



WPI

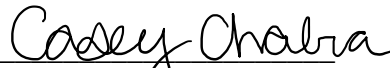
Manufacturing and Validation of a Microfluidic Bioreactor to Simulate Fluid Flow in Tissue Engineered Heart Valves

A Major Qualifying Project

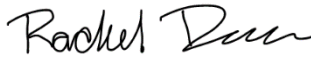
Submitted to the Faculty of
WORCESTER POLYTECHNIC INSTITUTE

In partial fulfillment of the requirements
for the degree of Bachelor of Science

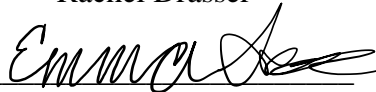
Submitted by:



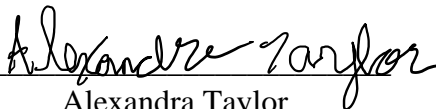
Casey Chabra



Rachel Drasser



Emma Smith



Alexandra Taylor

Date: 4/27/2023

Approved:

Professor Kristen L. Billiar, Advisor
Department of Biomedical Engineering

This report represents work of WPI undergraduate students submitted to the faculty as evidence of a degree requirement. WPI routinely publishes these reports on its website without editorial or peer review. For more information about the project's program at WPI, see <http://www.wpi.edu/Academics/Projects>.

Table of Contents

Table of Contents	1
Authorship.....	4
List of Figures	5
List of Tables	7
Acknowledgements.....	8
Abstract.....	9
1. Introduction	10
2. Literature Review	12
2.1 Aortic Valve Disease State and Anatomy	12
2.2 Current Treatments.....	13
2.3 Aortic Valve Environment	15
2.4 Tissue-Engineered Heart Valves (TEHVs).....	16
2.5 Endothelial to Mesenchymal Transition (EndMT)	18
2.6 Fluid Flow Bioreactors.....	19
3. Methodology and Approach.....	25
3.1 Initial Client Statement.....	25
3.2 Objectives and Parameters	25
3.3 Device Setup	27
3.3.1 Gravity Pump	27
3.3.2 Microfluidic Designs.....	29
3.4 Cell Culture	30
3.5 EndMT	30
3.6 Throughput	30
3.7 Ease of Use.....	31
3.8 Revised Client Statement	31
3.9 Engineering Standards.....	31
4. Alternative Designs and Proof of Concepts	33
4.1 Needs and Wants.....	33
4.2 Manufacturing Alternatives.....	33
4.3 Manufacturing Methodology.....	34
4.3.1 Photomask Design.....	34

4.3.2	Photolithography	34
4.3.3	Soft Lithography and Plasma Bonding	35
4.4	Previous Designs in Literature	35
4.5	Contact Angle Study	37
4.6	Alternative Devices	38
4.6.1	Design One: AIM Wider Spacing (150 μm)	39
4.6.2	Design Two: AIM Larger Post Angle	40
4.6.3	Design Three: AIM Internal Posts	41
4.6.4	Design Four: AIM Wider Spacing (200 μm)	42
4.6.5	Design Five: Farahat	43
4.6.6	Design Six: Yoon	44
4.6.7	Design Seven: Yoon Smaller Spacing	45
4.6.8	Design Eight: Polacheck	46
4.6.9	Design Nine: AIM	47
4.7	Final Photomask	47
4.8	Manufacturing Results	49
4.8.1	Fabrication of Devices	49
4.8.2	Gel Placement	58
4.9	Pump Validation	66
4.9.1	General Calculations for Gravity Pump	67
4.9.2	Experimental Validation of Steady Flow Gravity Pumps	68
4.9.3	Data Analysis	71
6.	Final Design	73
6.1	Microfluidic Designs	73
6.2	Steady Flow Gravity Pumps	74
6.3	Oscillatory Flow Circuit	75
7.	Ethical Consideration	78
7.1	Economic Factors	78
7.2	Environmental Impact	79
7.3	Social Influence	79
7.4	Global Ramifications	80
8.	Discussion	81

8.1	Imaging.....	81
8.2	Accuracy and Reproducibility.....	81
8.3	High Throughput.....	81
8.4	Shear Stresses.....	82
8.5	Compact and Contained.....	82
8.6	Ease of Use.....	82
8.7	Overall Cost.....	83
8.8	Cost Breakdown.....	83
8.9	Future Research Impacts.....	83
9.	Future Considerations.....	83
10.	Conclusions.....	84
	References.....	85
	Appendices.....	91
	Appendix A: Contact Angle Study Protocol.....	91
	Appendix B: Contact Angle Datasheet.....	93
	Appendix C: Gravity Pump Validation Procedure.....	94
	Appendix D: Pump Calculations.....	95
	Appendix E. MATLAB Code of Calculations.....	102
	Appendix F. MATLAB Code of Resistance Calculations.....	103
	Appendix G. Arduino Code for Circuit.....	105
	Appendix H. Making and Placing Gels in PDMS Devices.....	106
	Appendix I. Seeding Cells in Microfluidic Devices.....	108
	Appendix J: Soft Lithography Protocol.....	109
	Appendix K: Steady Flow Gravity Pump SOP.....	111
F.	Priming/Starting the Experiment.....	116
	Appendix L: AutoCAD Drawings of Microfluidic Designs.....	120

Authorship

Section	Author	Editor
Abstract	RD	ALL
Introduction	ES	ALL
Aortic Valve Disease State and Anatomy	AT	CC
Current Treatments	CC	AT
Aortic Valve Environment	AT	CC
Tissue-Engineered Heart Valves (TEHVs)	RD	RD
Endothelial to Mesenchymal Transition (EndMT)	ES	RD
Fluid Flow Bioreactors	ES	RD
Initial Client Statement	ES	RD
Objectives and Parameters	ES	RD
Device Setup	CC	AT
Gravity Pump	RD	RD
Microfluidic Designs	ES	ES
Cell Culture	CC	CC
EndMT	AT	CC
Throughput	CC	AT
Ease of Use	RD	ES
Revised Client Statement	ES	RD
Engineering Standards	CC	AT
Needs and Wants	AT	CC
Manufacturing Alternatives	ES	RD
Photolithography	ES	ES
Soft Lithography	AT	AT
Previous Microfluidic Designs	RD	ES
Contact Angle Study	ES	RD
Alternative Designs	RD	ES
Final Photomask	ES	RD
Fabrication of Devices	CC	CC
Gel Placement	CC, ES	ES
Pump Validation	AT	CC
General Calculations for Gravity Pump	AT, RD	AT
Experimental: Steady Flow	RD	RD
Data Analysis	AT	AT
Microfluidic Designs	ES	ES
Steady Flow Gravity Pumps	RD	RD
Oscillatory Flow Circuit	ES	ES
Discussion	ALL	ALL
Ethical Considerations	RD	ALL
Future Considerations	RD	RD

List of Figures

Figure	Pg. No.
Figure 1: Healthy and Stenotic Tricuspid and Bicuspid Valve.	12
Figure 2: Valves and Blood Flow in the Human Heart	13
Figure 3: Tilting Disc and Bileaflet Valve Replacements	14
Figure 4: Heart Valve Layers	15
Figure 5: Cross Section of a Heart Valve Under Normal Blood Flow Conditions	16
Figure 6: Flow Systems for Studying Fluid Flow on <i>in vitro</i> Models	20
Figure 7: Overview of Cellular Migration from the Media Channel into Microfluidic Gel Chamber	21
Figure 8: Microfluidic Device Used to Apply Interstitial Flow	22
Figure 9: AIM Biotech idenTx 3D Cell Culture Chip	23
Figure 10: Two schematics showing the basic setup for both low and high shear stress gravity pumps	28
Figure 11: Double Gravity Pump Setup with the labeled components	29
Figure 12: AIM Biotech's 3D Cell Culture Chip with an Acellular 4 mg/mL Fibrin Gel	30
Figure 13: Wafer Creation using Photolithography	35
Figure 14: Base Designs for Microfluidic Chips	36
Figure 15: AutoCAD Design One	39
Figure 16: AutoCAD Design Two	40
Figure 17: AutoCAD Design Three	41
Figure 18: AutoCAD Design Four	42
Figure 19: AutoCAD Design Five	43
Figure 20: AutoCAD Design Six	44
Figure 21: AutoCAD Design Seven	45
Figure 22: AutoCAD Design Eight	46
Figure 23: AutoCAD Design Nine	47
Figure 24: Photomask of Designs for Photolithography	48
Figure 25: 10x Image of Fabrication of AIM Chip replicas	49
Figure 26: Fabrication of AIM Chip replicas	50
Figure 27: Fabrication of AIM chip with Internal Posts	51
Figure 28: Fabrication of Yoon replicas	52
Figure 29: Fabrication of Polacheck replicas	53
Figure 30: Fabrication of Farahat replicas	54
Figure 31: Fabrication of Yoon device replica with 100 μm spacing	55
Figure 32: Fabrication of AIM Device with 150 μm spacing	56
Figure 33: Fabrication of AIM Device with 200 μm spacing	57
Figure 34: Fabrication of AIM Device with 75 degree post angle	58
Figure 35: Successful Gel Placement in AIM Chip	59
Figure 36: Pre-Gelation of AIM Chip Replicas	60
Figure 37: Pre-Gelation of AIM Chip Design with 150 μm Spacing	60
Figure 38: Pre-Gelation of AIM Chip Design with 200 μm Spacing	61
Figure 39: Pre-Gelation of AIM Chip Design with 75° Posts	62
Figure 40: Pre-Gelation of AIM Chip Design with Internal Posts	63
Figure 41: Pre-Gelation of Farahat Replicas	63

Figure 42: Pre-Gelation of Second Run of 200 μm Height Farahat Replica	64
Figure 43: Pre-Gelation of Polacheck Replicas	65
Figure 44: Pre-Gelation of Yoon Replicas	65
Figure 45: Pre-Gelation of Yoon Design with 100 μm Spacing	66
Figure 46: Diagram of gravity pump used for steady flow that produces a shear stress of 0.2 Pa	69
Figure 47: Diagram of gravity pump used for steady flow that produces a shear stress of 2.0 Pa	70
Figure 48: Average shear stress of the low system over three trials	72
Figure 49: Flow rates of the high shear stress pumping system compared to the theoretical flow rate	72
Figure 50: Both final setups for low and high shear stress gravity pumps with tubing dimensions	74
Figure 51: Final setup of high shear stress gravity pump running with the AIM Chip within the incubator	75
Figure 52: Full Circuit Diagram of Solenoid Pinch Valves in Parallel for Creating Oscillatory Flow	76
Figure 53: Circuit Diagram for one Solenoid Pinch Valve	77
Figure 54: Circuit Diagram for Powering the Breadboard and Arduino Uno	77

List of Tables

	Pg. No.
Table	
Table 1: Pairwise Comparison of Objectives for Fluidic Bioreactor	25
Table 2: Objectives and Weights	26
Table 3: Functions List	26
Table 4: Constraints List	26
Table 5: Flow Parameters	27

Acknowledgements

We would like to first thank our project advisor, Professor Kristen L. Billiar, for his guidance and support throughout the duration of this project. We also want to thank our client and mentor, Rozanne Mungai, for her guidance, patience, and expertise in this project. Her guidance and support contributed greatly to the success of this project.

In addition, we want to acknowledge Vanessa Kamara, from Professor Dirk Albrecht's lab. Her expertise and guidance in fabricating microfluidic devices aided our manufacturing and contributed to the success of our devices. We also appreciate the help from James Eakin, Professor Chris Nycz, and the Lab for Education and Application Prototypes; their knowledge contributed greatly to the decision regarding manufacturing methods for fabricating microfluidic devices. We also appreciated the help and continued support from those in Professor Billiar's Mechanobiology Lab and Professor Albrecht's Quantitative Neurotechnology Lab. Lastly, we would like to thank Lisa Wall, our Lab Manager, for her assistance in gathering all of the necessary materials and equipment for our project. This project would not have been possible without all of these individual's support, guidance, and expertise.

Abstract

Currently, the only treatment for aortic valvular disease is a valve replacement, and replacement valves on the market have limitations, especially for pediatric patients who need to undergo multiple invasive surgeries in a lifetime. Tissue-engineered heart valves (TEHV) hold the possibility to grow with patients, by having host cells repopulate it, however, this mechanism of repopulation is not understood, and TEHVs have mechanical limitations that are not conducive to the valvular environment. The cells within the TEHVs are directly influenced by the blood flow through the valves, therefore the goal of this project is to study the cellular response to blood flow conditions. We designed a microfluidic bioreactor that can contain cells and a gel matrix where endothelial cells are seeded adjacent to the matrix so that they can migrate into it as they experience phenotypic changes due to exposure to shear flow conditions. To achieve this, we designed multiple microfluidic devices out of PDMS using photolithography and soft lithography increasing the height of our devices to 200 μm and post spacing, while containing the gel matrix. We also designed two gravity pumps that produce steady flow at shear stresses of 2.0 pascals and 0.2 pascals and updated a double gravity pump which produces oscillatory flow. Based on our results, our microfluidic designs can contain gel and can be used for further testing under our gravity pump systems, indicating that we successfully designed a device with double the height and space between posts, increasing the area by four times. Hence, a microfluidic bioreactor was created with an accurate shear stress pumping system and a microfluidic device that maximizes the space for cell migration.

1. Introduction

In the United States, approximately 2.5% of the population has valvular heart disease, and 61% of these deaths are due to aortic valve disease (AVD) (Otto & Bonow, 2014; CDC, 2019). AVD is caused by calcification of the aortic valve or stenosis of a defective aortic valve (Lincoln & Garg, 2014). Currently the only treatment for this disease is a valve replacement, causing AVD to account for 10-20% of all cardiac procedures in the United States (Maganti et al., 2010). Treatment involves replacing the valve with either a mechanical or bioprosthetic valve (Butcher et al., 2011). In order for the replacement valves to function correctly and no blood clots form, medications are required for all patients, specifically blood thinners. Mechanical valves are made of biocompatible materials, such as pyrolytic carbon, and bioprosthetic valves are xenografted or autografted from living tissue (Gopal et al., 2022; Kostyunin et al., 2020). Since for both replacements blood thinners are needed, patients with abnormal blood pressure or an active lifestyle cannot get replacements (Zhu and Grande-Allen, 2018; Harris et al., 2015). Tissue-engineered heart valves (TEHVs) hold promise to limit these limitations of current valve replacements. TEHVs are made of a natural or synthetic scaffold structure (Neuenschwander & P. Hoerstrup, 2004). The scaffold is then either pre-populated with cells, prior to implantation, or implanted without cells, in hopes that native cells will populate the scaffold (Neuenschwander & P. Hoerstrup, 2004). To understand and develop efficient and successful treatments for AVD, researchers must understand how repopulation of this scaffold occurs in the body.

To understand repopulation, the valvular environment needs to be recreated *in vitro*. The aim of this mechanical model is to test the hypotheses of how cells repopulate TEHVs post-implantation. One of these hypotheses is that cells attach to the TEHV scaffold and undergo an endothelial to mesenchymal transition (EndMT), which allows cells to migrate into the scaffold, thereby repopulating it. Our goal is to construct a system that can produce flow on cells under a microscopic level to be able to observe the effects of fluid flow on cells that repopulate the scaffold, or matrix, of TEHVs.

Studying this phenomenon has been done through the use of systems that apply fluid shear stress (FSS) to cells. The focus for this project consists of multiple gravity pumps and a 3D *in vitro* model that determines where FSS is applied. The 3D *in vitro* model chosen is a microfluidic device, which has been used in preceding studies to examine the effects of FSS on cellular response (Meng et al., 2022). 2D cultures give some insight into bodily processes, but do not accurately represent the 3D environment. Microfluidics can contain flow channels, or media channels, and an inner gel chamber (Meng et al., 2022). The gel chamber contains the model of the TEHV scaffold for our experiment, and the media channels contain cell media, that the fluid will flow through to expose the cells to shear stress. The cells for this particular study will be injected along one media channel, and their migration into the gel will be assessed using the microfluidic device. We chose to design three gravity pumps in order to introduce the cells to high and low shear stress under steady and oscillatory flow conditions. Two single gravity pumps, one at a high shear stress and one at a low shear stress were designed. One double gravity pump was designed to produce oscillatory flow. The double gravity pump was designed to have one side send fluid through the microfluidic device in one direction and then the other side of the

pump would send fluid through the microfluidic device in the opposite direction. The gravity pumps in combination with the microfluidic device, were used as a bioreactor to mimic the environment of a heart valve, specifically the shear stress that cells face as blood flows through the valve. Using the pump and microfluidic device, cellular response due to fluid flow can be observed in real time under a microscope.

Our bioreactor design aims to resolve the limitations of current, commercially available, pumps and microfluidic devices. Using photolithography and soft lithography, we aim to manufacture a microfluidic device capable of containing a gel scaffold. In addition to manufacturing this microfluidic, we aim to design and validate two steady flow gravity pumps and improve upon the double gravity pump that has been previously designed by a WPI MQP Team.

2. Literature Review

2.1 Aortic Valve Disease State and Anatomy

In the United States, about 2.5% of the population has valvular heart disease, which leads to death if left untreated (Otto & Bonow, 2014). Of the deaths due to valvular heart disease, 61% of them were due to aortic valvular disease (AVD) (CDC, 2019). AVD is caused by either a bicuspid aortic valve, which is a congenital defect, or calcification around the cusps (Maganti et al., 2010; Fishbein & Fishbein, 2019). Both causes of AVD result in abnormal blood flow through the valve. This abnormality can lead to stenosis or regurgitation, straining the surrounding valvular tissues, creating an irregular force distribution along the valve (Fishbein & Fishbein, 2019). The cells in the valve need to compensate for this change, leading to an unbalanced extracellular matrix (ECM) composition. The composition changes result in the thickening of the aortic valve tissue and walls (Nishimura, 2002; Hinton & Yutzey, 2011). Figure 1 demonstrates the anatomical differences and visual changes between a bicuspid and tricuspid valve with and without stenosis.

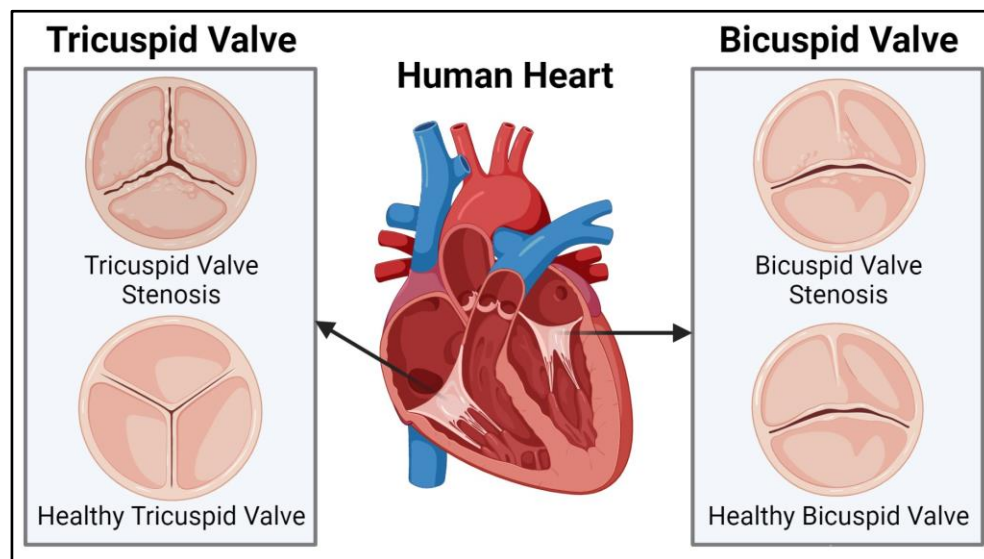


Figure 1: Healthy and Stenotic Tricuspid and Bicuspid Valve. A representation of a healthy and stenotic tricuspid valve (left). A representation of a healthy and stenotic bicuspid valve (right). (Nishimura, 2002; Hinton & Yutzey, 2011) Image created using Biorender.com.

Within the heart, there are four valves that work to maintain unidirectional blood flow, shown in Figure 2 (O'Donnell et al., 2020). There are two types of valves, atrioventricular and semilunar, which separate the different components of the heart. A semilunar valve, such as the aortic valve, are cusps that separate the ventricles from the outflow tract (Hinton & Yutzey, 2011; O'Donnell et al., 2020). The aortic valve aids in distributing blood throughout the body. It first opens to fill the aorta, and then closes to ensure no blood returns to the left ventricle (Nishimura, 2002). If deformation or disease of this valve occurs, classified as AVD, patients are

at risk of stenosis, restriction of blood flow, or regurgitation, backflow putting strain on other areas of the heart (Maganti et al., 2010; Fishbein & Fishbein, 2019).

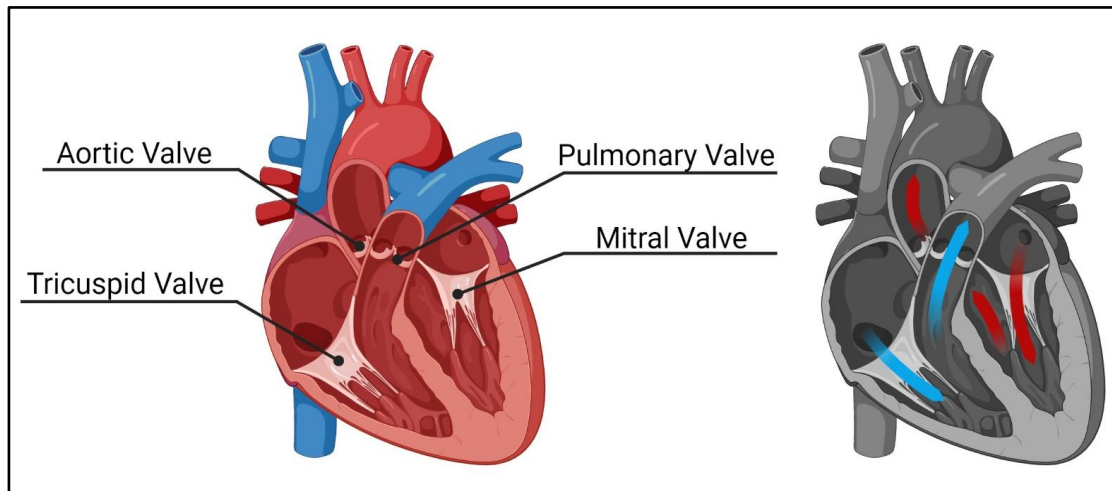


Figure 2. Valves and Blood Flow in the Human Heart. A representation of the four valves within the heart, including the aortic, pulmonary, tricuspid, and mitral valves (left). A representation of blood flow within the heart (right), including deoxygenated (blue arrows) and oxygenated (red arrows) blood. (O'Donnell et al., 2020) Image created with Biorender.com.

2.2 Current Treatments

Current treatment options for AVD are limited and have varying challenges. These treatments, and the medications prescribed alongside treatment, can help slow the progression of this disease, but they cannot cure it (Zhu & Grande-Allen, 2018). Typically, the treatment for AVD is a full valve replacement. The two most common options for valve replacement are mechanical and bioprosthetic (Cukierman et al., 2001).

Mechanical valve replacements (MVRs) are made of biocompatible materials, such as pyrolytic carbon, and are commonly used due to its durability, as they can last up to 20 years (Gopal et al., 2022). When choosing a mechanical valve, thrombogenicity, the ability to generate blood clots, is an important factor. There are two types of MVRs: tilting disc valve and bi-leaflet heart valves, shown in Figure 3. The tilting disc valve is made by a metal ring which holds the disc and is covered by fabric where sutures are placed to contain the valve. This valve opens when the chamber pressure drops to pump the blood out and then closes to prevent backflow. A bi-leaflet heart valve consists of two semicircular leaflets and is the most commonly used valve because it is the least thrombogenic (Gopal et al., 2022). However, one of the biggest limitations of mechanical heart valves is their thrombogenicity, meaning that patients must take blood thinners following replacement.

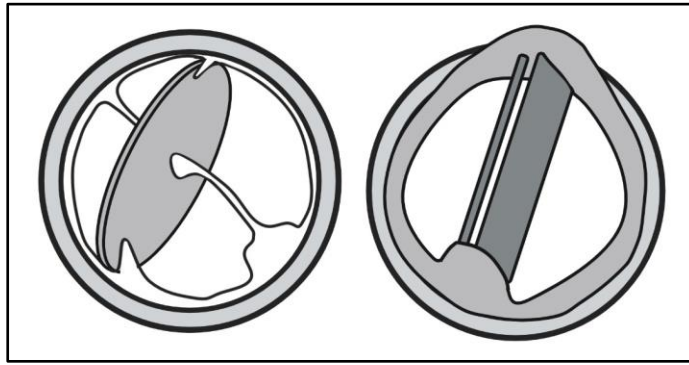


Figure 3: Tilting Disc and Bileaflet Valve Replacements. A representation of a tilting disc valve (left) and bileaflet valve (right) replacement. (Kaushik et al., 2022; Yun et al., 2014) Image created using Biorender.com

Blood thinners are needed to prevent clotting, and patients who undergo heart valve replacement surgery will need to be on blood thinners for the remainder of their lives (Hasan et al., 2018). Those who cannot take blood thinners, particularly those with uncontrolled high blood pressure or stomach ulcers, will not be able to get a MVR (Butcher et al., 2011). In addition, blood thinners are not advised during pregnancy, so patients who are pregnant or planning to become pregnant cannot receive a MVR (Harris et al., 2015). If no complications arise, a typical mechanical replacement should last 20 to 30 years (Ahmed, 2017).

The other option for heart valve replacement is a bioprosthetic valve, which can be a human autograft, bovine xenograft, or porcine xenograft valve (Kostyunin et al., 2020). Autografts are a patient's own tissues which are transplanted from one position to another, an example being a Ross procedure. This is when a patient's aortic valve is replaced with their own pulmonary valve, which is then replaced with a pulmonary allograft, which is from a donor (Brown & Kanmanthareddy, 2022). Xenografts are chemically stabilized tissues of animal origin and are the most common type of bioprosthetic valves because of their wide availability. Bioprosthetic valves are less durable than a healthy, human valve, as they lack living cells to regenerate the tissue, leading to degradation due to the forces applied to the valve (Zhu & Grande-Allen, 2018). Considering this degradation, bioprosthetic valves are not advised for patients who lead a very active lifestyle, as this further strains the valve. In addition to degradation, these valves only last 10 to 15 years, meaning they are not advised for patients that would need multiple replacements (Harris et al., 2015). In addition to degradation, bioprosthetic valve replacement failure can occur due to an adverse immune response, leading to rejection of the valve (Manji & Manji, 2020). However, these valves are recommended for patients who are over sixty and have limited regular physical activity and for patients who cannot handle blood thinners (Butcher et al., 2011).

As demonstrated, there is a strong need for an improved alternative to mechanical and bioprosthetic valves. Neither valve grows with the patient, meaning recipients of these valves will need multiple replacement surgeries. Due to the static growth and lack of longevity, both options are not suitable for pediatric patients as they will need multiple replacement surgeries throughout their lifetime (Hasan et al., 2018). Bioprosthetic valve replacements, in addition, have

a chance of rejection (Manji & Manji, 2020). Tissue Engineered Heart Valves (TEHVs) have the potential to overcome the aforementioned limitations as they are biocompatible and present lower risk than mechanical and bioprosthetic valves.

2.3 Aortic Valve Environment

Valve replacements aim to reestablish blood flow, as the diseased valve perturbed blood flow into and out of the valve. As healthy aortic valve leaflets open and close 30-40 million times per year, the replacements need to be able to withstand the significant stress put on them. The shear stress put on these valves ranges from 3.0 to 150 Pa, with an average of 2.0 Pa of stress (Mahler et al., 2014). The endothelial cells within the valve are subject to these stresses. To learn more about how these stresses affect cellular response, experiments with porcine aortic valve endothelial cells (PAVECs) were subjected to shear stresses of 0.2 and 2.0 Pa (Mahler et al., 2014). These two stress values fall within the physiological values of the valve and are key to understanding more about cellular response to blood flow. To create a replacement that can withstand these stresses, we must understand what comprises the micro and mechanical environment and how these stresses affect the cells within the environment.

Aortic valves consist of the ECM, valvular interstitial cells (VICs), and valvular endothelial cells (VECs), shown in Figure 4 (O'Donnell et al., 2020). VECs form a monolayer on the exterior of the valve, and the interior of the valve comprises ECM and VICs, which are separated into three distinct layers, the fibrosa, spongiosa, and ventricularis. Each of these layers has a different function. The valve's primary strength comes from the outflow layer of fibrosa. The spongiosa supports the motion of the other layers. The ventricularis, located on the inflow side of the valve, allows it to stretch and contract (Kodigepalli et al., 2020).

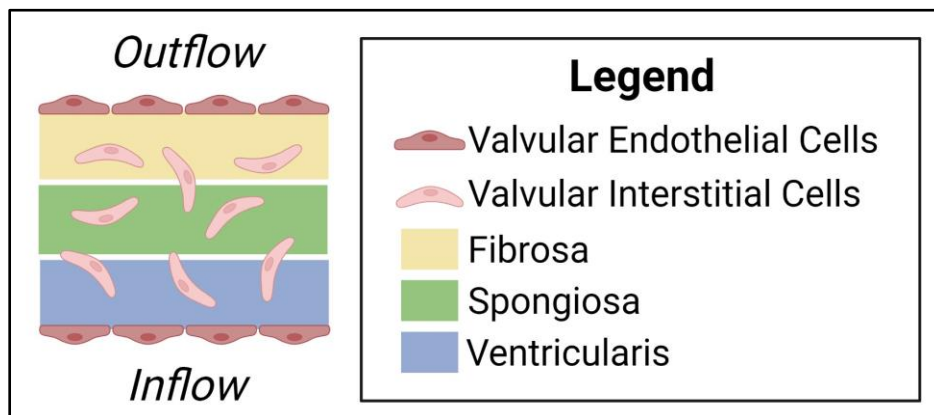


Figure 4: Heart Valve Layers. A representation of the layers of a heart valve, the fibrosa, spongiosa, and ventricularis, bordered by valvular endothelial cells (VECs) (right). This representation includes the valvular interstitial cells (VICs) in the fibrosa, spongiosa, and ventricularis. (O'Donnell et al., 2020; Kodigepalli et al., 2020) Image created using Biorender.com.

VECs have direct contact with blood flow and communicate with VICs, maintaining the architecture and functions of the heart valves (O'Donnell et al., 2020; Kodigepalli et al., 2020). Under normal blood flow conditions, shown in Figure 5, VECs in the ventricularis are subject to steady flow when blood flows through the valve. VECs in the fibrosa are subject to oscillatory flow when the valve closes. This flow subjects VECs to stresses from 3.0 to 150 Pa, with experiments using 0.2 and 2.0 to represent physiological values on VECs (Mahler et al., 2014). VICs mitigate the wear and tear of the valves by remodeling the ECM, which is done through degradation and deposition of ECM components (Kodigepalli et al., 2020). On the contrary, the overproduction of the ECM components due to VICs activation in malformed valves can cause stenosis or myxomatous degeneration, progressive degeneration of the valve, leading to abnormal blood flow (O'Donnell et al., 2020). If the aortic valve can no longer function sufficiently to maintain livable blood flow conditions, patients will need to undergo aortic valve replacement surgery (Fishbein & Fishbein, 2019). Although mechanical and prosthetic valves are currently used to replace diseased valves, there is a need for a better replacement. Tissue-engineered heart valves are being researched for their efficacy as a treatment option for valvular disease, especially with their potential to repopulate with native cells, preventing rejection and allowing growth with the patient.

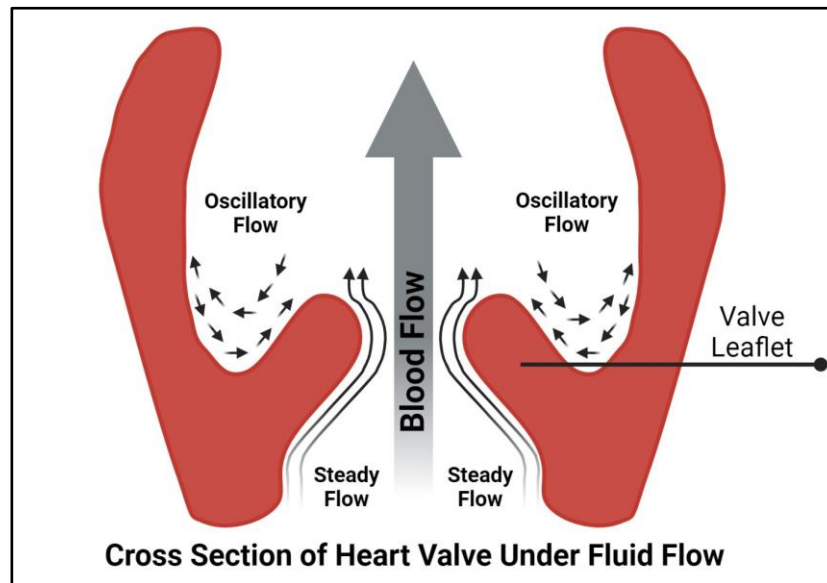


Figure 5: Cross Section of a Heart Valve Under Normal Blood Flow Conditions. A representation of blood flow into a heart valve. This shows a cross section of the valve leaflet and flow patterns. Steady flow occurs on the inflow side of the valve, and oscillatory flow occurs on the outflow side of the valve. (O'Donnell et al., 2020; Kodigepalli et al., 2020) Image created using Biorender.com

2.4 Tissue-Engineered Heart Valves (TEHVs)

Heart valve tissue engineering has the potential to overcome the limitations of existing valve replacements. Even though mechanical heart valves are stronger, TEHVs have the potential to regenerate and, ultimately, grow with the patient (Xue et al., 2017). This allows a

pediatric patient to undergo a heart valve replacement and limit their replacement surgeries in the future.

TEHVs are synthesized using natural or synthetic scaffolds. Scaffolds are three-dimensional constructs that direct cell attachment and tissue regeneration (Neuenschwander & P. Hoerstrup, 2004). Bioreactors are typically used to expose the cells and scaffold of the TEHV to the environment of a human heart, where it will be implanted, subjecting it to the mechanical environment TEHVs need to withstand. It is important for bioreactors to provide the optimal pH, temperature, pressure, and stress that a heart valve undergoes (Gandaglia et al., 2011). By using a bioreactor, it preconditions the scaffold and cells to behave as if it were inside the body, which can be observed prior to implantation.

Scaffolds for TEHVs can be utilized by seeding a provisional scaffold with cells, allowing the cells to remodel the ECM and then decellularizing in order to allow for mass-production. From there, the decellularized scaffolds can be implanted into a patient and repopulated by native cells. Natural scaffolds are composed of native extracellular matrix components (ECM). Purified components of ECM contain the biological information cells need to differentiate into the desired structure. Natural scaffolds elicit a smaller foreign body response than synthetic scaffolds when implanted in the body (Mendelson & Schoen, 2006). These properties are what make natural scaffolds a more viable option in TEHVs. One way to synthesize natural scaffolds is to use a donor valve from an animal or human then decellularizing the valve, removing all cellular components (Hari Priya et al., 2020). After removing all cellular components, the scaffold is left as native ECM, acting as a blueprint for repopulation of cells. Another way to synthesize a natural scaffold is to use biomaterials, such as fibrin, which have been grown *in vitro*, then decellularized and recellularized *in situ*. A synthetic scaffold is constructed using bioresorbable polymers that degrade over time. As the polymers degrade, the scaffold is seeded with living tissue cells from the patient (Neuenschwander & P. Hoerstrup, 2004). Since a synthetic heart valve scaffold has a porous macrostructure, it allows the cells to repopulate and grow within the structure. However, the cellular repopulation of host cells is not completely understood. It is hypothesized that the blood flow through the valve affects the cells, changing their behavior. When the TEHV undergoes constant blood flow into and out of it, the valve fails due to the cells not repopulating the valve at the same rate as they are damaged (Hari Priya et al., 2020).

To study the repopulation of decellularized TEHVs and better understand what drives and contributes to the repopulation of host cells, many experiments have been conducted *in vivo*. In one study, decellularized tissues were implanted in sheep models with two different generations. The first generation has a structure that was simple and non-physiological to valve geometry and the second generation was created with a computerized shape geometry (Motta et al., 2020). It was hypothesized that geometry affects the remodeling of TEHV and showed that abnormal repopulation contributed to the shortening and thickening of leaflets (Motta et al., 2020). The two generations of TEHVs were observed and it was found that the first generation experienced leaflet thickening and chronic inflammation. However, the second generation experienced decreased inflammatory response, and after eight weeks, the cells repopulated the walls of the

valve (Motta et al., 2020). With the different geometries, the second generation of TEHV experienced less complications and cells began to repopulate it. At the conclusion of this study, it was hypothesized that the presence of endothelial cells lowered the inflammatory response during the early stages of tissue remodeling (Motta et al., 2020). This was caused by the findings that the second generation TEHV experienced significantly less inflammatory response after being repopulated with cells (Motta et al., 2020). Endothelial cells are important to aid the integration of TEHVs within the body, but the mechanisms of their repopulations are still not understood. Another study that focuses on repopulation of cells in TEHV, consisted of a heart valve constructed using fibroblast-produced ECM and implanted into a sheep for 52 weeks (Syedain et al., 2021). The leaflet of this valve was only partially repopulated with cells. One observation of the study was that the cells migrated from the base of the pulmonary artery to the free edge of the leaflet (Syedain et al., 2021) Due to this observation, it is believed that cells start migration from the vessel wall. Another discovery was that the majority of cells remain on the surface of either the root or the leaflet (Syedain et al., 2021). The migration of cells into the decellularized TEHV has been documented but were not sufficient enough to undergo full repopulation. To effectively construct TEHVs, from decellularization to repopulation, further study of this repopulation within the valvular mechanical environment is necessary.

2.5 Endothelial to Mesenchymal Transition (EndMT)

One hypothesis of how cells repopulate decellularized TEHVs is via the endothelial to mesenchymal transition (EndMT) (Kovacic et al., 2019). EndMT is the transition from an endothelial to mesenchymal-like state through the response of the cell to its surrounding and internal environment (Kovacic, 2018). This transition is typically observed through protein production, as endothelial and mesenchymal cells have different proteins upregulated. Endothelial cells are known to have increased CD31, VE-Cadherin, and endothelial nitric oxide synthase (Kovacic et al., 2019). Mesenchymal cells have increased alpha-smooth muscle actin (α -SMA), calponin, and SM22 α (Kovacic et al., 2019). This change in phenotype is how cells are thought to invade the matrix of the TEHV, as it has been hypothesized that EndMT becomes a way for the body to replenish the cells of the cardiac valves, particularly the valve interstitial cells, in order to maintain the ECM (Aikawa et al., 2006). This replacement is most likely due to the valves being subjected to forces that cause wear. These forces are steady and oscillatory forces from the flow of blood through the valves (Kovacic et al., 2019). If these cells are not replaced, then the valve will not function properly; this is the same if there is too much replacement. The process of the EndMT requires a balance, which is not fully understood.

To further understand the role of EndMT, *in vitro* models are used because they allow for a more controlled environment than animal models. *In vitro* models allow for stimulus to be added to endothelial cells to examine EndMT. These models can use a variety of assays to look for a reduction in endothelial and increase in mesenchymal characteristics. Assays that study the endothelial characteristic reduction include endothelial cell tubule formation *in vitro* and thrombin generation (Moonen et al., 2010; Krenning et al., 2008). Assays that examine

mesenchymal characteristic increase include invasion and migration (Evrard et al., 2016; Krenning, et al., 2008). To get a whole picture of EndMT in an *in vitro* model, both reduction of endothelial markers and upregulation of mesenchymal markers should be studied. In the context of this project, the focus will be examining the effect of fluid flow on EndMT using an invasion assay.

Flow through the heart valves in adults is known to affect EndMT. In 2014, Mahler et al. examined the effects of flow on porcine aortic valve endothelial cells (PAVECs). Their study consisted of a microfluidic device with a collagen matrix that applied shear and oscillatory stresses of 0.2, 1.0, and 2.0 Pa on PAVECs, analyzing invasion and protein expression (Mahler et al., 2014). Within this study there were three different pressures with three wells in each pressure to study how the cells respond to fluid flow (Mahler et al., 2014). There was very little difference in the invasion of the cells into the matrix when comparing the wells experiencing the same amount of pressure, meaning that position of the well had minor effects on the invasion compared to flow. When comparing the control, static, to the oscillatory flow, they found an increase in invasion into the matrix and mesenchymal protein markers in oscillatory flow. Comparing the static cells to cells exposed to steady shear flow, they found that mesenchymal cell markers decreased as the steady shear stress increased (Mahler et al., 2014). In other words, as shear stress increases, the less mesenchymal cells become; this, in turn, means that cells should exhibit a less migratory phenotype. There are still gaps in the knowledge of cell invasion into TEHV matrices, including further understanding of neo tissue formation (Blum et al., 2018). One way to study these gaps is fluid flow bioreactors.

2.6 Fluid Flow Bioreactors

To study EndMT and neo tissue formation, fluid flow bioreactors have been developed, particularly for applications of fluid shear stress (FSS). In typical bioreactors, fluid flow is not applied, and cells and constructs are not subject to FSS. There are two different FSS of interest in this device, steady and oscillatory flow (Meng et al., 2022). To study cellular response to FSS, several types of fluidic devices have been developed, including parallel-plate, cone-and-plate, orbital shaker, and microfluidic systems, shown in Figure 6 below (Meng et al., 2022).

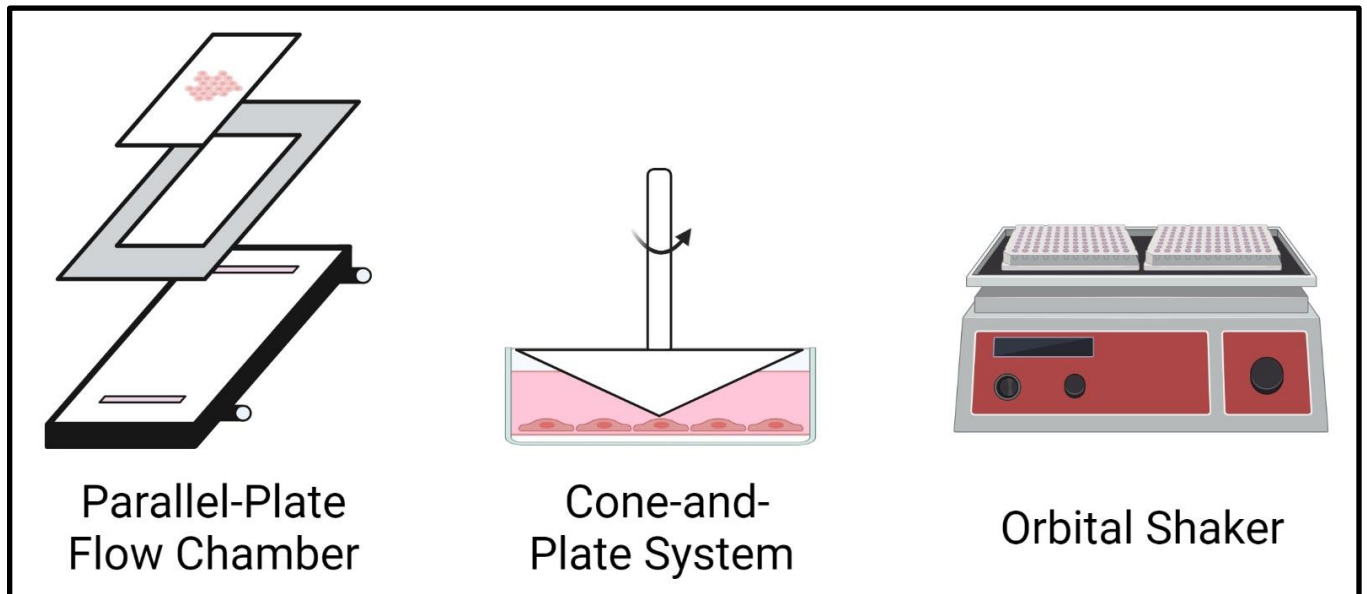


Figure 6: Flow Systems for Studying Fluid Flow on *in vitro* Models (Meng et al., 2022) Image created using Biorender.com

Parallel-plate systems involved placing two plates, a transparent plate on top to allow observation and a plate for culturing cells (Meng et al., 2022). The ends of the plate are open, allowing fluid flow, which can be driven by pressure, typically done using gravity or an active pump system. This system is typically used to study cellular response to fluid flow, particularly using live cell imaging. A limitation with this system is the throughput of medium; the device would require a large amount of medium for running experiments for long periods of time. The cone-and-plate system is similar to the parallel plate system, except it consists of a petri dish inside a cone, which is rotating (Meng et al., 2022). This system is particularly useful for experiments where pulsating and turbulent flow are desired (Dai et al., 2004). A limitation of this system is that evaporation plays a larger role, as the system is open. Orbital shakers are another system, consisting of a dish being swirled to simulate uniaxial and multiaxial shear stress on cells (Meng et al., 2022). A limitation of this system is the ability to calculate the FSS being exerted on the cells. Finally, microfluidic systems are widely used to generate a multitude of flow patterns, as they are personalizable (Meng et al., 2022). The main limitation of microfluidic systems is the small number of cells that can be studied at a time. All of these systems have varying applications and limitations; due to their ability for high experimental throughput and low cost, microfluidic systems were the primary focus for this project.

Microfluidic devices have been used to mimic flow conditions found in the human body. These devices can have either passive or active flow, where the flow remains unchanged and the flow is dynamic, respectively. Microfluidic devices can complete many different experiments involving cellular response, especially since the goal of the microenvironment is to be biomimetic. Experiments involving endothelial cell lines focused on analyzing pulsatile shear stress on HUVECs and shear stress on endothelial cell morphology on BAECs (Blackman et al., 2002; Girard & Nerem, 1995). Morphology through cell migration and differentiation,

proliferation, apoptosis, and metabolism are examples of cellular behaviors that can be observed using microfluidic devices (Meng et al., 2022). Aspects of cellular response, such as protein expression, in response to fluid flow are key to the experimental use of this device. The focus of this project's experimental design is cellular migration into a decellularized gel in response to fluid flow, particularly to test the hypothesis that EndMT is how cells repopulate the scaffolds of TEHVs. Figure 7, below, shows how this would occur in a microfluidic device.

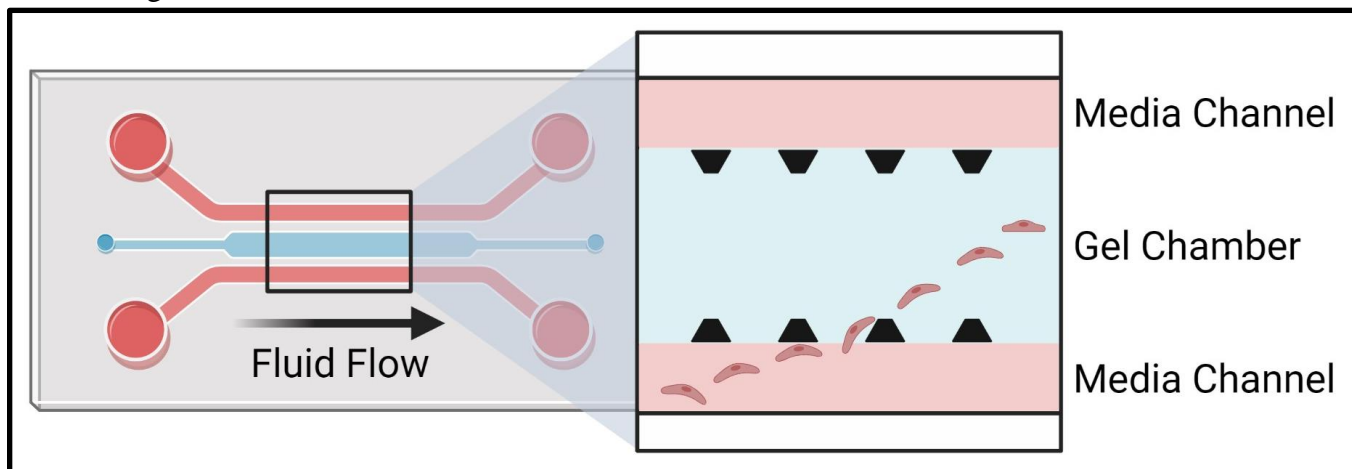


Figure 7: Overview of Cellular Migration from the Media Channel into Microfluidic Gel Chamber. As fluid flows through the media channels on either side, cell behavior changes, making them more migratory, and they migrate into the inner gel chamber. This is shown in the zoomed in picture above. Image created using Biorender.com

Microfluidic devices come in a variety of shapes and sizes, as many studies utilize them for their biomimetic properties. Due to the small size of the devices, the structure and dimensions of the device features directly influence the fluid dynamics they experience. For one, the flow rate through a microfluidic device is directly influenced by the dimensions of the channels. Regulation of flow can also be affected by protrusions within the channels. Other aspects of the microfluidic device, such as a gel chamber, can be modified to fit the needs of the user (Meng et al., 2022). There are calculations that go along with determining the optimal properties of the microfluidic device. The Navier Stokes equations and Hagen Poiseuille law are used to calculate the theoretical FSS and flow rate in the microfluidic. The Navier Stokes equations are used primarily to describe the flow of incompressible fluids, and the Hagen Poiseuille law describes the laminar flow rate of an incompressible fluid along a pipe (Meng et al., 2022).

Understanding these concepts, in addition to the understanding resistance along the wall of the channels, is important to designing a microfluidic for this particular application. These concepts are the baseline for the type and magnitude of stress that is applied to the cells within a given experiment, and since the cells will be seeded along the wall of the channel, calculating the resistance of the wall is important to ensure that the cells are subjected to the correct stress values. Given this information, it is important to look at devices that are applied in similar experimental applications, as they can inform the microfluidic design for a fluid flow experiment on endothelial cells.

Given that the focus of the experimental design is a cell invasion assay, examining microfluidic devices used in cell invasion and migration studies is pertinent. The two devices of interest, particularly as a baseline, are a design in Dr. William J. Polacheck and colleagues' 2014 cellular migration study and AIM Biotech's 3D Cell Culture Chip. The 2014 device, shown in Figure 8, contains two flow channels for medium and one for a collagen type one hydrogel (Polacheck et al., 2014). A pressure gradient was created using both channels, one being a higher pressure and the other being a lower pressure; this created flow across the gel (Polacheck et al., 2014). Cells within the gel were the target of the pressure gradient. This study provides evidence of fluid flow inducing adhesion activation, polarization, and migration of cells through the adhesion stress in a gel matrix (Polacheck et al., 2014).

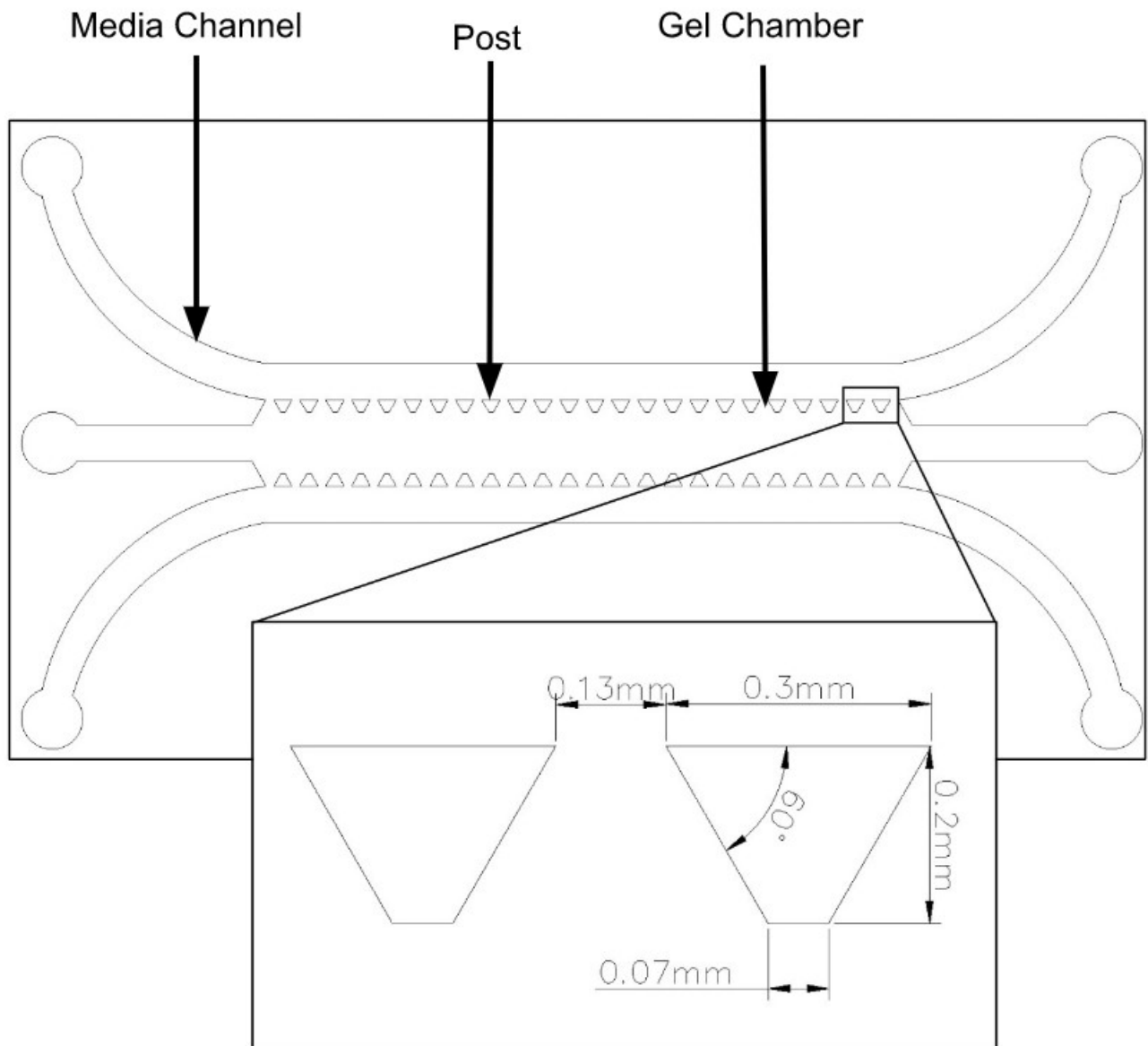


Figure 8: Microfluidic Device Used to Apply Interstitial Flow (Polacheck et al., 2014)

Another device of interest, due to its similarity in function to the desired device, is the AIM Biotech idenTx 3D Cell Culture Chip (AIM Biotech® DAX-1™), shown in Figure 9 below. This chip contains two flow channels for medium and a gel channel, and it is made of plastic, not polydimethylsiloxane (PDMS). This device has been used to study the effects of luminal and trans-endothelial fluid flow on tumor cell migration (Hajal et al., 2021). This study, completed by Dr. Roger D. Kamm and colleagues, shows that flow can promote tumor cell extravasation, and subsequent transmigration, which paves the road for exploring the roles of flow on other tumor cell responses in a microscale platform (Hajal et al., 2021). Transmigration of tumor cells out of blood vessels involves cells upregulating and downregulating proteins that aid in migration and invasion, much like endothelial cells do in response to fluid flow (Chen et al., 2014). The AIM Biotech Chip is an important baseline for this work, as it provides a platform that is known to work for experiments examining fluid flow. Working off of this baseline will involve optimizing a microfluidic device that can be manufactured cheaply and used efficiently. Using this modified microfluidic device, the client can effectively study how TEHVs are repopulated with cells when exposed to the fluid flow conditions within the heart valve.

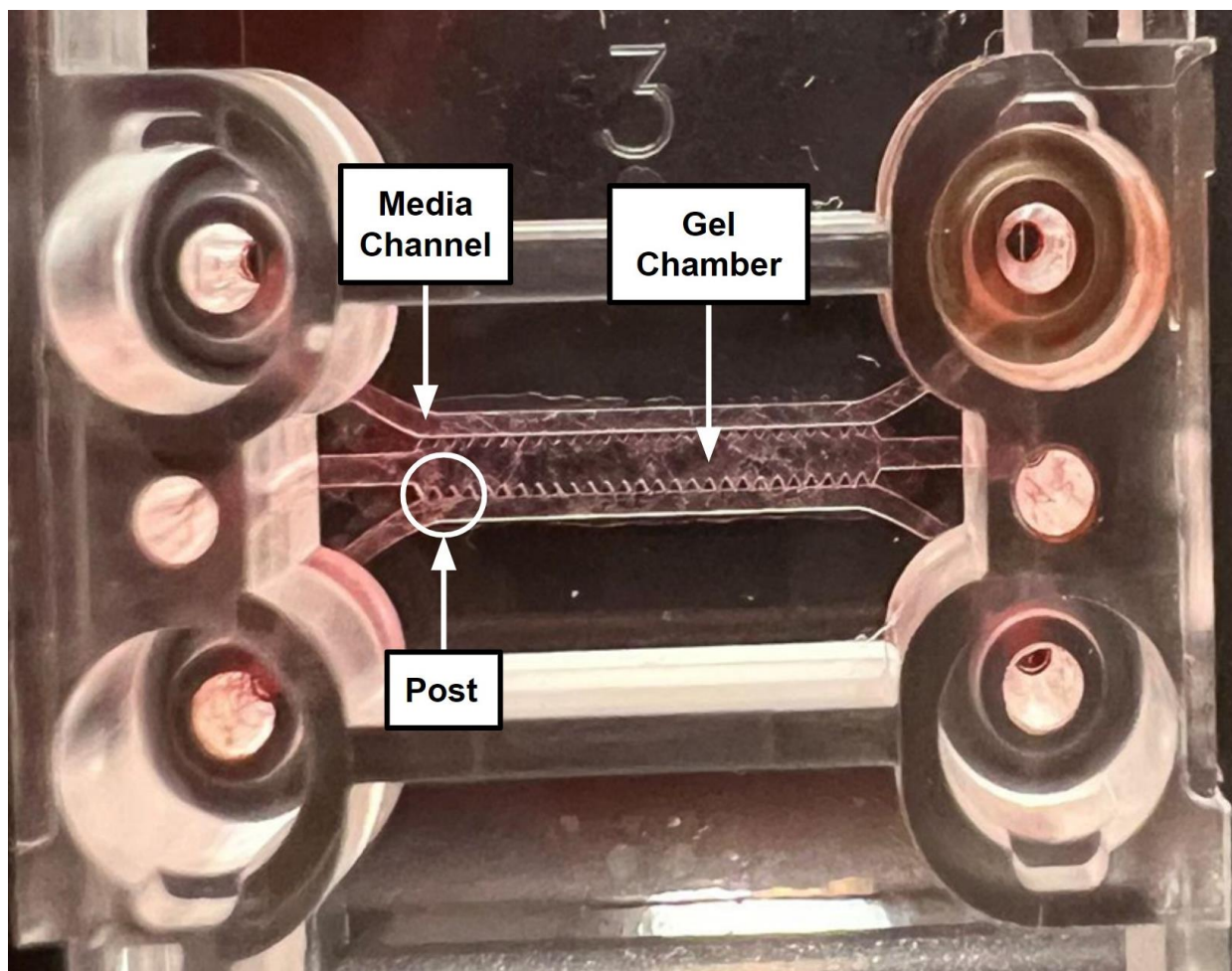


Figure 9: AIM Biotech idenTx 3D Cell Culture Chip (AIM Biotech® DAX-1™). Media channel, gel chamber, and post (white circle) within the AIM chip are labelled.

In our study, we apply fluid flow along the wall of a rectangular channel, as the cells will be seeded along the wall of the channel. The cells will be exposed to our chosen target shear stresses of 0.2 and 2.0 Pa, as these values are within a range of simulated shear stress values. These values have also been used in experiments examining the effect of shear stress on cells (Mahler et al., 2014). To complete this, we designed a microfluidic device, as well as a pump system to flow media through the microfluidic.

3. Methodology and Approach

3.1 Initial Client Statement

The goal of this project is to design and validate a bioreactor system that can exert shear stress on endothelial cells through steady and oscillatory flow and observe the migration of endothelial cells into a 3D gel matrix, which acts as a scaffold of a tissue-engineered heart valve.

3.2 Objectives and Parameters

The objectives, shown below in Table 1, are based on the client’s requests for the development of the fluidic bioreactor for studying repopulation of cells. Objectives are listed on the second row and first column to be compared to one another in order to determine the priority of each. This comparison was created by averaging the client’s own answers for the table. The rank in the final column represents the priority of each objective. In Table 2, the weights of the objectives are assigned percentages, which add up to one. The objective ranked highest was that cells are able to invade the matrix.

Table 1: Pairwise Comparison of Objectives for the Fluidic Bioreactor

Objectives - Pairwise Comparison										
	<i>High through-put</i>	<i>Cells able to invade the matrix</i>	<i>Easy to Use</i>	<i>Able to subject cells to a wide range of shear</i>	<i>Easy to image cell infiltration</i>	<i>Accurate / reproducible</i>	<i>Compact & contained</i>	<i>Inexpensive</i>	<u>Totals</u>	<u>Rank</u>
<i>High through-put</i>	x	0	1	0	0.25	0.5	1	1	3.75	4
<i>Cells able to invade the matrix</i>	1	x	1	1	1	1	1	1	7	1
<i>Easy to Use</i>	0	0	x	0	0.25	0	1	1	2.25	6
<i>Able to subject cells to a wide range of shear</i>	1	0	1	x	0	0	0	1	3	5
<i>Easy to image cell infiltration</i>	0.75	0	0.75	1	x	1	1	1	5.5	2
<i>Accurate / reproducible</i>	0.5	0	1	1	0	x	1	1	4.5	3
<i>Compact & contained</i>	0	0	0	1	0	0	x	1	2	7
<i>Inexpensive</i>	0	0	0	0	0	0	0	X	0	8

Table 2: Objectives and Weights

Objectives	Weights
Cells able to invade the matrix	0.25
Easy to image cell infiltration	0.20
Accurate / reproducible	0.16
High throughput	0.13
Able to subject cells to a wide range of shear	0.11
Easy to Use	0.08
Compact & contained	0.06
Inexpensive	0.01

The functions of the bioreactor are listed in Table 3, and the constraints are in Table 4. These functions and constraints were determined through conversations with the client. In addition to these functions and constraints, the stresses required for the device are listed in Table 5.

Table 3: Functions List

Functions
Produce Steady & Oscillatory Flow
Contain Gel in Chamber
Fit in Incubator
Prevent Evaporation
Contain Multiple Replicates
Produce Accurate Shear Stresses
Allow <i>In Situ</i> Decellularization
Allow Fix & Stain <i>In Situ</i>

Table 4: Constraints List

Constraints
min. eight samples concurrent at two levels (control & treatment)
min. 180 μm high 100 μm wide locations for cell attachment
able to be used by one person; not require precision placement of gels/cells
min. 0.2 and 2.0 Pa; min. steady and oscillatory at 1Hz

must be able to measure depth of infiltration min. 900um
must have an inlet min. 1000 μm wide to fit 10 μL pipette tip
min. +/- 10% of stated parameter values (e.g., 2Pa +/- 0.2Pa)
must use max. two incubator standard shelves (i.e., max 10" high)
max. \$1000 for system and \$25 per experimental point (i.e., \$200 for eight units in parallel)
must be sterile/aseptic

The flow parameters listed below, in Table 5, were determined using an average resting heart rate of 60 to 72 beats per minute (BPM). The two shear stresses that will act as our high and low values are 0.2 and 2.0 Pascals (Pa) (Mahler et al., 2014).

Table 5: Flow Parameters

Flow Pattern	Magnitude of Shear Stress (Pa)	
Static (Control)	0	
Steady	0.2	2.0
Oscillatory (60-72 bpm)	0.2	2.0

3.3 Device Setup

When setting up the microfluidic bioreactor, it is important that the central gel chamber of the microfluidic device can contain the gel while fluid runs along the side media channels. This ensures that the cells that are attached to the side of the gel are not sheared off during the experiments. If the cells shear off due to fluid flow or possible air bubbles, a disruption to the gel can occur and the observation of cell migration cannot be conducted. Therefore, the system needs to be set up with careful attention under proper sterile conditions as the imaging of cells *in situ* is crucial for the purpose of studying cell migration.

3.3.1 Gravity Pump

The first component of the microfluidic bioreactor is three different gravity pumps that provide fluid flow to the gel chamber. A gravity pump is driven by the forces of gravity, where pressure difference pushes the fluid to flow downwards. Due to the acceleration of gravity, the higher the initial reservoir is placed from the outlet, the faster the fluid will flow through the system. Two gravity pumps were designed to produce steady flow conditions at a high and low shear stress and another double gravity pump was designed to produce oscillatory flow conditions. All setups consist of tubing and connectors of varying heights to provide the

necessary flow rate, which can be seen in the schematics in Figure 10. For steady flow conditions, one unfiltered T175 flask was used to hold the initial amount of cell media to run through the system. The reservoir was placed at different heights to produce a larger or smaller pressure difference and therefore a different flow rate. The fluid flows in a uniaxial direction and constantly through the two inlets through the media channels of the microfluidic device and flowing out of the outlets, pictured in Figure 10.

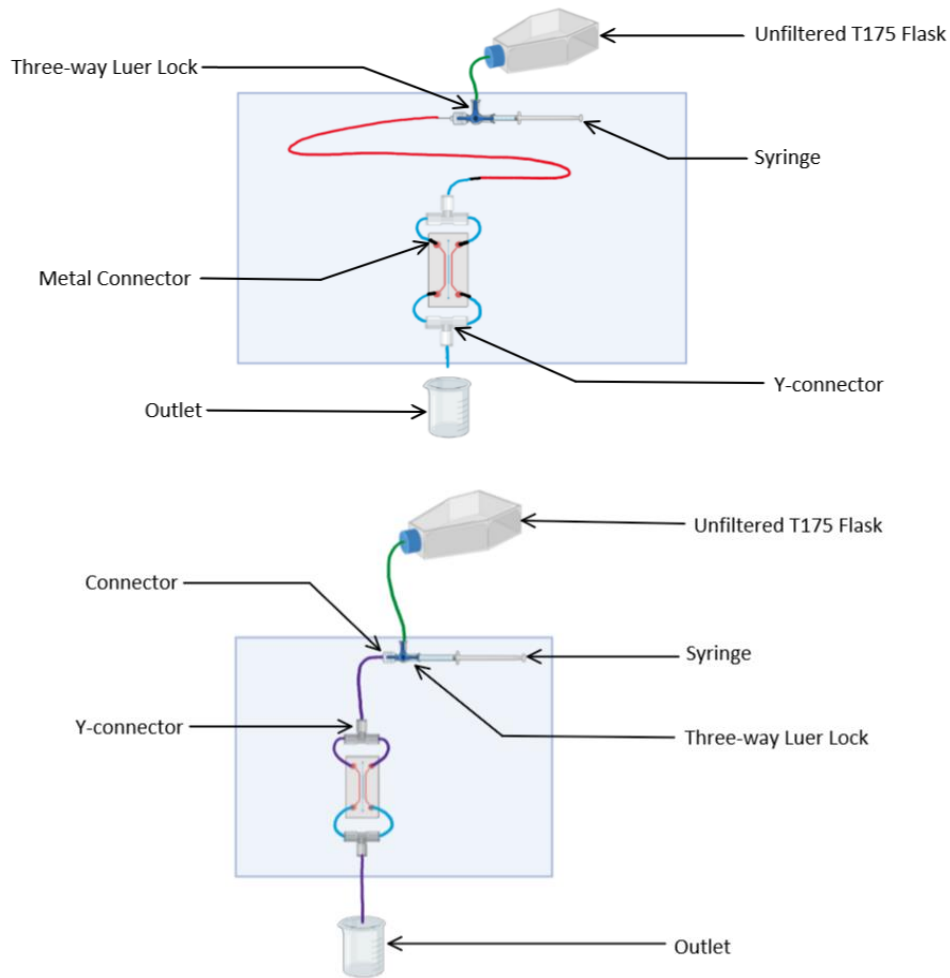


Figure 10. Two schematics showing the basic setup for both low and high shear stress gravity pumps.

To create an oscillatory flow, four 24 V solenoid pinch valves were used to modify the gravity pump. Tubing is placed at the four corners of the microfluidic, which are attached to the media channels, with two inlets and two outlets. The tubing connected to the two inlets, where the fluid enters the media channels, has two solenoid valves attached and the remaining two solenoid valves are attached to the tubing connected to the two outlets, where the fluid exits the media channels, pictured in Figure 11. The pumps push fluid forward and backwards through the media channels, producing the oscillatory flow pattern, this pattern is created by alternating tubing constriction via the solenoid valves. The pinch valves are programmed using Arduino software, where when the first group opens it pushes media from inlet one to outlet one (left to right), the second group closes and vice versa, but the media goes from inlet two to outlet two

(right to left). Oscillatory flow pattern is created by pushing media forward and backward, the first set of solenoids are turned on for twice as long as the second set to introduce fresh media to the cells. The first set of solenoid valves are open, allowing fluid to flow, for 666 milliseconds and the second set are open for 333 milliseconds. Hence, fluid flows right to left for 666 milliseconds across both media channels then alternately fluid flows left to right for 333 milliseconds.

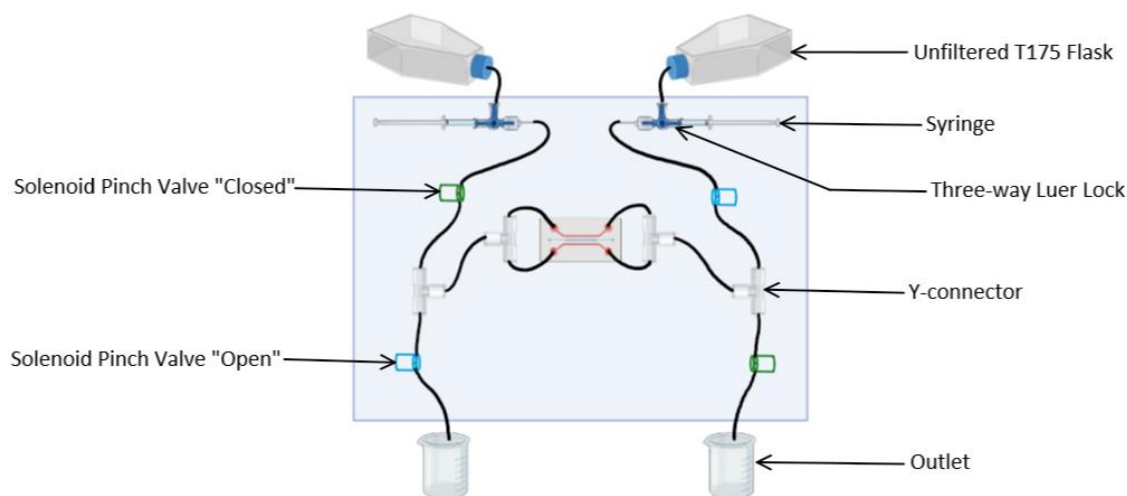


Figure 11: Double Gravity Pump Setup with the labeled components.

By varying the height, tubing size and length the pump is able to produce the desired shear stress (0.2 Pa to 2.0 Pa) on the wall of the microfluidic channel. To minimize variation of flow rates and fit the solenoid valves a tubing of 250 μm was selected. To achieve the shear stress needed in the gel chamber with the height of 250 μm and a width of 500 μm a flow rate of 2.08 $\mu\text{L/s}$. The corresponding calculations are in Appendix D.

3.3.2 Microfluidic Designs

The second component of this fluidic bioreactor is the microfluidic device design. The design was based on previous literature. Four designs were used as the base for ours, including AIM Biotech's 3D Cell Culture Chip (AIM Biotech® DAX-1™) and microfluidic devices from the work of Dr. Dayoung Yoon, Dr. Waleed A. Farahat, Dr. William J. Polacheck and colleagues. The AIM Chip, as well as these other devices, have been proven to contain and confine the gel placed in the gel chamber, pictured below in Figure 12, without gel leaking into the media channel. The four devices we are basing ours off of are depicted in Section 4.4. Aspects of each device were taken to create microfluidic device designs.

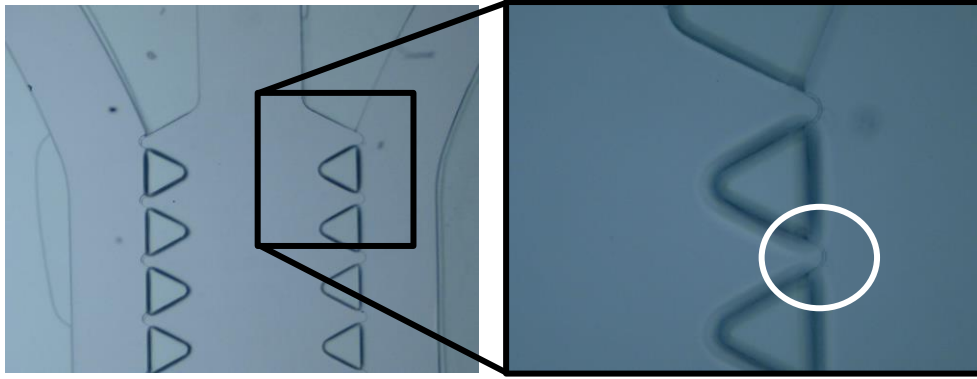


Figure 12: AIM Biotech's 3D Cell Culture Chip with an Acellular 4 mg/mL Fibrin Gel. The meniscus of the gel (circled in white) indicates that the gel has been retained.

Following the creation of the designs, AutoCAD was used to draw the designs in a 2D space. The drawing file created was then used to create a photomask for use during photolithography. In addition to creating this photomask, other manufacturing methods available at WPI were thoroughly explored, to ensure that photolithography would be the best option for manufacturing this device. CAD/Art Services is the company that will be used to print the photomask. Details of the photomask size and resolution will be explained further in a later section.

3.4 Cell Culture

Neonatal human dermal fibroblasts (NHF) from foreskin were seeded and plated at one million cells/mL. These fibroblasts were then passaged weekly, and fed bi-weekly to ensure that the media is changed and is the correct color, and to ensure that the cells do not die. The cells were passaged to ensure confluence would not exceed 80%. Porcine aortic valvular endothelial cells (PAVEC) were seeded and plated at one million cells/mL. These endothelial cells were passaged to ensure confluence would not exceed 80%. The PAVECs were stored in T25 flasks which were coated with 2% gelatin to improve cell attachment. The protocol for seeding cells is found in Appendix I. PAVECs were seeded into the microfluidic devices through the media inlets to examine the migration of these cells from the media channels into the gel matrix.

3.5 EndMT

The device should allow the measurement of cell migration and the tracking of phenotype to analyze the effects of EndMT. Per the experimental procedure, it should allow the imaging, fixing and staining of the cells *in situ*.

3.6 Throughput

The majority of microfluidic devices can contain one gel chamber, which only allows for one trial to run at a time. Increasing throughput is important as it ensures that multiple trials can

be completed at the same time. Increasing the number of chambers that hold the cells is critical as it allows for a greater representation of the cells under investigation, which will generate more trials and data during the specific time frame. In addition, increasing the number of microfluidic devices connected to the gravity pump can increase throughput.

3.7 Ease of Use

Ease of use is in regard to how easy the whole device can be used by somebody trained in the laboratory techniques required to study fluid flow on cells. This criteria is important for this project, as the device uses a combination of an Arduino Uno microprocessor, gravity pump, and positive polydimethylsiloxane (PDMS) microfluidic. All of these components must not inhibit the client's ability to complete their experiment, however, the bioreactor needs to function prior to optimizing the ease of use.

3.8 Revised Client Statement

The goal of this project is to design a device that can observe the effects of shear stress, through different magnitudes of steady and oscillatory flow, on endothelial cells. The device must produce a wall shear stress of 0.2 Pa and 2.0 Pa in order to mimic the blood flow of the heart. In addition, the device needs a pump system that can produce 60-72 oscillations per minute, which is consistent with an average resting heart rate of 60 beats per minute. Ideally, the device would be easy to manufacture, use, and inexpensive. The user should be able to easily place the gel, decellularize *in situ*, and seed cells in media channels. This device should allow for fixing, staining, and imaging cells to measure invasion into the gel matrix and phenotype. The device would also be compact, contained within a standard incubator, and able to prevent the evaporation of media.

3.9 Engineering Standards

Engineering standards are an essential component in research, design, and engineering as they provide best practices and safety measures to ensure the maximum benefit for the patients using these products. For this project, there are several standards that represent a guideline in which the product will follow to ensure the utmost quality and safety to the patient. One important standard that is important in relation to the microfluidic portion of this project is ISO 22916: 2022 - microfluidic devices. This standard explains the specific requirements for microfluidic devices to ensure a facile incorporation with microfluidic components such as sensors, actuators, and connectors. Another standard that is relevant to this project is IWA 23: 2016- Interoperability of microfluidic devices: provides specific dimensions in terms of geometry for pitch connectors in microfluidic devices and provides the designer with rules for an initial device classification. Another important standard is F2739:19- Standard Guide for Quantifying Cell Viability and related attributes within Biomaterial Scaffolds. This standard is relevant to the project as it provides the requirements for quantifying cell viability within

biomaterial scaffolds which is important because cell viability is an essential aspect for determining the in vivo product performance of biomaterial constructs.

4. Alternative Designs and Proof of Concepts

4.1 Needs and Wants

To achieve the goal of the project, the microfluidic device and pump must meet the constraints and functions set forth in the objectives and parameters section. After these constraints and functions are met, to optimize and for ease-of-use additional design changes can be made. The combination of the needs and wants of the device would be the ideal system.

The microfluidic device must meet the following functions: contain multiple replicates, prevent evaporation, be able to contain the gel in the central chamber, allow for in situ decellularization, and fix and stain *in situ*. These functions must be able to occur under these constraints: minimum of eight samples concurrent at two levels, minimum of 200 μm high and 100 μm wide location for cell attachment, used by one person, measure depth of infiltration, inlet channel minimum of 500 μm wide, sterile and inexpensive. The pump needs to meet the following functions: produce shear stress, produce steady and oscillatory flow, fit within the incubator, and produce accurate shear stresses. It needs to function under these constraints: produce shear stress of 0.2 and 2.0 Pa, +/- stated parameter values, be sterile, and be no taller than the inside of a standard incubator (26 inches).

After all of these constraints and functions are met the system should achieve additional design constraints. The microfluidic device needs to be inexpensively made using PDMS with accurate replication. The height of the device should be 200 μm tall. The mold should be manufactured using soft lithography. The pump should fit in the incubator taking up no more than one shelf. It should also be powered by a DC power supply that can be plugged into an outlet rather than a battery.

4.2 Manufacturing Alternatives

One of the key pieces for designing these microfluidic devices is through examining different manufacturing methods that could be used to manufacture the negative, or mold, that the device is made off of. We spoke with multiple staff, graduate students, and faculty to determine the resolution and feasibility of using 3D printing, Nano printing, and Milling to manufacture this mold.

3D printing is a state-of-the-art additive manufacturing method used in many different industries. The 3D printers available to us at WPI include the Formlabs Form Two and Markforged Mark Two, both at the PracticePoint facility at 50 Prescott St, Worcester, MA, 01609. The resolution of the 3D printers are as follows, 500 μm and 250 μm . After looking at the specifications of these devices, particularly the resolution of them, we decided that the 3D printers available could not feasibly be used to manufacture the negative. Following this, Nano printing was the next best option for additive manufacturing.

Nano printing is additive manufacturing at a nano-level. This is used for devices that require a size and resolution much smaller than a typical 3D printer, like the Formlabs Form Two, can provide. This is available in the Lab for Education and Application Prototypes (LEAP). The resolution of this printer on the X-Y plane is 400 to 500 nm, and the minimum feature size that can be manufactured is 160 to 200 nm. This printer fits the specifications necessary, but the costs of manufacturing are beyond our budget, so this method was ruled out. Following the additive manufacturing, we looked into two different subtractive methods, milling and photolithography.

Milling is a common subtractive manufacturing method used for many different applications, including medical robotics. At PracticePoint, they have a HAAS CM-1 milling machine, which can use a variety of end mills. Speaking with Dr. Chris Nycz, a professor at WPI, indicated that the milling machine could fabricate features as small as 250 μm with a 0.1 mm end mill. This was determined to be too large of a resolution for the device specifications, leading to the manufacturing method being ruled out. Of all manufacturing methods listed above, nano printing had the best resolution, but due to the expense associated with it, photolithography was chosen.

4.3 Manufacturing Methodology

4.3.1 Photomask Design

The microfluidic designs were created individually using AutoCAD. The designs are shown in Section G, and complete engineering drawings are in Appendix L. All nine designs were labeled and added into a photomask template, with a guide and target height of 200 μm at the top of the mask. After ensuring the mask followed guidelines for printing, the mask was sent to Artnet. Pro. Inc for printing.

4.3.2 Photolithography

Photolithography is the process by which a multitude of molds for microfluidic devices are manufactured, including those from the Kamm Laboratory at Massachusetts Institute of Technology. Photolithography is completed in three different steps, spinning an epoxy-based photoresist to a desired height, which, in our case, was SU-8, aligning and exposing the photomask to UV light, and developing the pattern on a silicon wafer master. The resolution of the mask aligner available to us, the UV-KUB, is one micron (μm). A diagram of the master fabrication process is shown below in Figure 13. This creates the master mold by which PDMS replicas are created using soft lithography.

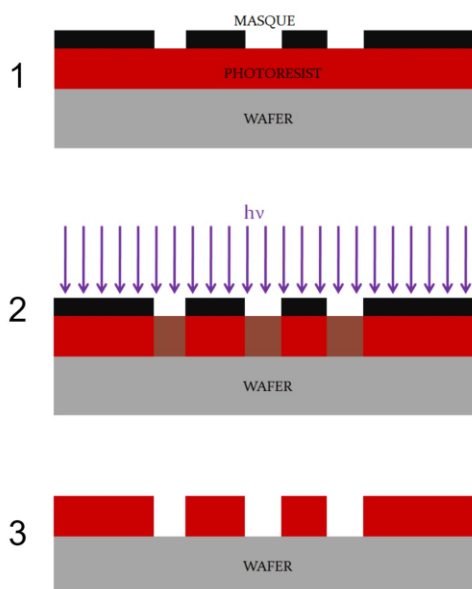


Figure 13: Wafer Creation using Photolithography. "[Photolithographie 1](#)," "[Photolithographie 2 - exposition](#)," and "[Photolithographie 3 - après développement](#)" by [Rhadamante](#) is licensed under [CC BY-SA 3.0](#).

4.3.3 Soft Lithography and Plasma Bonding

The negative mold can be used several times to make single-use microfluidic chips. The wafer is placed inside a petri dish and PDMS is poured over the mold to create the devices, the full protocol is outlined in Appendix J. The first use of the mold 100-120 g of PDMS is used and the subsequent times use about half the initial amount. Once the PDMS has been degassed, poured, and cured in the oven overnight, the microfluidic devices are cut out. Using a straight edge surgical knife, straight edge razor, and a dermal punch the microfluidic chips are cut into their individual devices. After the microfluidics are cut, they are prepared to be plasma bonded to a glass cover slip. The microfluidic chips are cleaned with 70% ethanol and sprayed dry with compressed air. The coverslips are cleaned with soap and water and sprayed dry with compressed air. The coverslip and the PDMS are adhered to one another through a process known as plasma bonding, which changes the surface properties of an item to enhance its adhesion properties. Once the coverslip and microfluidic device are plasma bonded, they are pressed together with the design-side of the microfluidic device to the coverslip.

4.4 Previous Designs in Literature

There are four devices on the market or in literature that our designs are based off of. AIM Biotech and the Kamm Lab have created different microfluidic devices that can successfully contain a gel within their respective center, gel chamber. This is a key parameter that our device needs to accomplish to achieve our goal, therefore we based our designs on these devices. An AutoCAD drawing of each base design is in Figure 14, below.

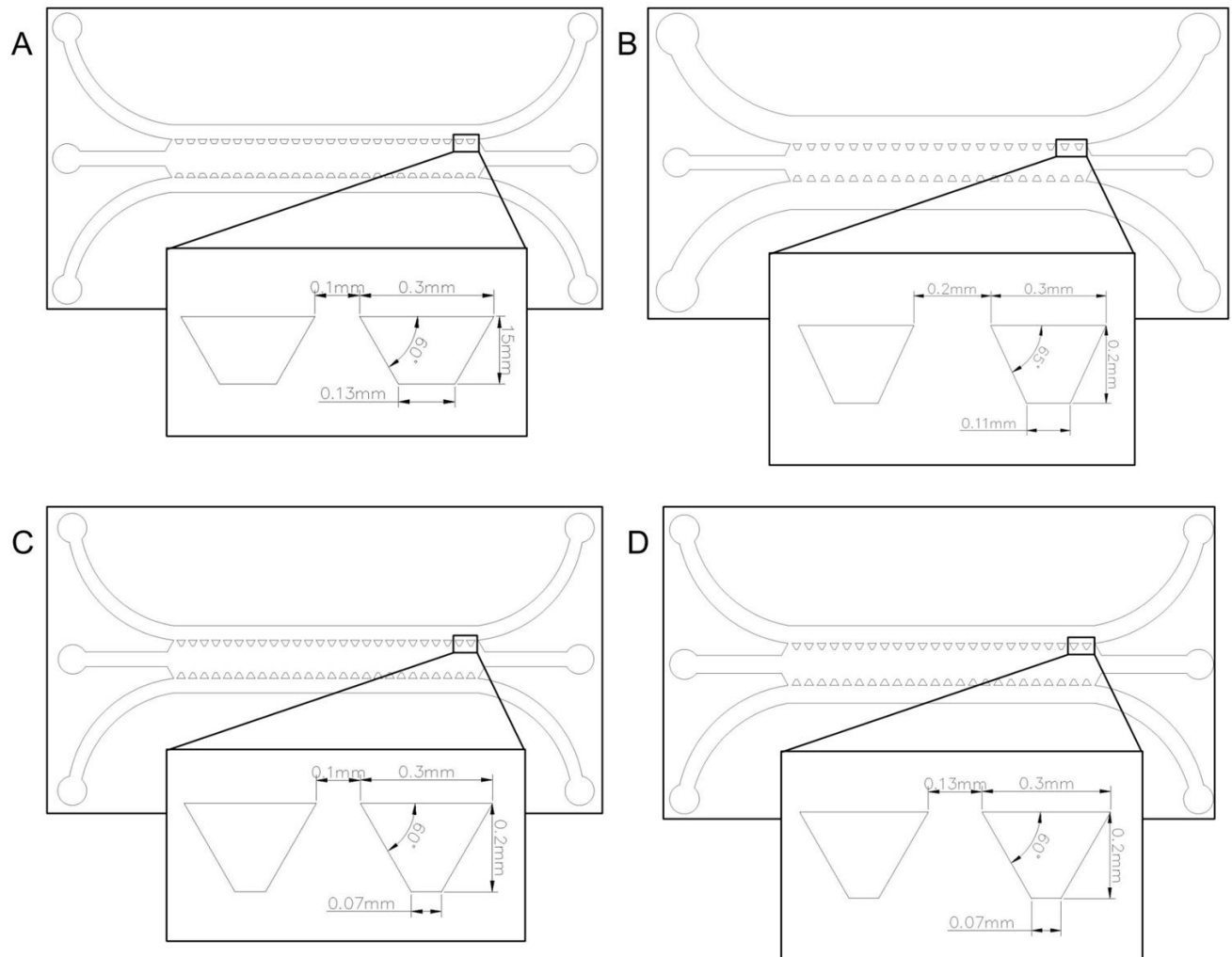


Figure 14: Base Designs for Microfluidic Chips. A) AIM Chip; B) Yoon; C) Farahat; D) Polacheck

AIM Biotech is a company that focuses on creating devices to further research of medicine (AIM Biotech, 2022). The AIM Biotech idenTx 3D Cell Culture Chip (AIM Chip) product is a plastic microfluidic device, containing two media channels and a central gel chamber, shown above in Figure 14A. This device has been used by our lab to study the effects of fluid flow on cells that have repopulated a piece of decellularized TEHV. Previously, this same device has been used to study the effects of fluid flow on cells, particularly on extravasation and invasion of tumor cells (Hajal et al., 2020). This study successfully used the AIM Chip to create a 3D *in vitro* platform for studying extravasation and tissue invasion of tumor cells, and although it does not mimic exactly this project's aim, it provides a baseline for the project to build off of. In addition to this study, there has been success with containing fibrinogen gel in the AIM Chip gel chamber. For the success of our project, the microfluidic devices need to contain the gel within the gel chamber to act as a TEHV scaffold. To accomplish this, we modeled designs based off of the AIM Chip dimensions using AutoCAD, which was then printed to create the photomask. This photomask was then used in photolithography to

create a mold of the device. This will create a device that is made from PDMS instead of plastic, as well as allow us to replicate the device for multiple experiments.

Dr. Yoon, Dr. Farahat, and Dr. Polacheck authored papers that examine the effects of fluid flow, with different applications, on cellular response at the Kamm Laboratory. Dr. Yoon's 2016 study on the effects of a chemical gradient on the migration of human bone-marrow derived stem cells uses a microfluidic device that is similar to the AIM Chip, containing two media channels and a gel chamber (Yoon et al., 2016). This device is depicted in Figure 14B, along with the others. Dr. Farahat's 2012 study on the angiogenic growth of endothelial cells due to vascular endothelial growth factor (VEGF) and sphingosine-1-phosphate (S1P) gradients (Farahat et al., 2012). Similar to the AIM Chip, it contains two media channels and a gel chamber, shown in Figure 14C. This device was able to successfully contain the gel, with the dimensions of trapezoidal posts, particularly the angle of the post, established through determining the contact angle of the gel being used. This contact angle was determined, and subsequently subtracted from 180° (Farahat et al., 2012). The theory behind this experiment was that the contact angle of the gel would inform how the gel was contained within the chamber, thus the posts were designed with a 60° angle. Finally, much of our work is based on Dr. Polacheck's work with microfluidic devices. We had decided to move forward with a design from Dr. Polacheck's work in a 2014 study on the effects of fluid stress on cell migration (Polacheck et al., 2014). This microfluidic device has similarities to the others mentioned above; it contains two media channels and a gel chamber, shown in Figure 14D. Much of our work is based on previous research due to their effectiveness in keeping the gel contained to the gel chamber. The hope is that emulating previous work will provide us with a baseline to solve the main issue with the microfluidic designs containing the fibrinogen gel.

4.5 Contact Angle Study

One of the initial experiments we completed was a contact angle study because Dr. Farahat and colleagues indicated that contact angle is a critical parameter in the design of the posts for retention of the gel by surface tension (Farahat et al., 2012). Contact angle forms between a liquid and a surface, which is determined by its surface tension. In work done by Farahat and colleagues, they utilized the contact angle of the gel to inform the angle of the posts within the gel chamber (Farahat et al., 2012). The idea behind this was that the contact angle would aid in determining the optimal angle of the trapezoidal posts. This was something we felt was important to explore. Diving deeper into literature, a study done by Dr. Carlos P. Huang and colleagues aided in our understanding of this phenomenon (Huang et al., 2009). Dr. Huang, in a study in 2009, explored differences in the effectiveness of posts in gel retention when modifying the gel composition, thereby modifying the contact angle, spacing between the posts, and hydrophobicity/hydrophilicity of a material. This study concluded that all three aspects were important in gel retention, and increasing contact angles, in particular, supported their hypothesis that hydrophobicity aids in gel retention (Huang et al., 2009). With this in mind, we decided to

determine the contact angle of the gel, with the hope that the angle will aid in maintaining gel retention in the chamber.

The protocol used is in Appendix A, and further calculations and experimental values can be found in Appendix B. This study utilized two sets of contact angles, one taken prior to incubation and one taken post incubation. This was to determine whether there was a significant difference between the two gel conditions. The contact angles were measured on two control conditions and one experimental condition. The two controls were on the inside of a petri dish and a coverslip, and the experimental condition was on a PDMS device. The PDMS device was meant to give an approximate contact angle of the gel on the microfluidic device. The contact angle on PDMS before incubation was $106^\circ \pm 3^\circ$. This was then subtracted by 180° to determine the optimal angle of the posts, which was $74^\circ \pm 3^\circ$. This angle was used in one of the microfluidic designs to compare gel retention with this (experimental) angle, 75° , to the AIM Chip (control) angle, 60° . This was done in addition to modifying the space between the posts and other dimensions in the microfluidic device.

4.6 Alternative Devices

To meet the needs of the project, multiple different designs were created based on prior research and outside experiments previously discussed. All the initial designs have two rectangular cell media channels with one gel chamber in between them. The size of the gel chamber ranges from 900-1000 μm wide to allow the cells to migrate through the gel. Each channel has a circular inlet and outlet to allow easy injection of the gel and entrance/exit of fluid to create a controlled flow. There are two rows of trapezoidal posts that run along the edge of the gel chamber, with the larger base on the side of the cell media channels and the smaller base on the inside of the gel chamber. These posts use surface tension to help hold the gel in the chamber without spreading into the flow channels. Each design has different sized trapezoidal posts and spacing between them. The range of spacing is 100-200 μm . This was to understand the maximized space between posts to allow the most cell migration without breaking the surface tension of the gel. In addition to the spacing between posts, the angle between posts was modified based on values found from the studies from the Kamm lab, as well as the contact angle study done.

4.6.1 Design One: AIM Wider Spacing (150 μm)

Our first design is based on the AIM Chip (AIM Biotech, 2022). The design consists of two media channels 500 μm wide, and an internal gel chamber that is 1300 μm wide from the bases of the trapezoidal posts. The spacing between the trapezoidal posts is 150 μm . This is larger than the original AIM chip, which is 100 μm in order to increase the migration of cells into the gel chamber.

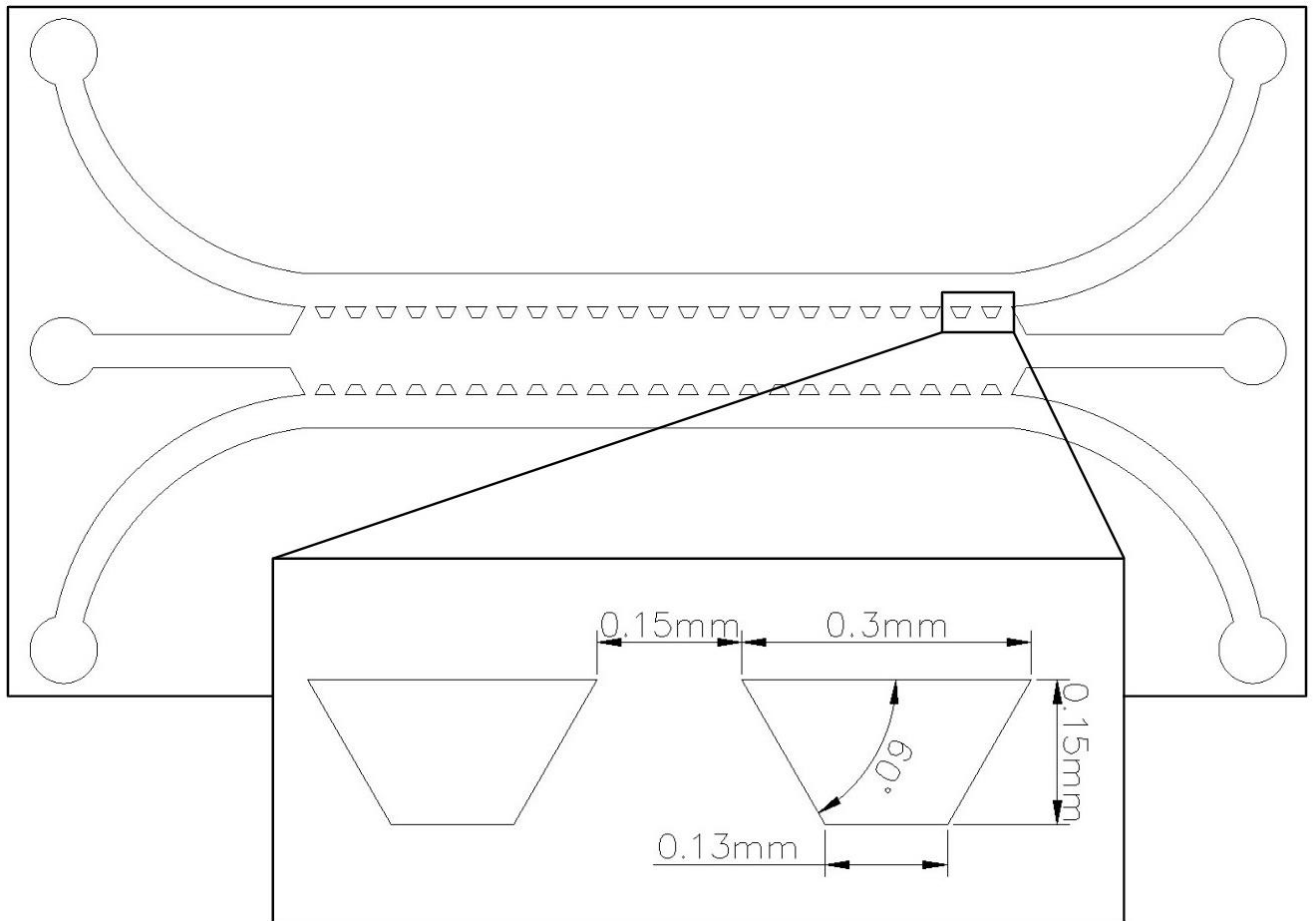


Figure 15. AutoCAD Design One. The length of the gel chamber is 10.50 mm long and 1300 μm wide. Each inlet and outlet are one mm in diameter to fit a standard pipette tip.

4.6.2 Design Two: AIM Larger Post Angle

Design two is also based on the AIM chip, however due to our results in our contact angle experiment, the angle of the trapezoidal posts was changed to 75° instead of 60° (AIM Biotech, 2022). This will improve the surface tension of the gel with the posts to keep the gel from flowing into the media channels. The trapezoidal posts are spaced apart $100\ \mu\text{m}$ as a control to see if the angle of the trapezoids improves the surface tension of the gel as we hypothesized.

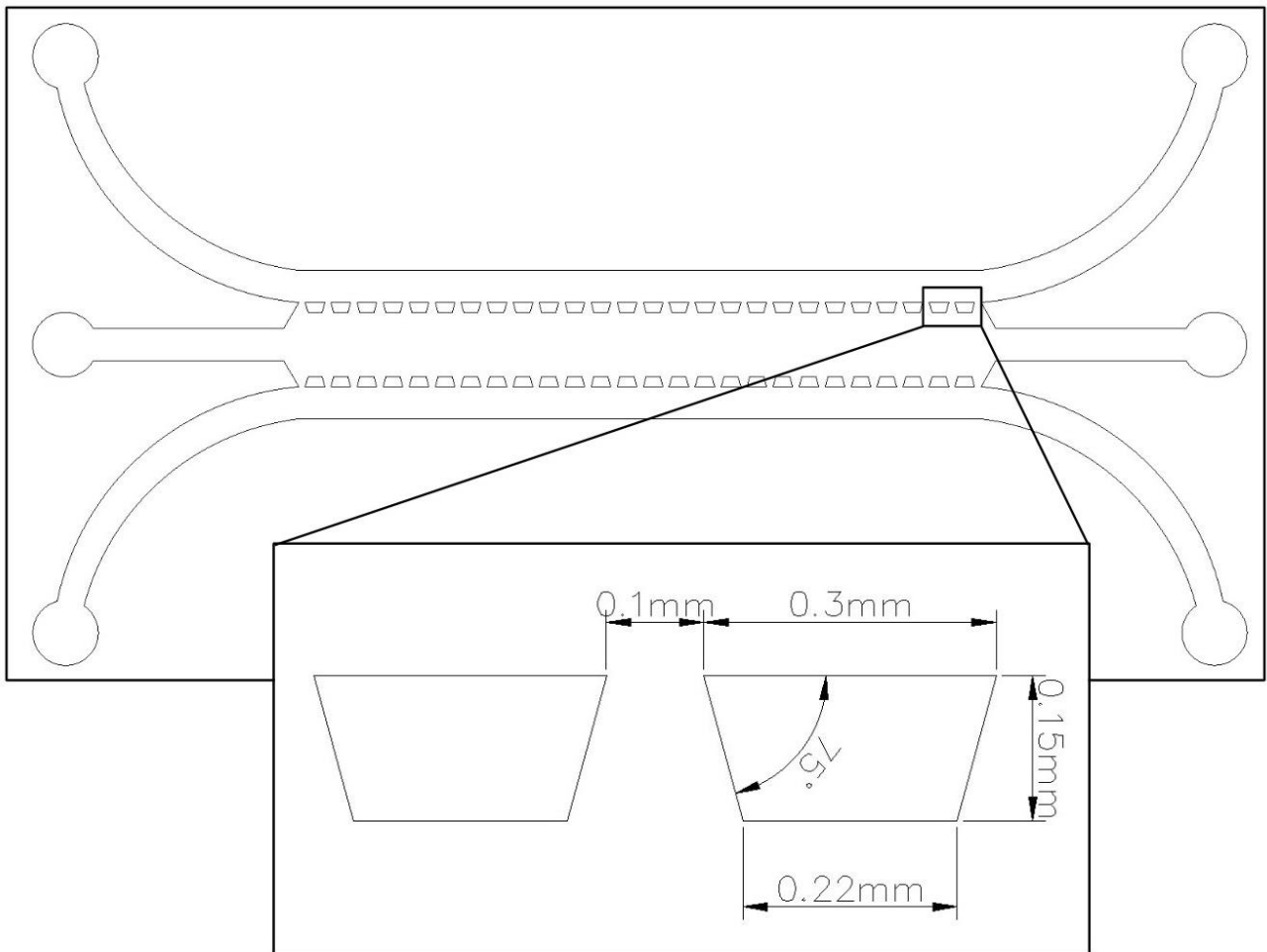


Figure 16. AutoCAD Design Two. The dimensions of the gel chamber are 10.50 mm long and $1300\ \mu\text{m}$ wide. Each inlet and outlet are one mm in diameter to fit a standard pipette tip.

4.6.3 Design Three: AIM Internal Posts

The next design is also based on the AIM chip (AIM Biotech, 2022). All dimensions are consistent to the AIM chip; however, a row of internal posts was added to the center of the gel chamber. The internal posts are each $200\ \mu\text{m}$ by $200\ \mu\text{m}$ spaced apart so that each internal post sits in between two trapezoidal posts along the edge of the gel chamber. The internal posts allow for more support to contain the gel.

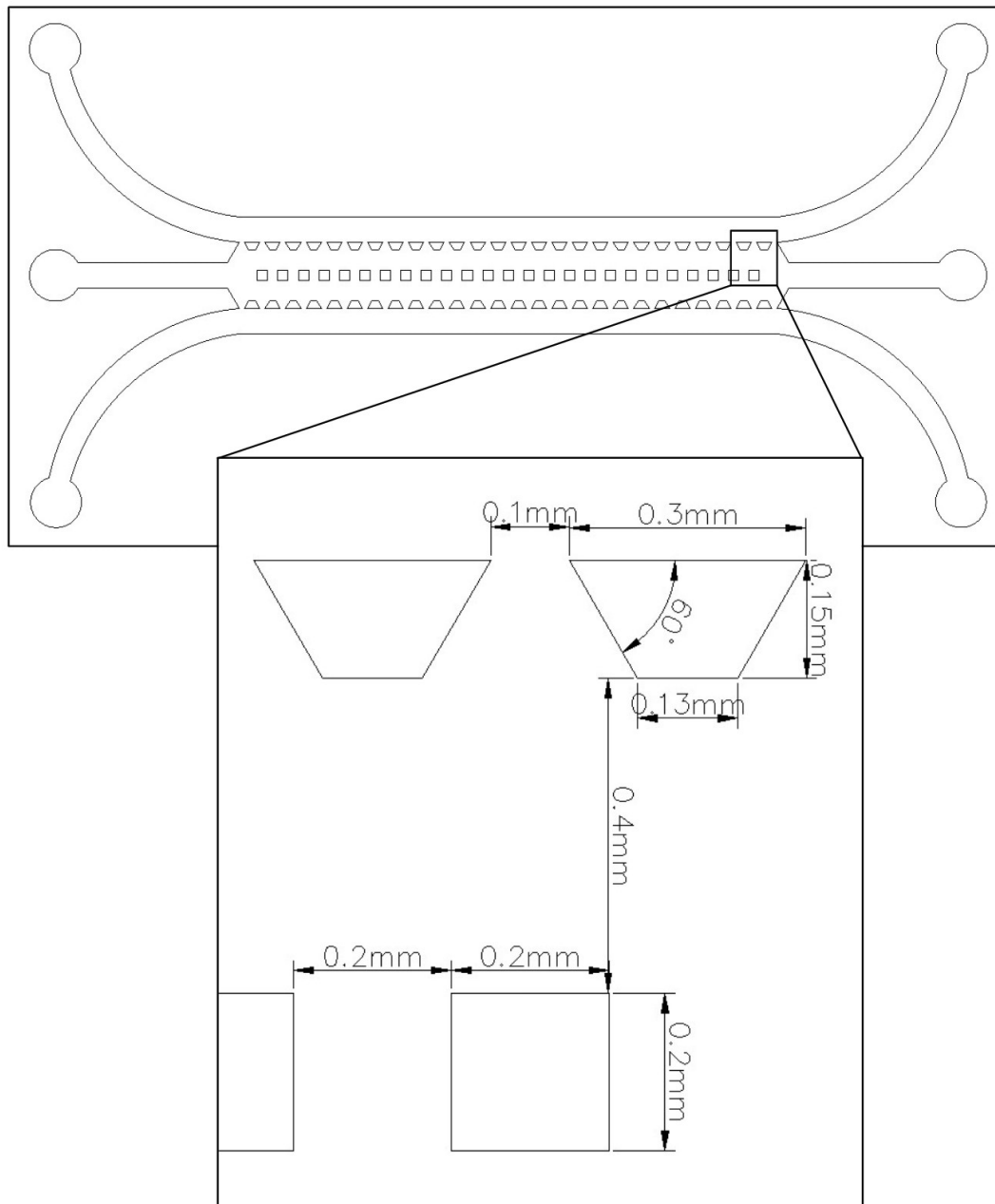


Figure 17. AutoCAD Design Three. The length of the gel chamber is 10.50 mm long and $1300\ \mu\text{m}$ wide. Each inlet and outlet are one mm in diameter to fit a standard pipette tip. Square internal posts, $200\ \mu\text{m}$ by $200\ \mu\text{m}$, run along the center of the gel chamber.

4.6.4 Design Four: AIM Wider Spacing (200 μm)

Design four is based on the AIM Chip, with all the same dimensions except for the spacing between the trapezoidal posts (AIM Biotech, 2022). This is similar to the idea of Design One, however the spacing between posts is 200 μm , instead of 150 μm . We decided to design two different AIM Chips with larger spacing to observe if the gel can be contained at the larger spacing. It is ideal for the gel to remain contained at the larger spacing because it will help maximize cell migration into the gel matrix.

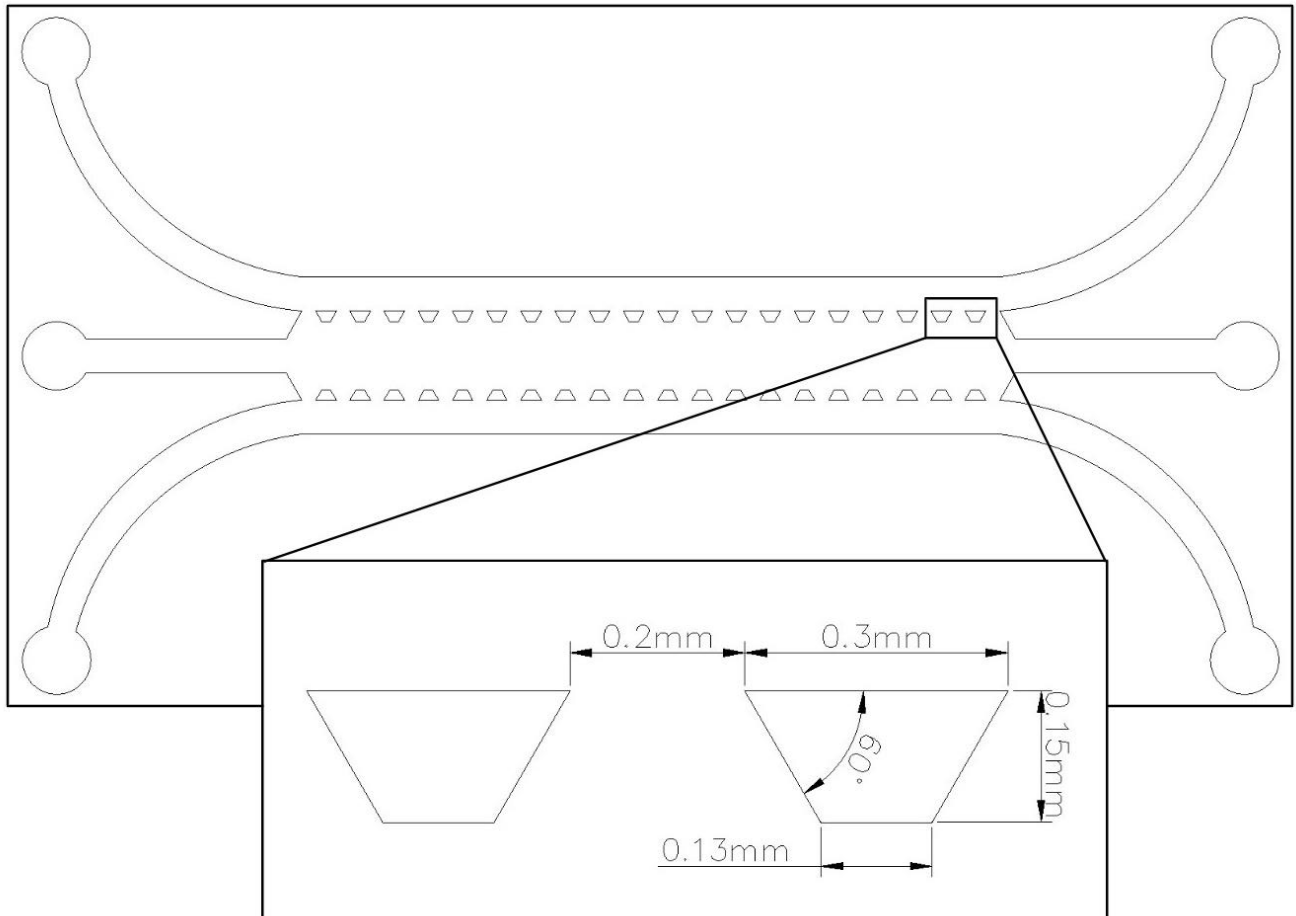


Figure 18. AutoCAD Design Four. The length of the gel chamber is 10.50 mm long and 1300 μm wide. Each inlet and outlet are one mm in diameter to fit a standard pipette tip. The spacing between the posts is 200 μm .

4.6.5 Design Five: Farahat

Our fifth design is an exact copy of the Kamm Lab's work from 2012 (Farahat et al., 2012). The design has a gel chamber of 10.50 mm long and 1.3 mm wide, same as the previous designs. There are trapezoidal posts along the edge of the gel chamber with an internal angle of 60° . However, the trapezoidal posts are $300\ \mu\text{m}$ at the base and $200\ \mu\text{m}$ tall (from the base to the top of the trapezoid), which is larger than the AIM Chip. The space between the posts is $125\ \mu\text{m}$, which is slightly larger than the original AIM Chip. The larger posts help contain the gel within the gel chamber due to more surface area for the gel to attach, increasing surface tension.

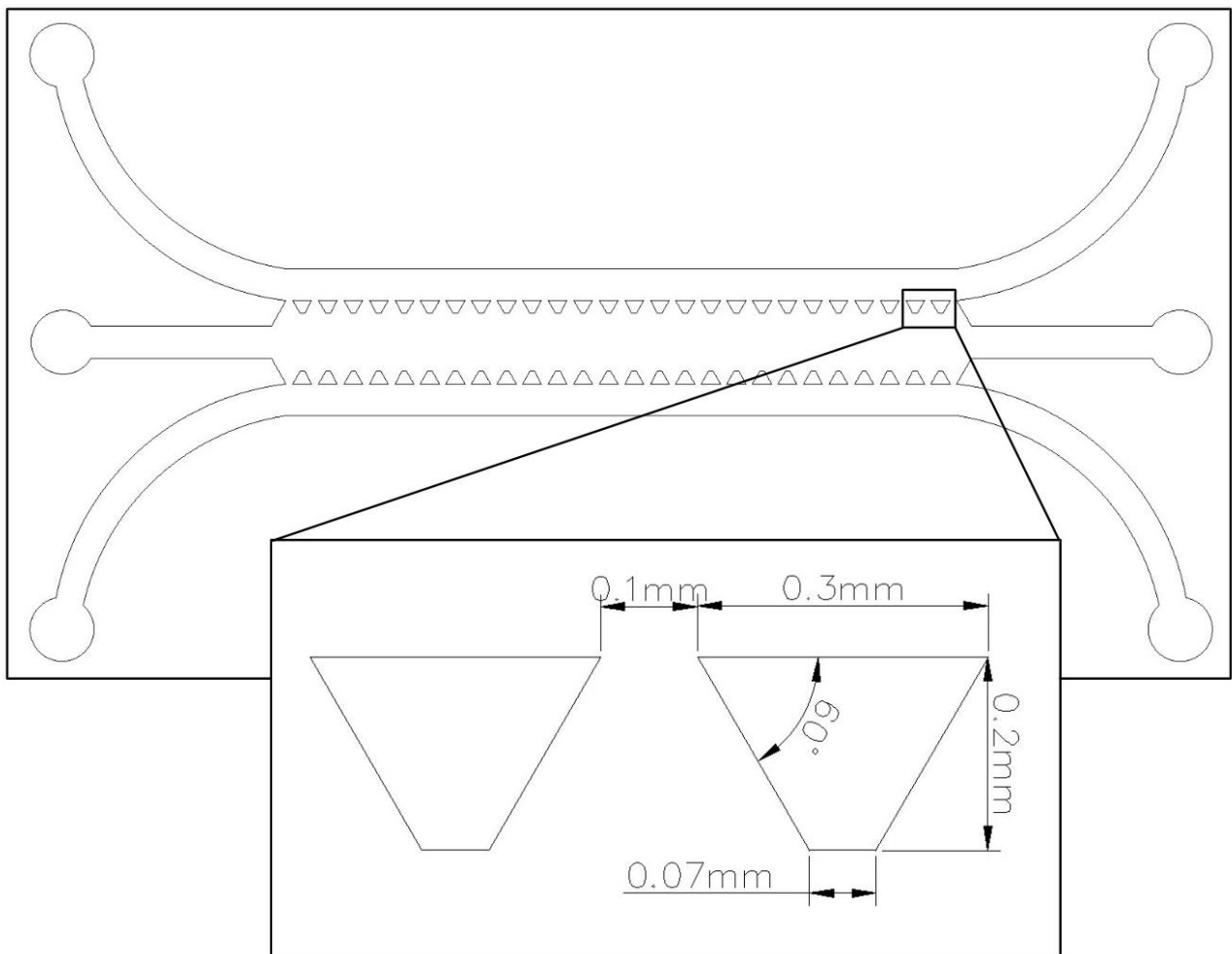


Figure 19. AutoCAD Design Five. Media channels are $500\ \mu\text{m}$ wide with inlets and outlets of one mm to fit a standard pipette tip. Trapezoidal posts equally spaced $125\ \mu\text{m}$ apart along the edge of the gel chamber.

4.6.6 Design Six: Yoon

Design Six is based on the Kamm Lab's work from 2016 (Yoon et al., 2016). The design contains two media channels that are one mm wide with a gel chamber of 1.3 mm wide in between them. The trapezoidal posts have the same dimensions as Design Five but are spaced 200 μm apart and have an internal angle of 65°. This is larger than Design Five to allow more cell migration into the gel chamber. The change in angle helps increase surface tension of the gel also.

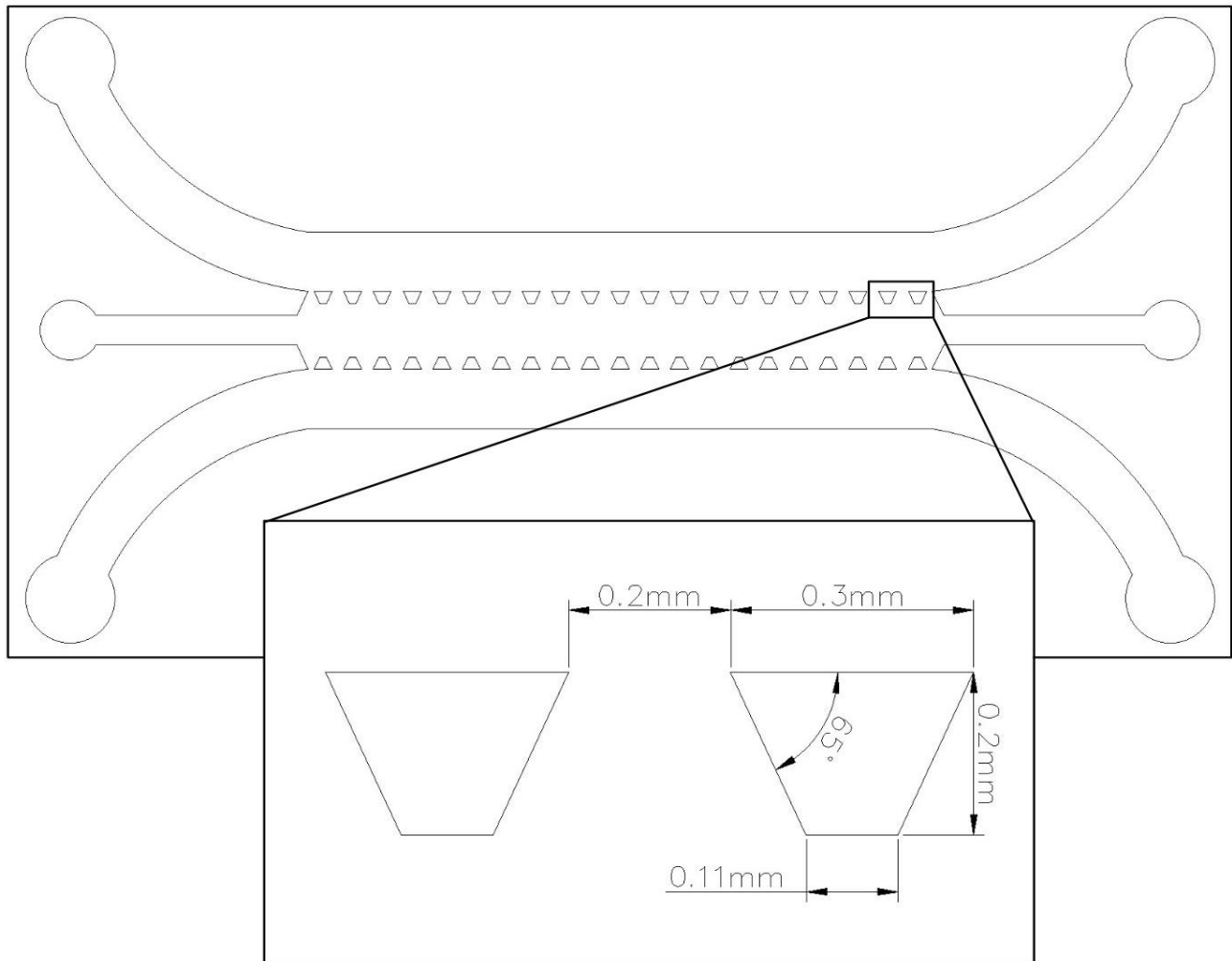


Figure 20. AutoCAD Design Six. Media channels are 1000 μm wide with inlets and outlets of 1500 μm . The central channel into the gel chamber is 500 μm with inlets of 1000 μm . Trapezoidal posts are equally spaced 200 μm apart along the edge of the gel chamber.

4.6.7 Design Seven: Yoon Smaller Spacing

The next design is based on the Kamm Lab's work from 2016 as well (Yoon et al., 2016). The design is the same as Design Six, however the spacing between the posts is $100\ \mu\text{m}$. This is to test how well the gel is contained in the gel chamber with a smaller gap between posts.

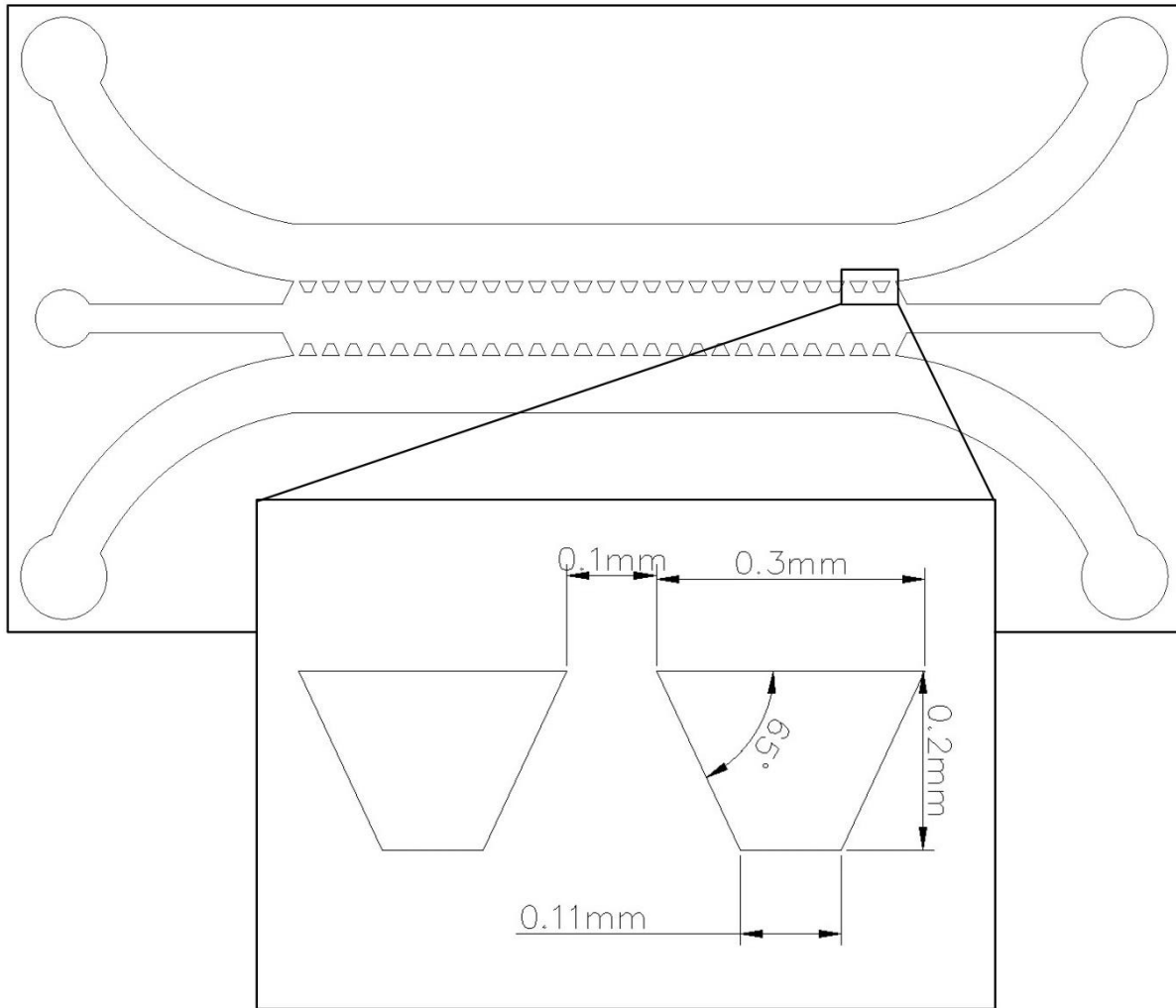


Figure 21. AutoCAD Design Seven. Media channels are $1000\ \mu\text{m}$ wide with inlets and outlets of $1500\ \mu\text{m}$. The central channel into the gel chamber is $500\ \mu\text{m}$ with inlets of $1000\ \mu\text{m}$. Trapezoidal posts are equally spaced $100\ \mu\text{m}$ apart along the edge of the gel chamber.

4.6.8 Design Eight: Polacheck

Our eighth design is an exact copy of the Kamm Lab's work from 2014 (Polcheck et al., 2014). The design has a gel chamber of 10.50 mm long and 1.4 mm wide, which is slightly larger than the previous designs. This allows more space to observe cell migration into the gel. There are trapezoidal posts along the edge of the gel chamber with an internal angle of 60° . However, the trapezoidal posts are 300 μm at the base and 200 μm tall, similar to the other designs from the Kamm Lab. The space between the posts is 125 μm .

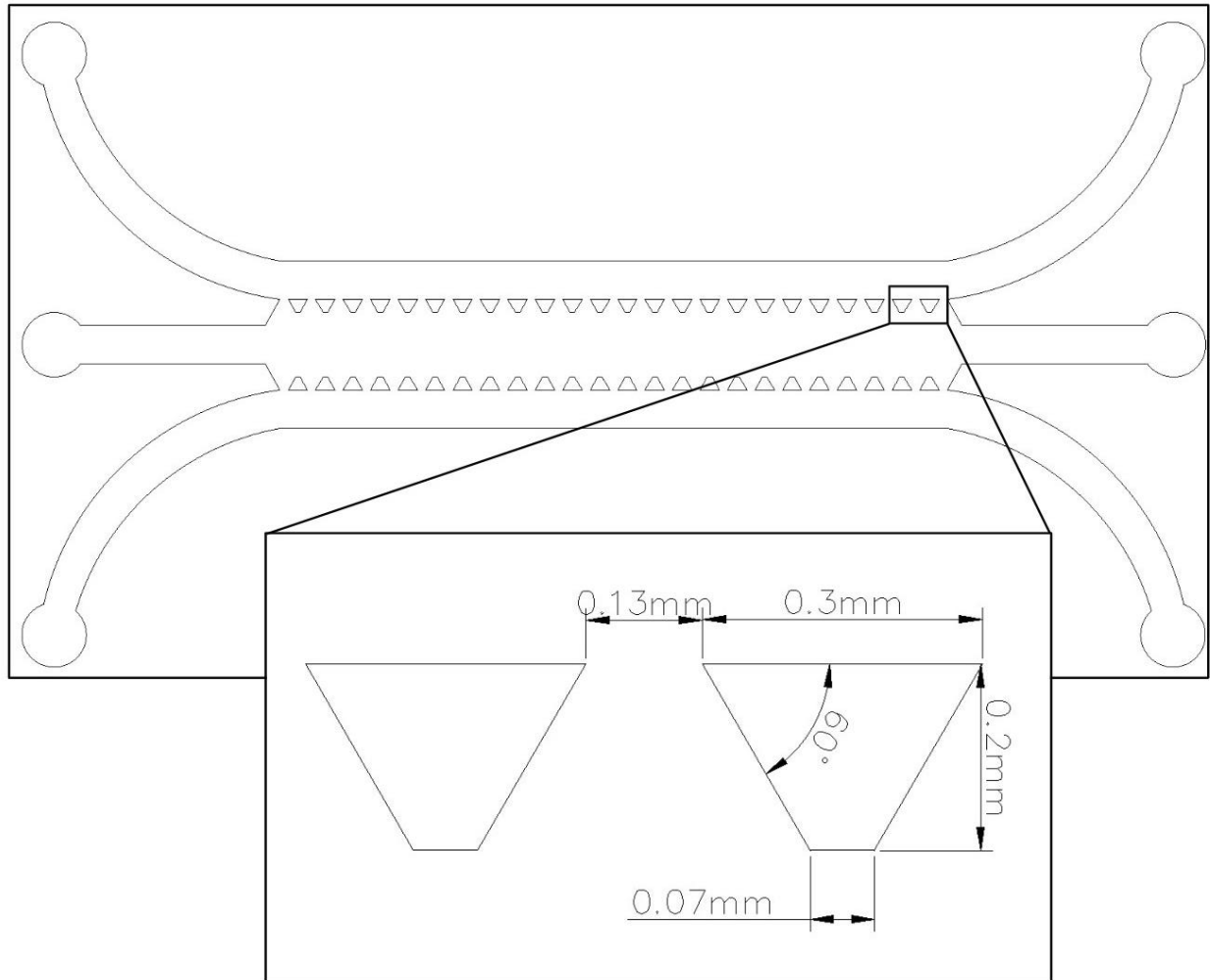


Figure 22. AutoCAD Design Eight. Media channels are 600 μm wide and a gel chamber of 1.4 mm wide with inlet and outlets of one mm to fit a standard pipette tip. Trapezoidal posts equally spaced 125 μm apart along the edge of the gel chamber.

4.6.9 Design Nine: AIM

Our last design is the exact copy of the AIM Chip (AIM Biotech, 2022). The design consists of two media channels 500 μm wide, and an internal gel chamber that is 1300 μm wide from the bases of the trapezoidal posts. The spacing between the trapezoidal posts is 100 μm . The trapezoidal posts are 300 μm at the base and 150 μm tall. The angle of the trapezoid edge is 60°. Since the AIM Chip is successful at containing the gel, by using the design in AutoCAD, a PDMS mold can be used and still hold the gel in place.

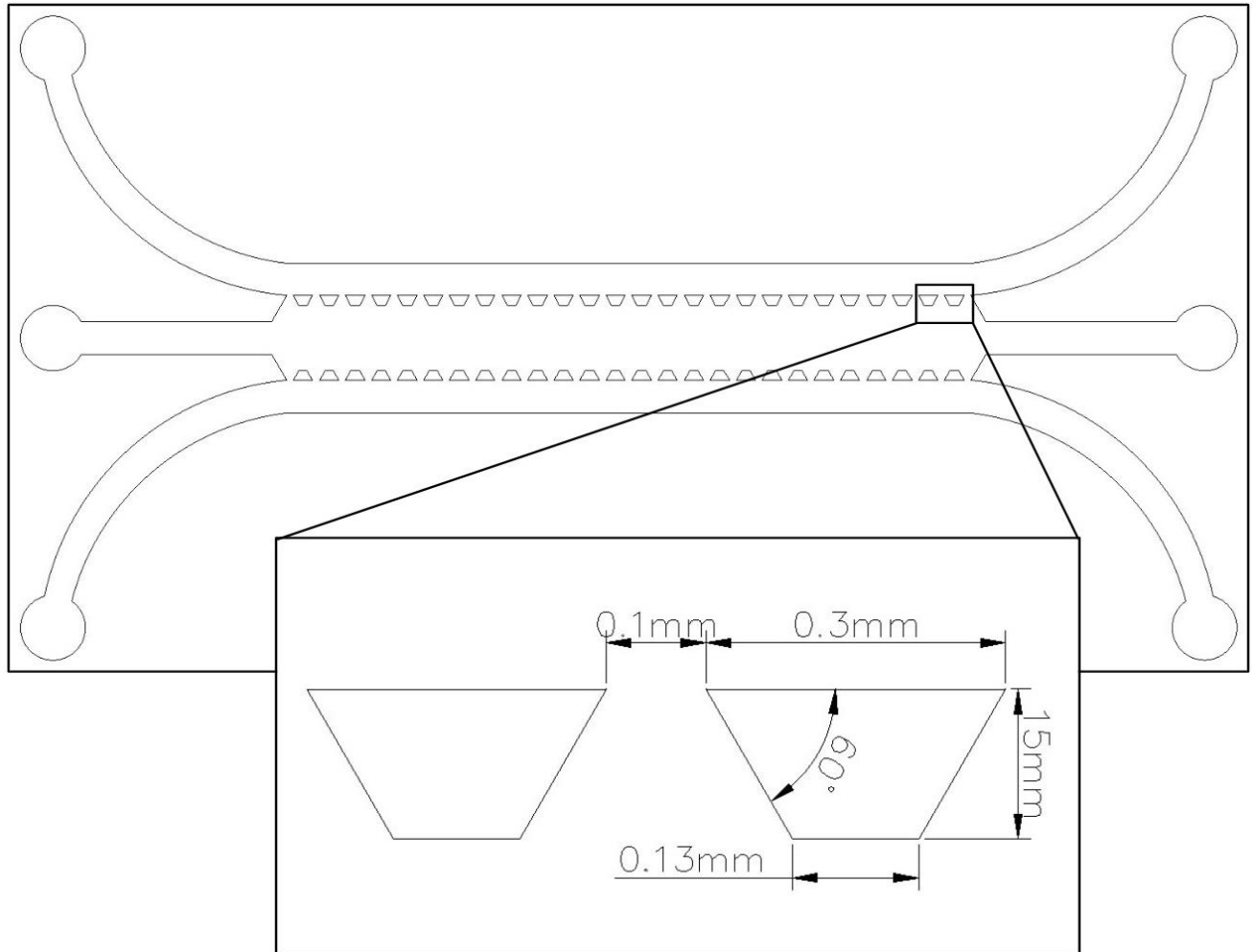


Figure 23. AutoCAD Design Nine. The length of the gel chamber is 10.50 mm long and 1300 μm wide. Each inlet and outlet are one mm in diameter to fit a standard pipette tip. The spacing between posts is 100 μm .

4.7 Final Photomask

The photomask created has nine different designs on it, as mentioned in our previous sections. A screenshot of the photomask is in Figure 24, below. This mask has four base designs that are replicas of designs from the Kamm lab. Designs five, six, eight, and nine are replicas,

and the others are built off of those replicas. Designs one, four, and seven were modified to increase or decrease the spacing between the posts, depending on the design it is based off. This was to test whether there was a difference in gel retention with devices with larger and smaller spacing. The goal of this test is to maximize the spacing between the posts. The other two designs, both based on the AIM Chip, were testing whether internal posts or a different trapezoidal post angle would affect gel retention. This photomask was sent to Artnet. Pro. Inc for printing.

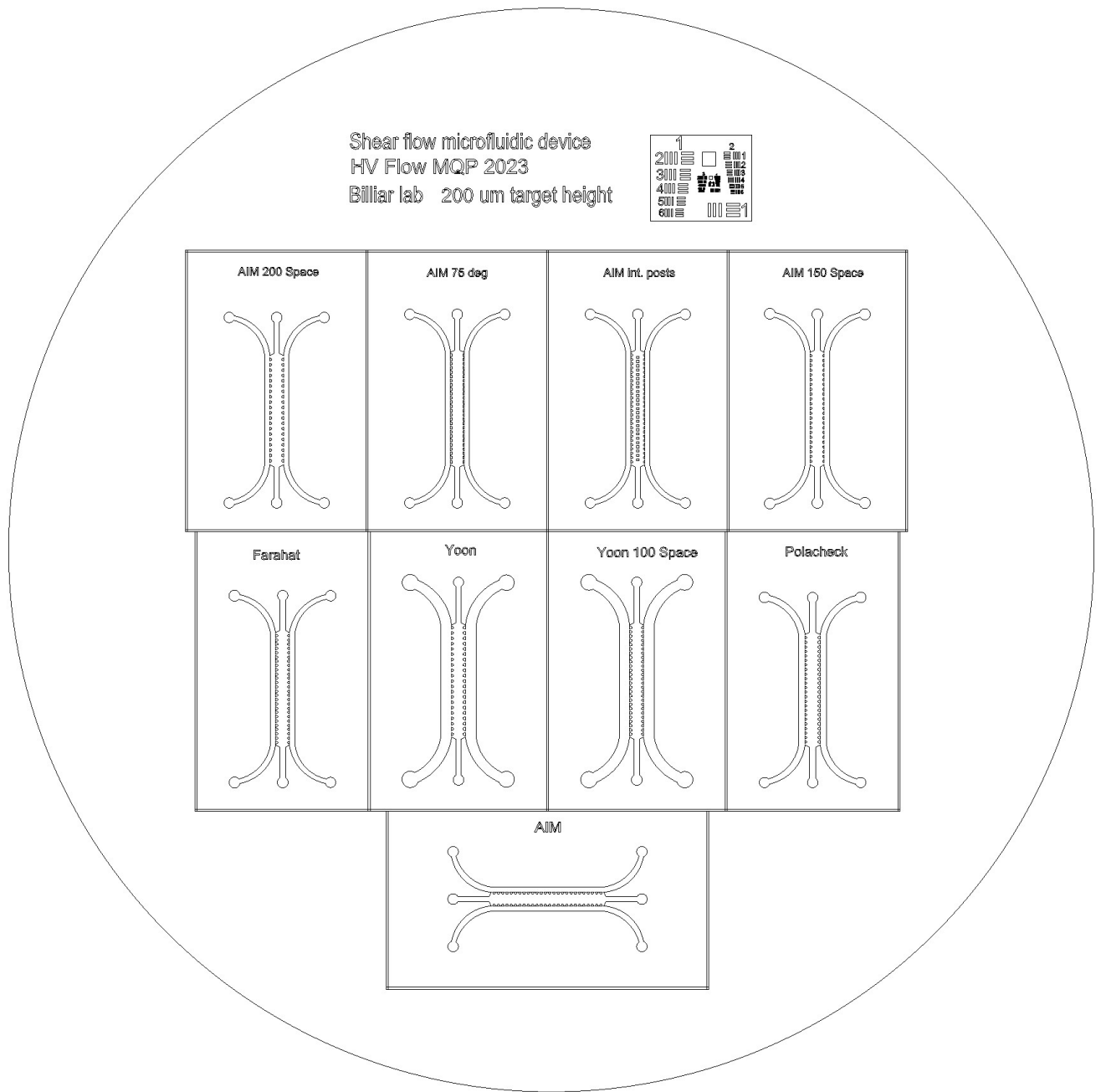


Figure 24: Photomask of Designs for Photolithography

4.8 Manufacturing Results

4.8.1 Fabrication of Devices

Microfluidic Devices were fabricated using a 100 μm and 200 μm silicon wafer. These devices were imaged before gel insertion to ensure the fabrication process was successful. Successful fabrication is shown with the posts being clearly developed and no fabrication issues occurred; for example, debonding which occurs when the microfluidic device becomes detached from the glass coverslip. The correct development of the posts are essential as this aids in full gel retention. The top of the post is smaller than the bottom of the post. In the image below, Figure 25, the dark outline, which borders represents the bottom of the post which is not bonded to the coverslip. The clear outline, which is on the inside of the dark outline, represents the top of the post and is bonded to the coverslip.

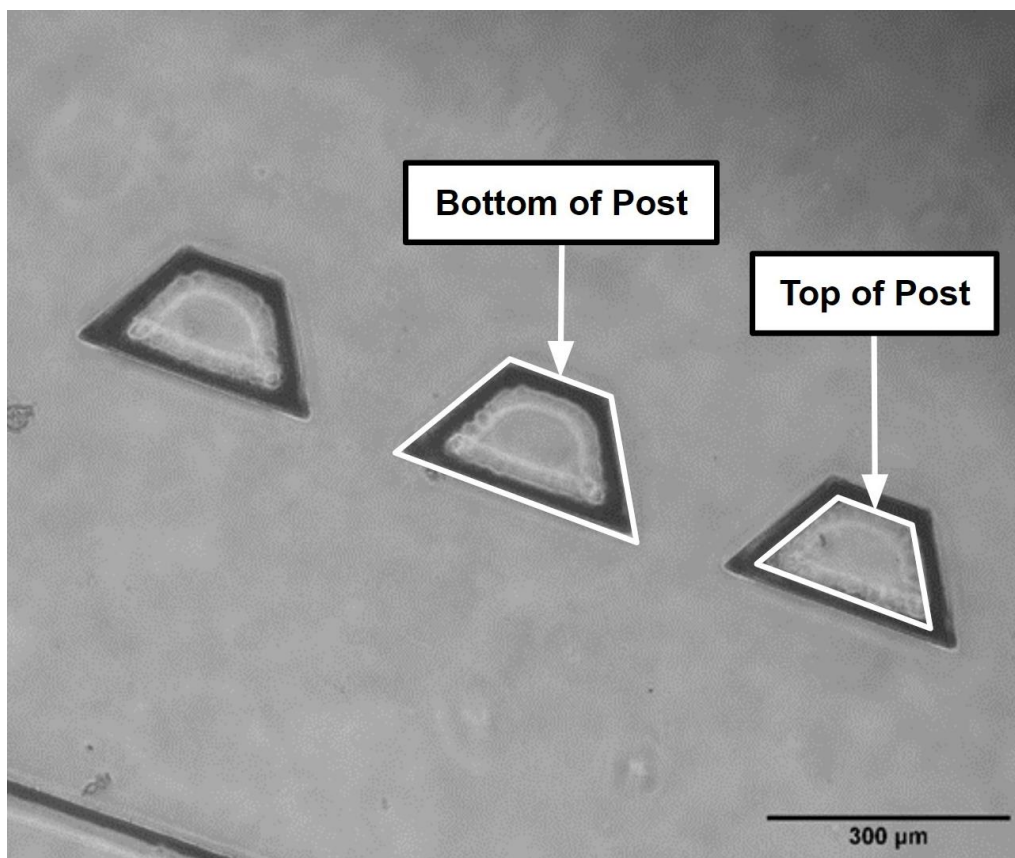


Figure 25: 10x Image of Fabrication of AIM chip replica of 100 μm height. This phase contrast image was taken with a Nikon Eclipse TS100 microscope.

The design of a replica of the AIM chip was used as a control for our designs. As shown below in Figure 26, the fabrication of this design was successful which is shown with the correct development of the posts.

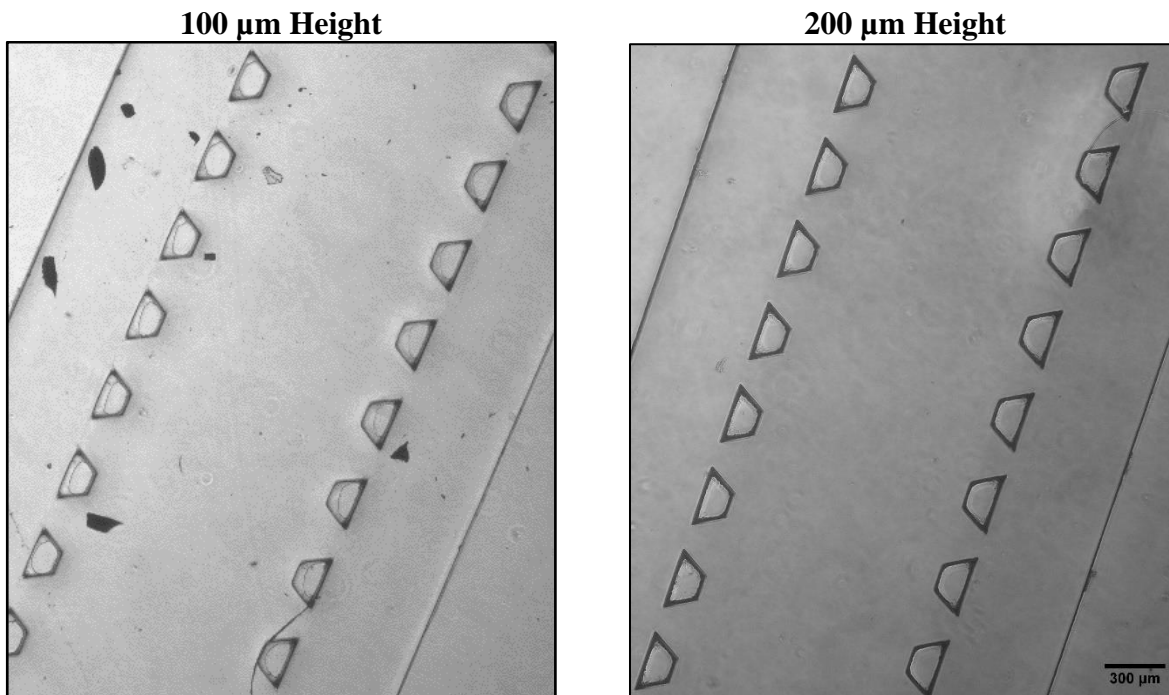


Figure 26: Fabrication of Pre-Gelation AIM Chip replicas. These phase contrast images were taken with a Nikon Eclipse TS100 microscope. The images, from left to right, are 4X images of the 100 μm and 200 μm heights.

The fabrication of the AIM device with internal posts at 100 μm height and 200 μm height were successful which is shown below with the correct development of the posts in Figure 27.

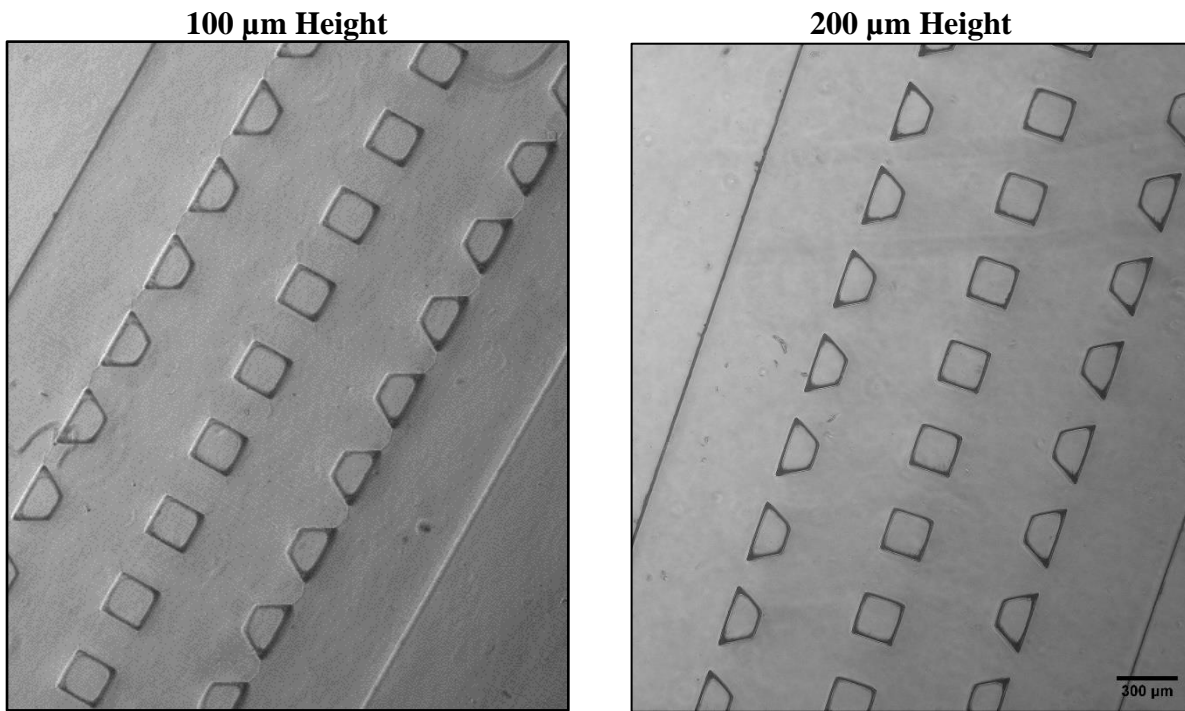


Figure 27: Fabrication of Pre-Gelation AIM Chip with Internal Posts design with 200 μm Spacing. These phase contrast images were taken with a Nikon Eclipse TS100 microscope. The images, from left to right, are 4X images of the 100 μm and 200 μm height.

The fabrication of the Yoon devices at 100 μm height and 200 μm height were successful which is shown below with the correct development of the posts in Figure 28.

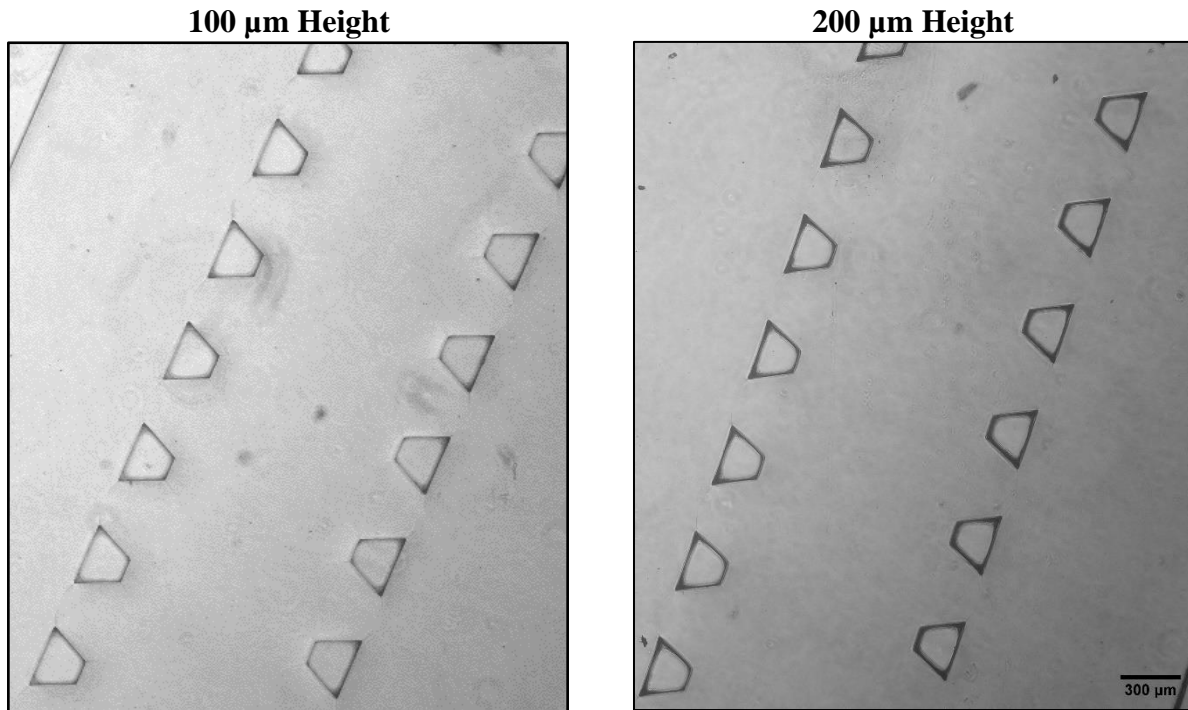


Figure 28: Fabrication of Yoon replicas. These phase contrast images were taken with a Nikon Eclipse TS100 microscope. The images, from left to right, are 4X images of the 100 μm and 200 μm heights.

The fabrication of the Polacheck device at 100 μm height was successful which is shown with the correct development of the posts. There were issues with the fabrication of the Polacheck device at 200 μm height which is shown below in Figure 29. To remove the excess SU-8 from the wafer, we sprayed the devices one at a time using the developer spray bottle. The Polacheck design shows evidence of being overdeveloped, due to spraying too much developer at the posts, or leaving the developer on for too long. This could have been caused by failing to remove the excess developer when spraying the wafer with distilled water. These fabrication issues led to the posts of the devices being overdeveloped, which can be shown below. We can tell the posts are overdeveloped due to the appearance of the posts being black.

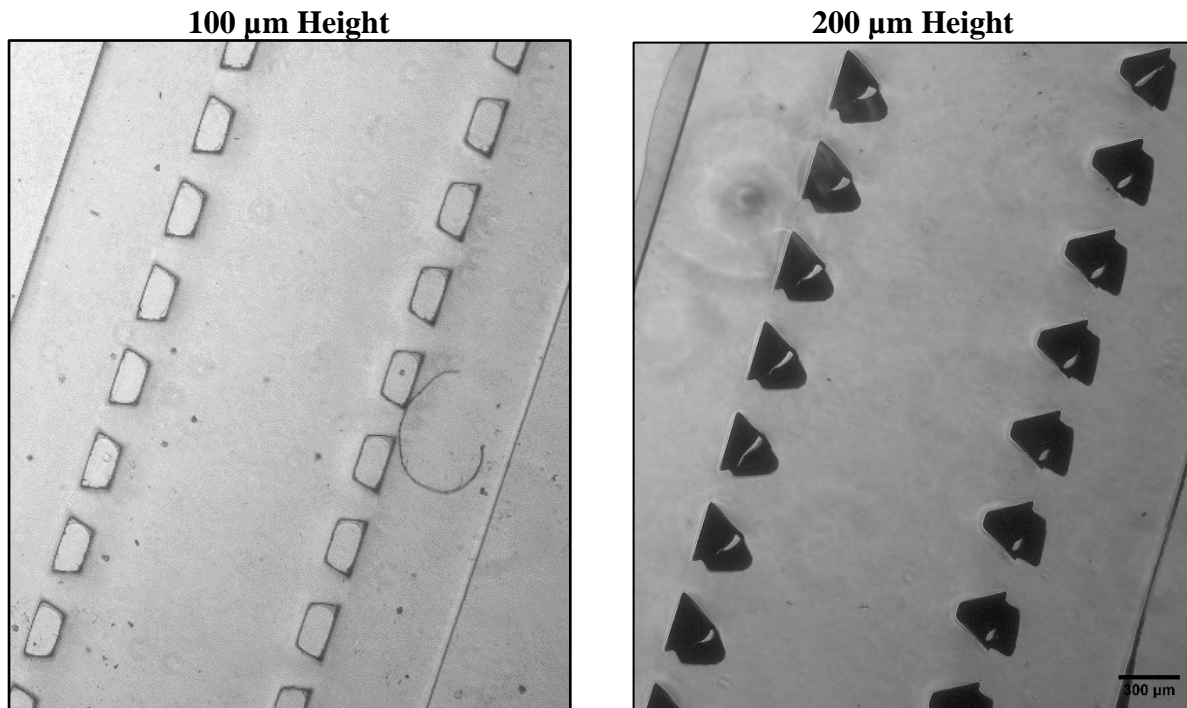


Figure 29: Fabrication of Pre-Gelation Polachek replicas. These phase contrast images were taken with a Nikon Eclipse TS100 microscope. The images, from left to right, are 4X images of the 100 μm and 200 μm heights.

The fabrication of the Farahat replica was successful, which shows the correct development of the posts which is shown below in Figure 30. The Farahat replica at 200 μm height was also successful despite the posts being slightly overdeveloped. However, this had no effect on the functionality of the device.

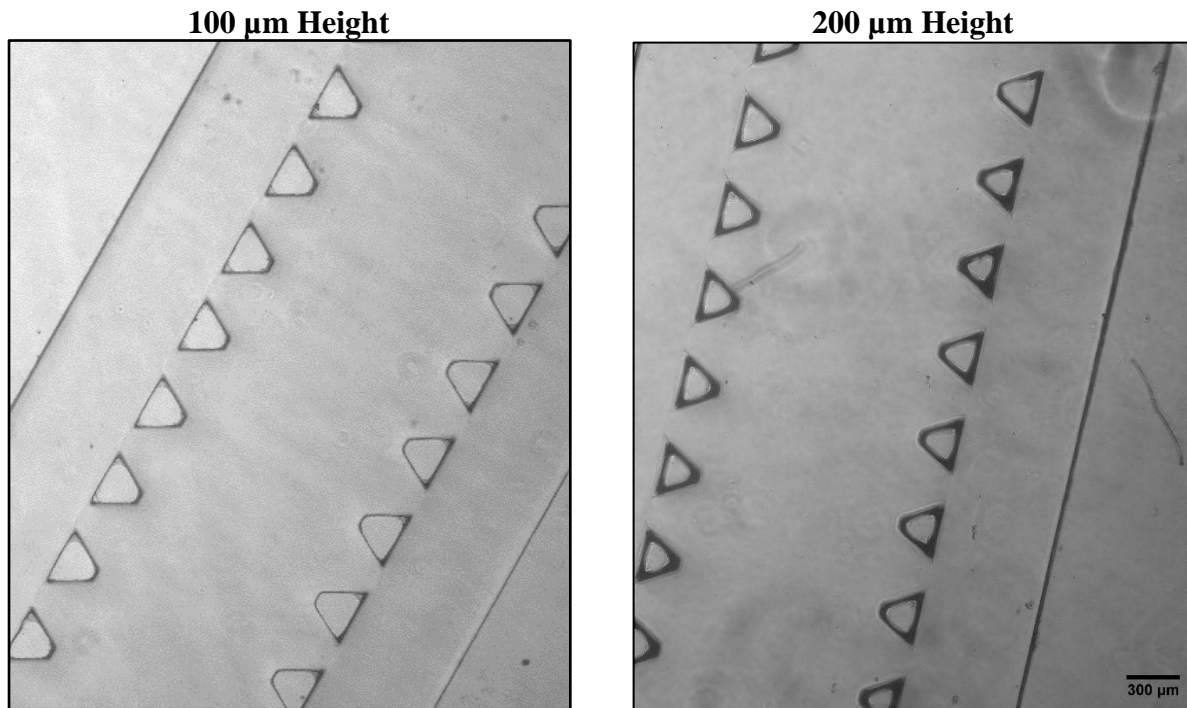


Figure 30: Fabrication of Pre-Gelation Farahat replicas. These phase contrast images were taken with a Nikon Eclipse TS100 microscope. The images, from left to right, are 4X images of the 100 μm and 200 μm heights.

The fabrication of the Yoon replicas with 100 μm spacing at 100 μm height and 200 μm height were successful which is shown below in Figure 31 with the correct development of the posts.

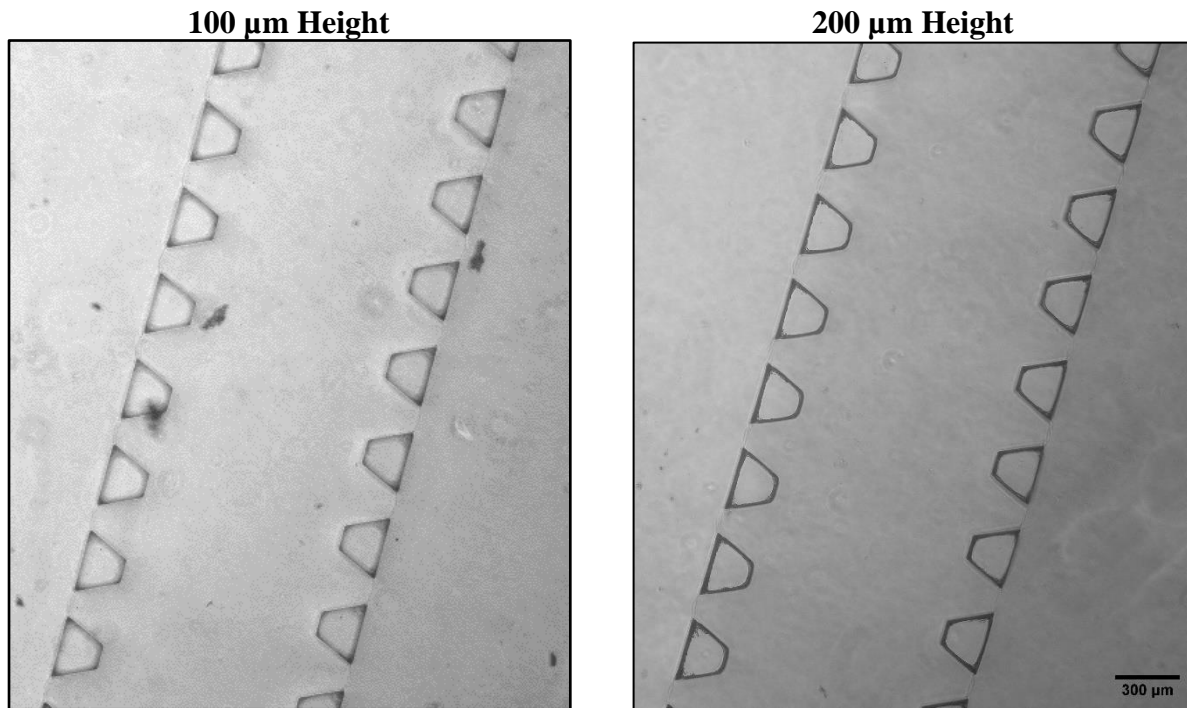


Figure 31. Fabrication of Pre- Gelation Yoon device replicas with 100 μm spacing. These phase contrast images were taken with a Nikon Eclipse TS100 microscope. The images, from left to right, are 4X images of the 100 μm and 200 μm heights.

The fabrication of the AIM device with 150 μm spacing at 100 μm height was successful which is shown with the correct development of the posts. There were issues with fabrication at 200 μm height which is shown below in Figure 32. The issues with fabrication led to the posts being overdeveloped. However, this had no effect on the functionality of the device.

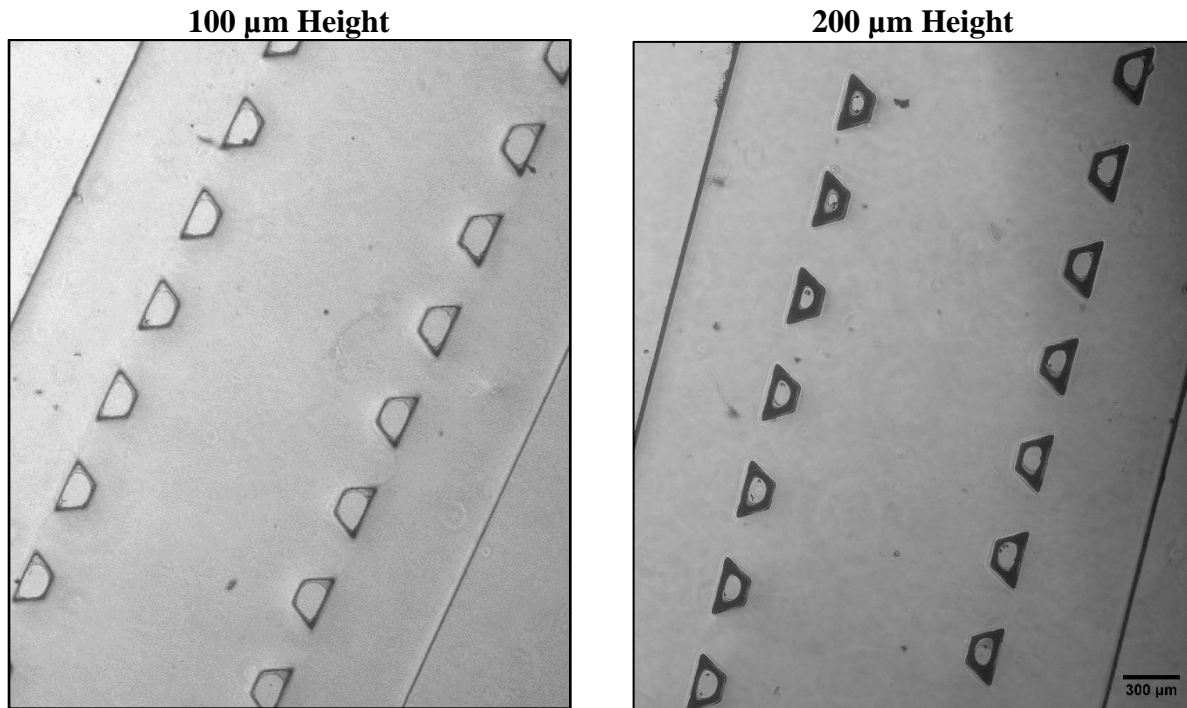


Figure 32. Fabrication of Pre-Gelation AIM Device replicas with 150 μm spacing. These phase contrast images were taken with a Nikon Eclipse TS100 microscope. The images, from left to right, are 4X images of the 100 μm and 200 μm heights.

The fabrication of the AIM device with 200 μm spacing at 100 μm height was successful which is shown with the correct development of the posts. There were issues with the fabrication of the device at 200 μm height which is shown below in Figure 33. The fabrication issues led to the posts being overdeveloped.

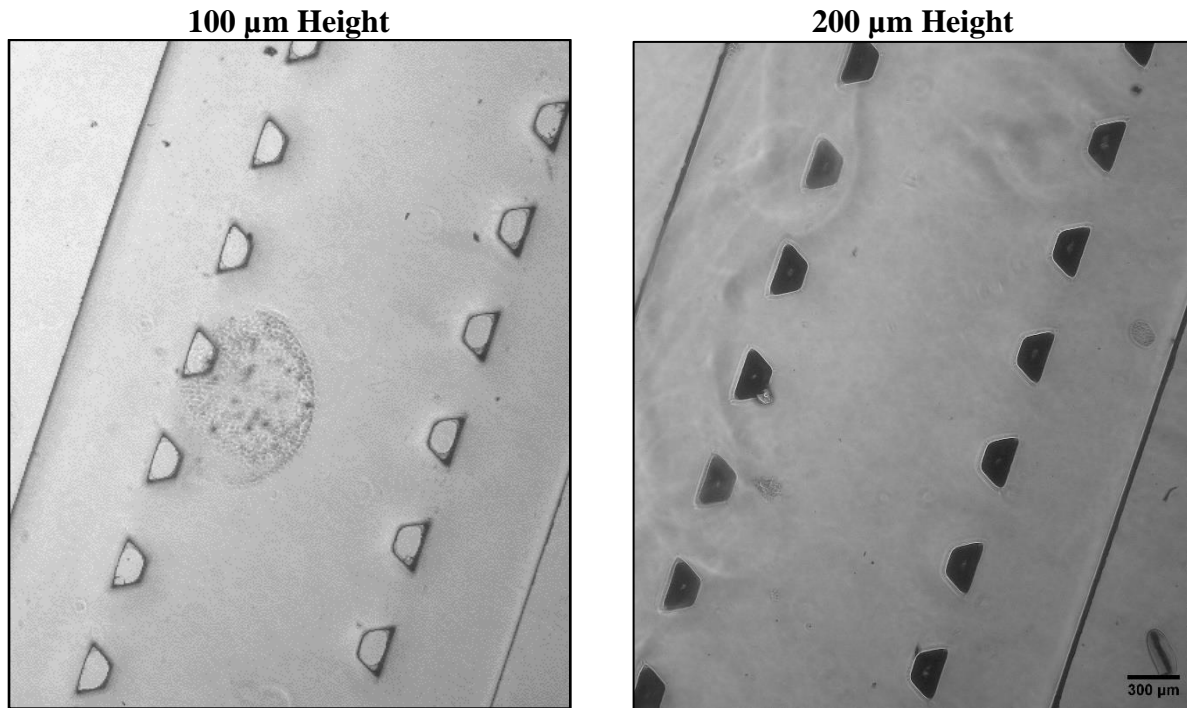


Figure 33. Fabrication of Pre-Gelation AIM Device replicas with 200 μm spacing. These phase contrast images were taken with a Nikon Eclipse TS100 microscope. The images, from left to right, are 4X images of the 100 μm and 200 μm heights.

The fabrication of the AIM devices with 75° post angle at 100 μm height and 200 μm height were successful which is shown below with the correct development of the posts in Figure 34.

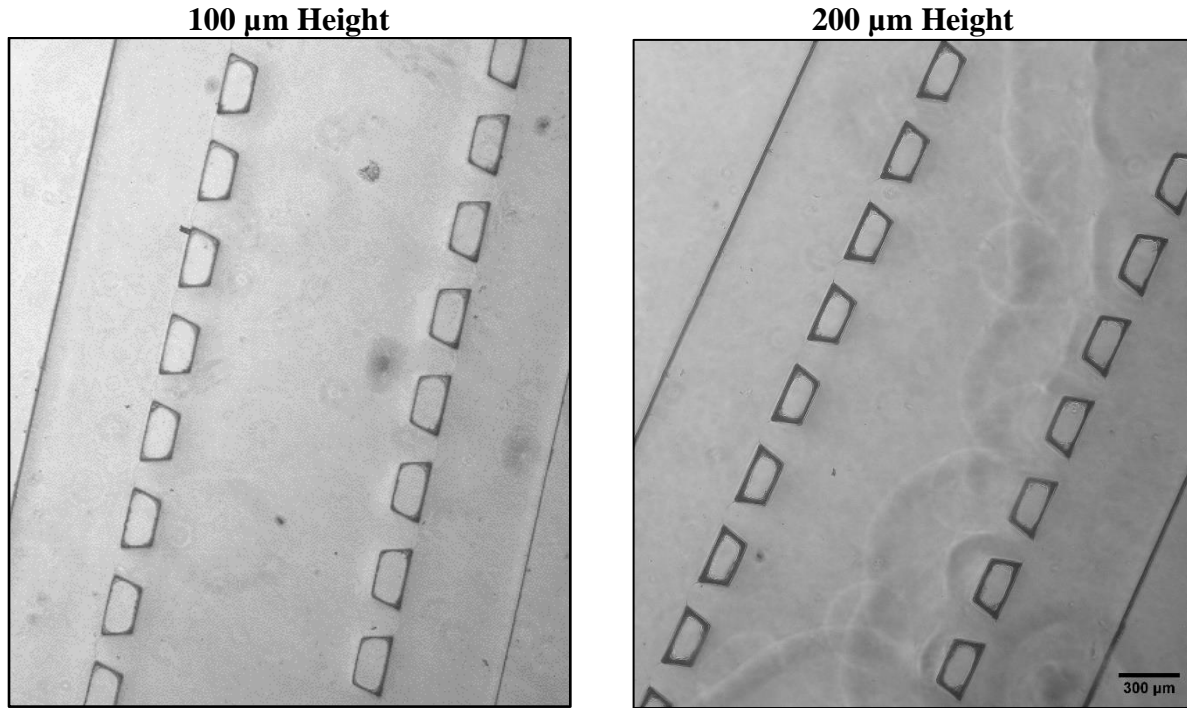


Figure 34. Fabrication of Pre- Gelation AIM Device replicas with 75° post angle. These phase contrast images were taken with a Nikon Eclipse TS100 microscope. The images, from left to right, are 4X images of the 100 μm and 200 μm heights.

4.8.2 Gel Placement

To prepare the microfluidic devices for experimentation, fibrin gels need to be placed into the central gel chamber. The components of the fibrin gels are created, an 8.0 mg/mL fibrinogen solution and 1.52 U/mL thrombin solution. These solutions are then mixed in a tube, and 10 μL of the 4 mg/mL fibrin solution is slowly placed into the central gel chamber microfluidic device, with half of the volume placed in each inlet. The full protocol used for preparing and placing gels is in Appendix H. We initially placed gels into a device that has been proven to retain gel before, the AIM Chip, shown below in Figure 35. We utilized the results in Figure 35 to determine whether gel retention was successful in the fabricated devices. Shortly after device fabrication, which was completed on a benchtop, gels were placed into each device while following aseptic technique.

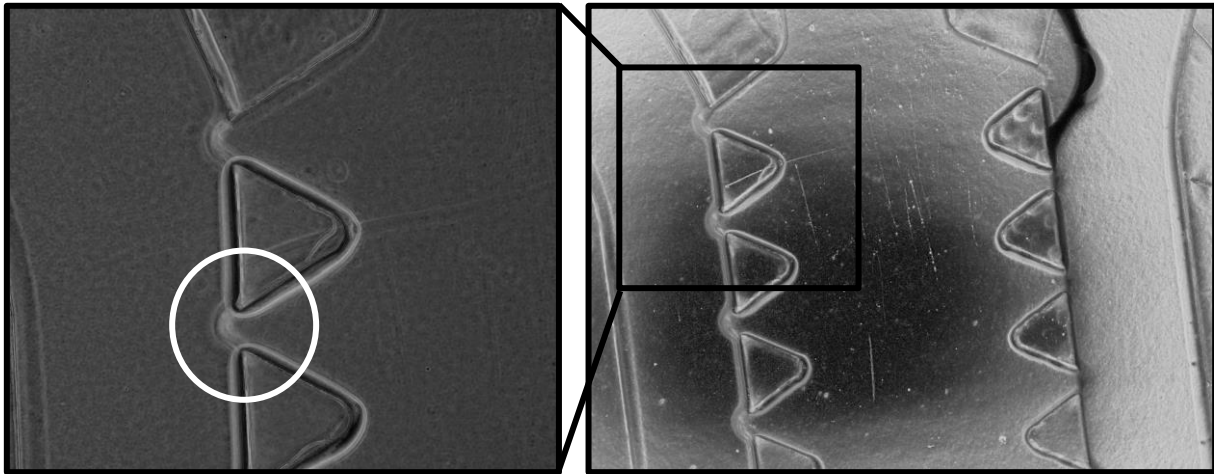


Figure 35: Successful Gel Placement in AIM Chip. These phase contrast images were taken with a Nikon Eclipse TS100 inverted microscope. The image on the left is a 10X image of an AIM Chip post gel insertion, with its subsequent 4X image on the right. In the image on the left, the meniscus is circled in white. In the image on the right, the inset of the image on the left is shown in a black square.

All gels were created and placed using the protocol in Appendix H for each design. Each design was fabricated using a 100 μm and 200 μm silicon wafer, with the 200 μm wafer used twice for further validation. Below is an analysis of the gel retention results for all designs, each with one 100 μm height device and two 200 μm height devices.

First, the AIM Chip designs will be analyzed, as success with the plastic AIM Chip has been observed previously. The modifications made to the AIM Chip design are as follows, increasing the post spacing to 150 μm and 200 μm , increasing the post angle to 75°, and adding square internal posts. As a baseline, or control, the original AIM Chip design was fabricated. In Figure 36, below, are images of the original AIM Chip design pre-gelation, when the gel is thinner and is water-like. Starting with the device at a height of 100 μm , gel retention is maintained through the entire device, with no leakage into the media channels along the side. This is the same for the first run of the 200 μm height device. The second run of the 200 μm did not successfully retain gel along the entire chamber. The left side of the chamber leaked, as shown by a lack of meniscus. However, the menisci are held along the right side of the chamber, indicating that this design has potential and leakage was due to user error. This is a common trend with most of the designs shown.

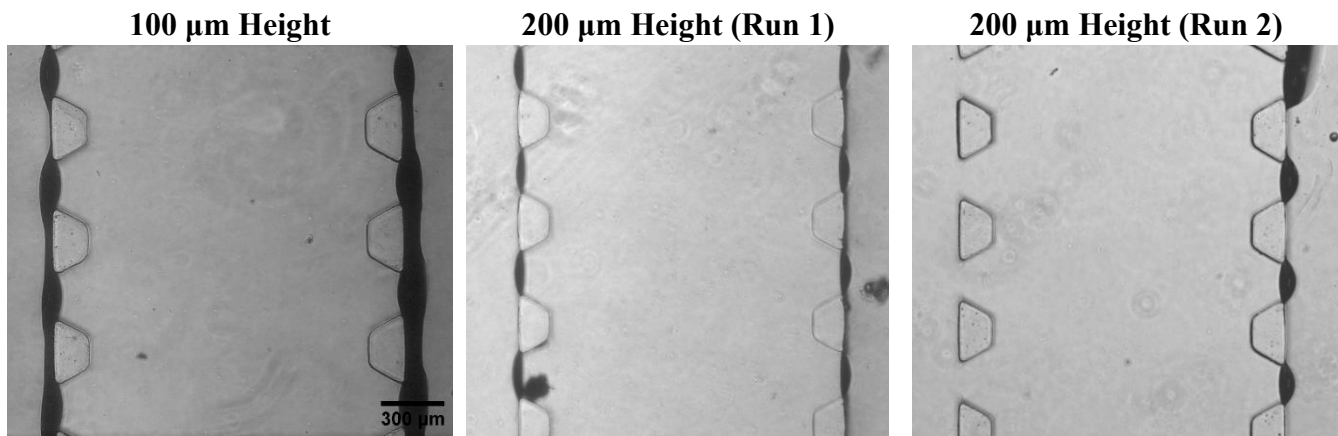


Figure 36: Pre-Gelation of AIM Chip Replicas. These phase contrast images were taken with a Nikon Eclipse TS100 inverted microscope. The images, from left to right, are 4X images of the initial 100 μm height, first run of the 200 μm height, and second run of the 200 μm height of the PDMS AIM Chip replicas with gels inserted into the central gel chamber.

The next AIM Chip designs of interest are those with larger spacing between posts, one at 150 μm and the other at 200 μm . In Figure 37, below, are images of the AIM Chip design with 150 μm spacing. The 100 μm height device did not retain the gel completely, as indicated by the leakage into the media channel on the right. However, along the left side of the device, menisci are along the channel, indicating that user error was the cause of the leakage. An additional note for the 100 μm height device is the bubble present in the gel chamber. This bubble indicates user error during gel insertion, as there may have been bubbles in the pipette tip prior to insertion or the pipette plunger was retracted during insertion. Despite leakage with the 100 μm height, both 200 μm height devices retained gel along the entire channel, indicated by the menisci along both sides of the gel chamber.

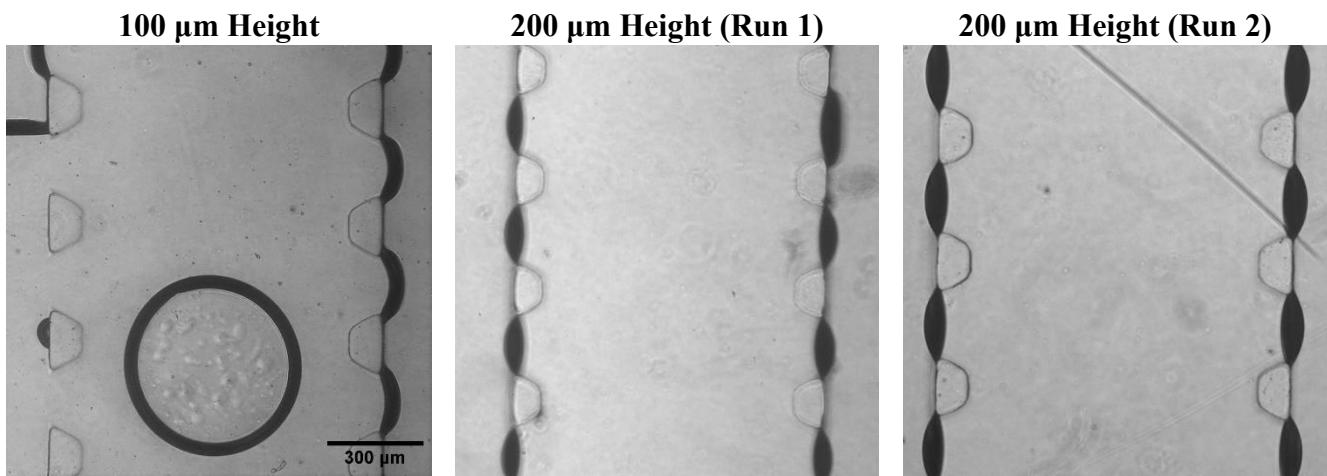


Figure 37: Pre-Gelation of AIM Chip Design with 150 μm Spacing. These phase contrast images were taken with a Nikon Eclipse TS100 inverted microscope. The images, from left to right, are 4X images of the initial 100 μm height, first run of the 200 μm height, and second run of the 200 μm height of the PDMS AIM Chip Design with 150 μm spacing with gels inserted into the central gel chamber.

The next AIM Chip design of interest is the one with post spacing of 200 μm . In Figure 38, below, are images of the AIM Chip design with 200 μm spacing. The 100 μm height device successfully retained gel, however some menisci are bowing out more, indicating that the gel had a chance of leaking out into the media channel. This most likely would have occurred if gel placement had been quicker. Both of the 200 μm height devices were not fully successful at retaining the gel. There is leakage into the left media channel in both of the images, indicating a lack of retention. This may have been partially to user error, as the device may have partially debonded during placement. However, when comparing the posts between the two heights 100 μm and 200 μm , the posts in the 200 μm device look much smaller than those in the 100 μm photo, despite them being the same size in the design. This led us to believe that this leakage was due to errors during fabrication of the devices. Despite this, gel retention still occurred between posts, such as those on the right of the gel chamber in 200 μm devices.

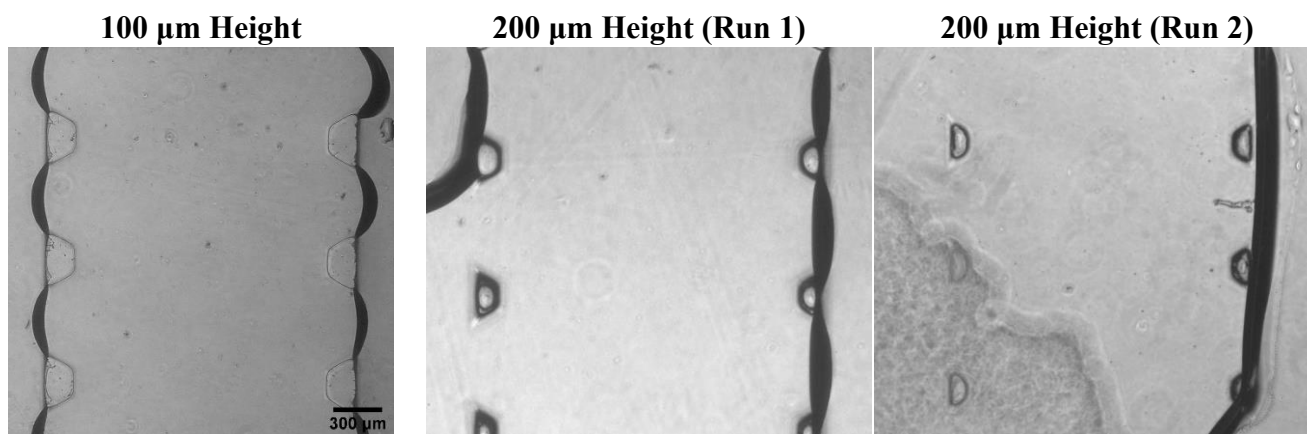


Figure 38: Pre-Gelation of AIM Chip Design with 200 μm Spacing. These phase contrast images were taken with a Nikon Eclipse TS100 inverted microscope. The images, from left to right, are 4X images of the initial 100 μm height, first run of the 200 μm height, and second run of the 200 μm height of the PDMS AIM Chip Design with 200 μm spacing with gels inserted into the central gel chamber.

The next AIM Chip design of interest is the one with a larger, 75°, post angle. It is important to note that this design was based on data gathered in the contact angle study in Section 4.5. In Figure 39, below, are images of the AIM Chip design with posts at a 75° angle. In all of the devices below, gel retention was achieved along both sides of the gel chamber, as seen by the menisci. This indicates successful gel retention at both heights, 100 μm and 200 μm . An additional note for the 100 μm height device is the bubble present in the gel chamber. This bubble indicates user error during gel insertion, as there may have been bubbles in the pipette tip prior to insertion or the pipette plunger was retracted during insertion.

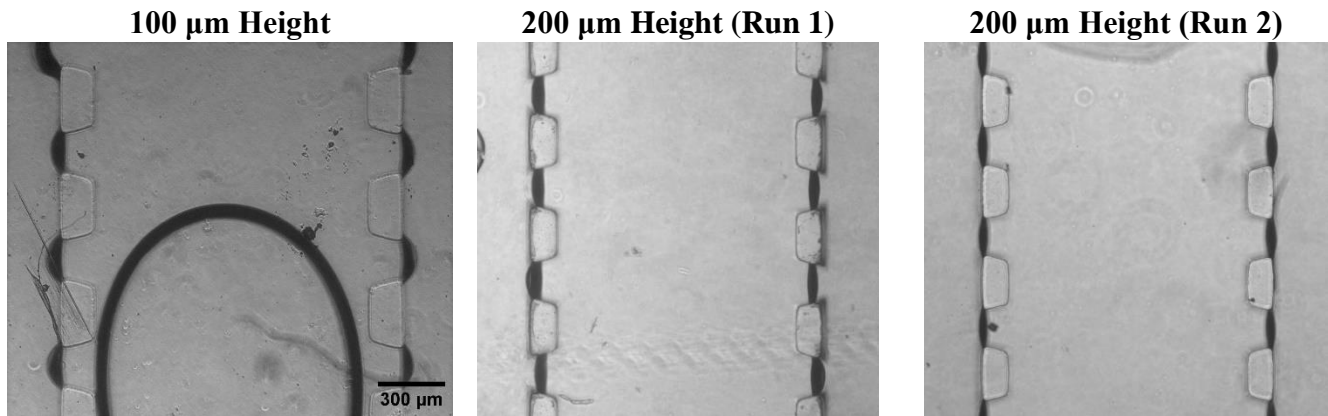


Figure 39: Pre-Gelation of AIM Chip Design with 75° Posts. These phase contrast images were taken with a Nikon Eclipse TS100 inverted microscope. The images, from left to right, are 4X images of the initial 100 μm height, first run of the 200 μm height, and second run of the 200 μm height of the PDMS AIM Chip Design with 75° posts with gels inserted into the central gel chamber.

The next AIM Chip design of interest is the one with internal posts. In Figure 40, below, are images of the AIM Chip design with square internal posts. The 100 μm height device was unable to retain gel, as indicated by the leakage into the left media channel. However, this is thought to be due to user error, as menisci are present along the right side of the gel chamber. In addition, the first run of the 200 μm height devices retained gel along both sides of the gel chamber. The second run of the 200 μm height also leaked into the left channel; however, this is believed to be due to user error, as the right side of the gel chamber maintained menisci. An important note for this design is that bubbles formed between the square internal posts, whereas in the other designs, no bubbles formed between the posts along the side. This may have been due to user error, with pipetting the gel in, or the gel being unable to fill that space due to a lack of adequate volume to fill the space.

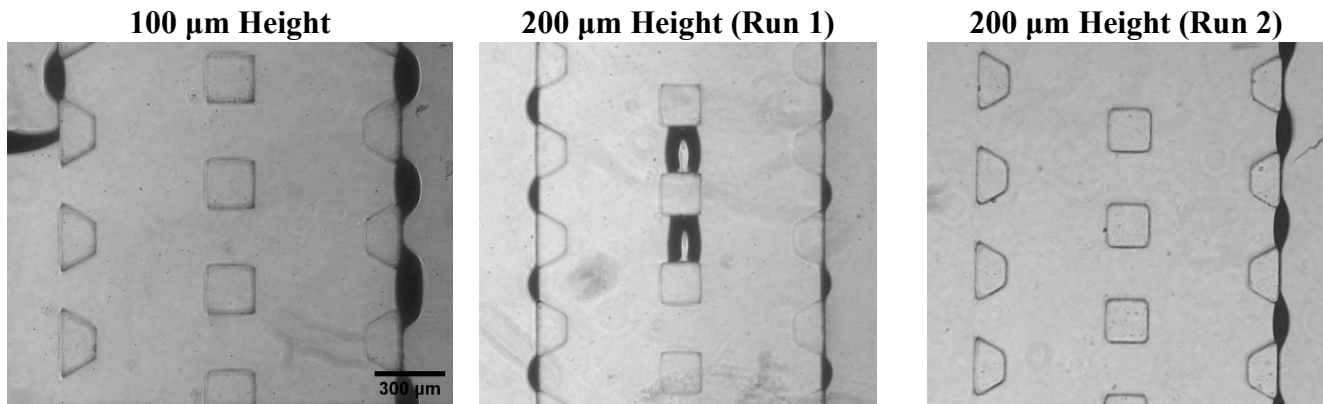


Figure 40: Pre-Gelation of AIM Chip Design with Internal Posts. These phase contrast images were taken with a Nikon Eclipse TS100 inverted microscope. The images, from left to right, are 4X images of the initial 100 μm height, first run of the 200 μm height, and second run of the 200 μm height of the PDMS AIM Chip Design with internal posts with gels inserted into the central gel chamber.

Overall, the devices based on the AIM Chip were fairly successful at gel retention, and all of the leakage into the media channels was due to user error. The next set of designs of interest are the Farahat and Polacheck replicas. The Farahat replica is shown in Figure 41, below. The 100 μm height device had leakage into the left media channel; however, menisci are retained all along the right of the gel chamber and for sections of the left gel chamber. This indicates that the leakage was due to user error. The first run of the 200 μm height devices retained gel all along the chamber, indicating that the device can successfully retain gel despite the leakage in the 100 μm height device. The second run was not successful, as indicated by the image in Figure 41. The center gel chamber is not full of gel, as the menisci is in the opposite direction that they should be in. This was due to user error during gel insertion.

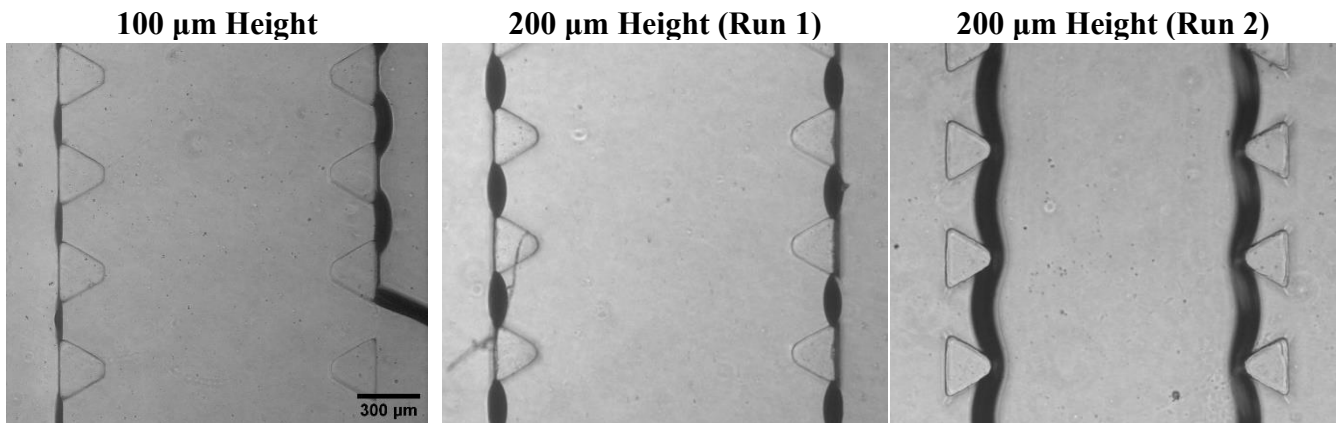


Figure 41: Pre-Gelation of Farahat Replicas. These phase contrast images were taken with a Nikon Eclipse TS100 inverted microscope. The images, from left to right, are 4X images of the initial 100 μm height, first run of the 200 μm height, and second run of the 200 μm height of the PDMS Farahat replicas with gels inserted into the central gel chamber.

Figure 42, below, shows the more sections of this device. As seen in Figure 42, gel insertion was successful along the central gel chamber, until leakage occurred. This leakage caused the bubble to occur in the image on the left, causing the gel to fill along the media channels instead of the gel chamber. This was most likely due to a lack of pressure during gel insertion. Despite the leakage into the media channels due to user error, the design has good gel retention.

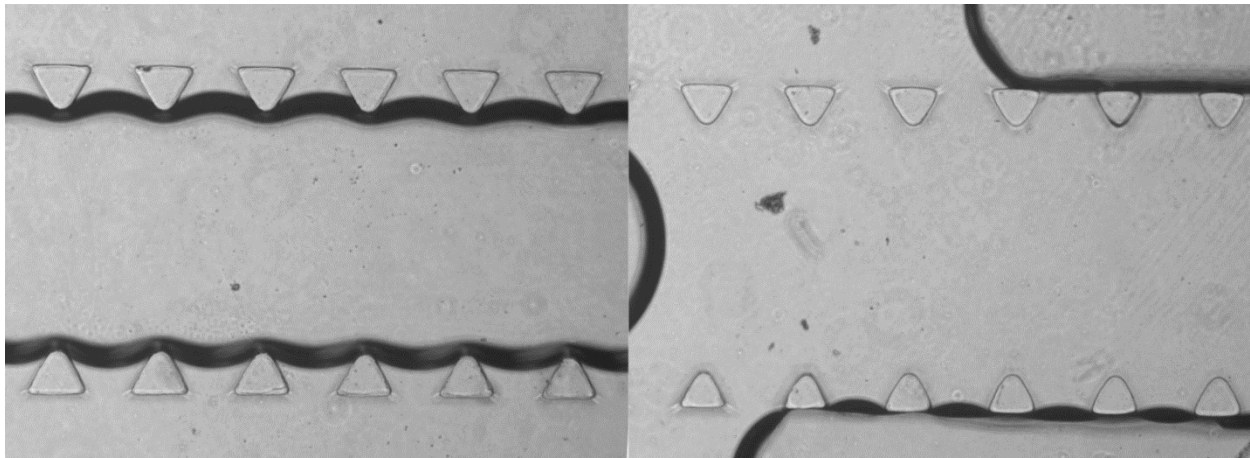


Figure 42: Pre-Gelation of Second Run of 200 μm Height Farahat Replica. These 4X phase contrast images were taken with a Nikon Eclipse TS100 inverted microscope. The image on the left is closer to the gel inlet, and the image on the right is toward the center of the device, between the two inlets. The image on the right indicates gel insertion was successful along the central gel chamber, until leakage occurred. This leakage caused the bubble to occur in the image on the left, causing the gel to fill along the media channels instead of the gel chamber.

The next design of interest is the Polacheck replica, shown in Figure 43, below. The 100 μm height device has no menisci along either side of the gel chamber, as the entire device debonded from the coverslip during gel placement, a user error. However, the first run of the 200 μm height device was able to successfully retain gel within the gel chamber, indicated by the menisci on both sides of the gel chamber. This is in contrast to the second run, which resulted in leakage into the right media channel, shown below. With the successful retention in the first run, it is reasonable to assume that the leakage was due to user error during gel placement.

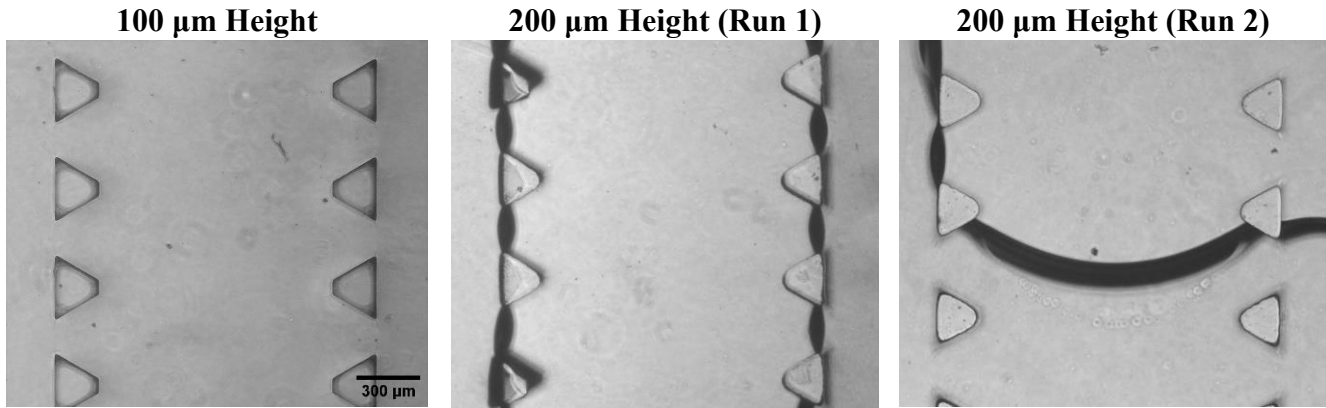


Figure 43: Pre-Gelation of Polacheck Replicas. These phase contrast images were taken with a Nikon Eclipse TS100 inverted microscope. The images, from left to right, are 4X images of the initial 100 μm height, first run of the 200 μm height, and second run of the 200 μm height of the PDMS Polacheck replicas with gels inserted into the central gel chamber.

Lastly, the Yoon devices, both at the original 200 μm spacing and modified 100 μm spacing, are of interest. The Yoon replica is shown in Figure 44, below. The 100 μm height device had leakage into the left media channel, most likely due to user error. This is indicated by the menisci along the right and above the leakage in the image. In addition to the menisci in the 100 μm height device, both 200 μm height devices successfully retained gel along the entire gel chamber, indicated by the menisci along both sides of the gel chamber in Figure 44.

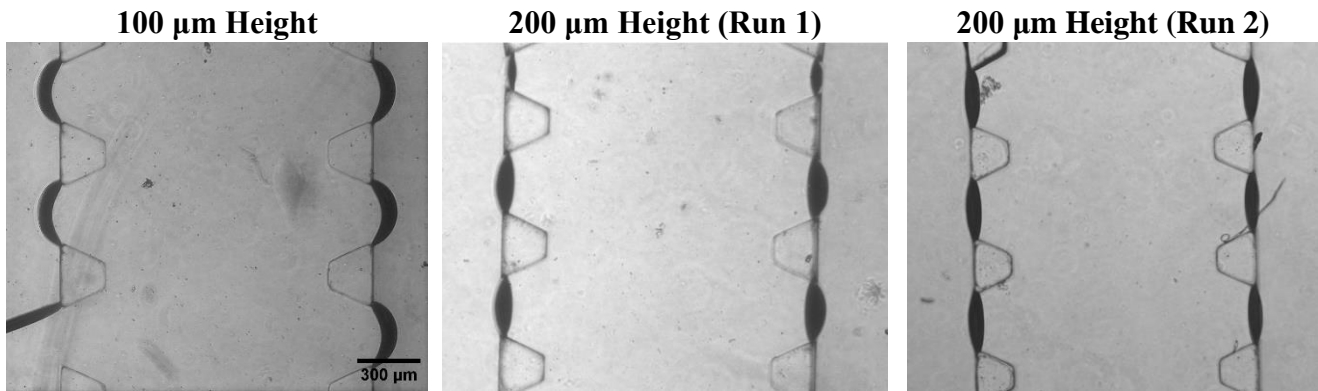


Figure 44: Pre-Gelation of Yoon Replicas. These phase contrast images were taken with a Nikon Eclipse TS100 inverted microscope. The images, from left to right, are 4X images of the initial 100 μm height, first run of the 200 μm height, and second run of the 200 μm height of the PDMS Yoon replicas with gels inserted into the central gel chamber.

Lastly, the Yoon device of interest was modified to have a smaller post spacing, at 100 μm instead of 200 μm . The images in Figure 45, below, indicate its potential for gel retention. Both heights of the device, 100 μm and 200 μm , retained the gel and showed no leakage into the media channels. This is indicated by the menisci along both sides of the gel chamber.

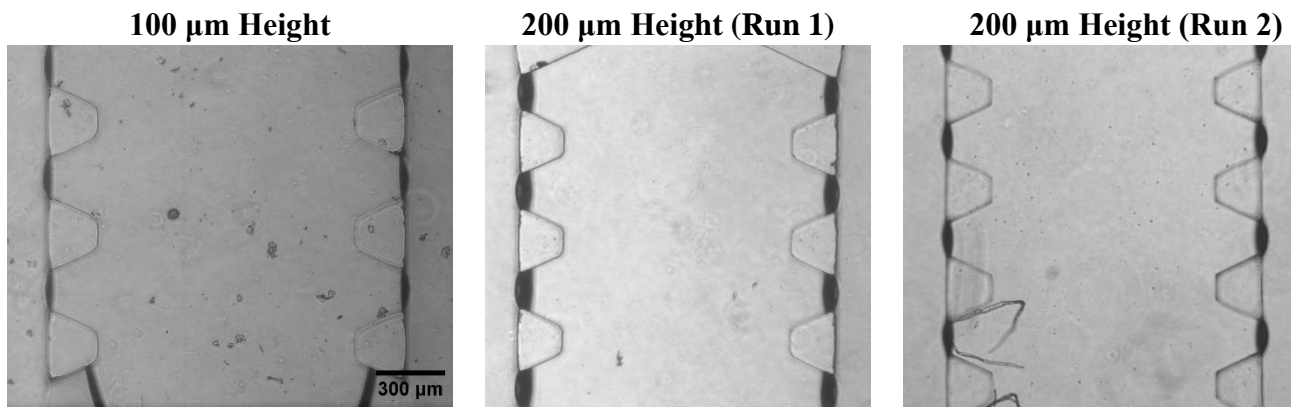


Figure 45: Pre-Gelation of Yoon Design with 100 μm Spacing. These phase contrast images were taken with a Nikon Eclipse TS100 inverted microscope. The images, from left to right, are 4X images of the initial 100 μm height, first run of the 200 μm height, and second run of the 200 μm height of the PDMS Yoon design with 100 μm spacing with gels inserted into the central gel chamber.

The results above indicate that all of these designs have the potential to retain gel. Two AIM Chip designs, in particular, retained gel in all fabricated devices, the one with a 150 μm spacing and the one with 75° post angles. All of the other designs had indications of gel retention through at least some of the gel chamber despite leakage into the media channels. The leakage, given the data shown, was due to either user error during gel placement or fabrication. The two examples of these errors are the 100 μm height Polacheck device, which was debonded during gel placement, and the 200 μm height AIM Chip devices with 200 μm spacing between posts, which had posts that were overdeveloped in the master mold. It is evident that if gel placement and fabrication went perfectly, all of the devices would retain gel.

4.9 Pump Validation

To ensure that the pump is running at the needed flow rate to achieve the desired shear stress it must be validated. Using the procedure that is outlined in Appendix C, multiple data points were collected to verify the necessary flow rate of the pump in order to produce a high and low shear stress on the wall of the media channel of the microfluidic device. The high and low values we aimed to achieve were 2.0 and 0.2 Pa which is the approximate shear stress cells experience from blood flow through the heart valve at a resting heart rate. For steady flow conditions, gravity was used to drive flow downwards through the microfluidic device. In order to produce oscillatory flow, an Arduino Uno was used to turn the solenoid pinch valves on and off. Since the Arduino program runs on a frequency of Hertz (HZ), we needed to convert the resting heart rate of 60 BPM to HZ so that the system ran at the rate of a normal heart beat. The beats per minute was converted into Hertz then into milliseconds to properly run the program. The conversion used was 1.0 hZ=60 BPM=1000 milliseconds. The way our double gravity pump works is the fluid flows through the microfluidic device in one direction by one reservoir and then the fluid runs in the opposite direction from the other reservoir. In order to mimic the

environment of the heart, including the opening and closing of the valves. To bring fresh media into the chamber, the first set of solenoids are open twice the amount of time as the second set. The first set of valves are open, allowing media to flow, for 666 milliseconds and the second set are open for 333 milliseconds. In order to validate that our gravity pumps can function under sterile conditions without negatively affecting the cells, we ran one of our pumps in the incubator with an AIM Biotech Chip that was seeded with endothelial cells.

4.9.1 General Calculations for Gravity Pump

The gravity pump was designed to produce shear stresses within 10% of 2.0 Pa and 0.2 Pa along the walls of the media channels of the microfluidic device. There are several variables that are a factor in being able to produce those shear stresses including tubing resistance, device channel resistance, pump height, tubing length, and radius sizing. Shear stress is directly proportional to flow rate, which can be solved and measured. To aid in the design many of the variables and flow rate were calculated using MATLAB. The variables and MATLAB code can be found in Appendix E & F. To achieve 0.2 Pa, the flow rate needs to run at 2.08 $\mu\text{l/s}$ and for 2.0 Pa, the flow rate needs to be 20.8 $\mu\text{l/s}$, which were calculated based on the shear stress with the following equation. For our experiment we were interested in the shear stress of the wall of the rectangular media channel, therefore the height and width of the channel was flipped which is shown in the equation below:

Flow Rate through the Rectangular Channel from each Pump

$$Q = \frac{\tau h^2 w}{6\mu} \rightarrow Q = \frac{\tau w^2 h}{6\mu} \rightarrow \frac{(0.2 \text{ Pa}) * (0.5 \text{ mm})^2 * (0.25 \text{ mm})}{6 * (0.001 \text{ Pa} * \text{s})} = 2.08 \frac{\text{mm}^3}{\text{s}} = 2.08 \frac{\mu\text{L}}{\text{s}}$$

where Q is the flow rate, τ is shear stress, h is height of the media channel, w is the width of the media channel, and μ is the viscosity of fluid. The flow rate is affected by the tubing and channel resistances, which change based upon the dimensions of the tubing. The gravity pump set ups use various types of tubing with different radiuses and lengths. Therefore, the resistance of each tubing was calculated, as was the channel of the microfluidic device.

Resistance of the Tubing Modeled as a Pipe (example of tubing from reservoir to syringe)

$$R = \frac{8 * \mu * L}{\pi * r^4} \rightarrow \frac{8 * (0.001 \text{ Pa} * \text{s}) * (101 \text{ mm})}{\pi * (1.13 \text{ mm})^4} = 0.158 \frac{\text{Pa} * \text{s}}{\text{mm}^3}$$

Resistance per One Unit of Length

$$R \text{ per mm} = \frac{R}{L} \rightarrow \frac{0.158 \frac{\text{Pa} * \text{s}}{\text{mm}^3}}{101 \text{ mm}} = 0.00156 \frac{\text{Pa} * \text{s}}{\text{mm}}$$

Resistance of the Microfluidic Device Channel

$$R = \frac{12 * \mu * L}{w * h^3} * \frac{1}{1 - (0.63 * \frac{h}{w})}$$
$$\rightarrow \left| \frac{12 * (0.001 Pa * s) * (10.5 mm)}{(0.25 mm) * (0.5 mm)^3} * \frac{1}{1 - (0.63 * \frac{0.5 mm}{0.25 mm})} \right|$$
$$= 15.5 \frac{Pa * s}{mm^3}$$

Finally, the height was calculated to provide the pump with enough pressure. Since the pump's driving force is gravity, the higher the reservoir was from the outlet point, the larger the pressure head and faster the flow rate. The following equation was used during validation:

Pump Height from the Reservoir to the Outlet

$$\Delta P = \rho g \Delta h$$

where ΔP is the change in pressure, ρ is the density of fluid, g is the acceleration of gravity, and Δh is the change in height from the inlet, or reservoir, to the outlet, or end of tubing.

4.9.2 Experimental Validation of Steady Flow Gravity Pumps

To produce a steady flow that continuously travels through both sides of our microfluidic device at the same rate, we constructed two single reservoir gravity flow systems that ran at a low and high shear stress. Both systems consisted of one reservoir, a syringe, two Y connectors, and tubing of various sizes. The reservoir provides a supply of cell media, which is siphoned using the syringe. In order to ensure there are no air pockets in the tubing which can damage the cells in the microfluidic device, the syringe is connected to a three-way valve that can push liquid through the tubing removing the air pockets. Our final designs to produce the flow rates that create a 0.2 Pa shear stress and 2.0 Pa shear stress on the microfluidic device were determined through multiple trials. These trials include changing the height of the reservoir and size and length of tubing to either increase or decrease the flow rate. A schematic of the low shear stress gravity pump is shown below. Due to limited resources, the tubing size needed to change in order to be connected to the Y connector as well as the microfluidic device.

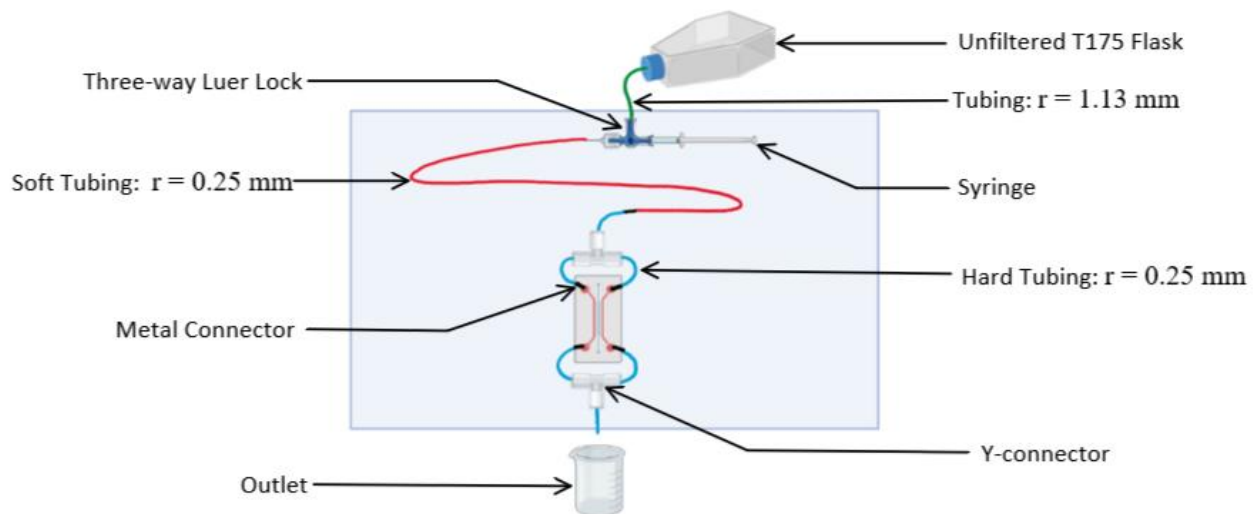


Figure 46: Diagram of gravity pump used for steady flow that produces a shear stress of 0.2 Pa

In the diagram above, it shows the preliminary setup of our pumping system that can achieve the flow rate required for 0.2 Pa. The length of tubing needed to change during the validation process many times due to the flow rate being too fast or too slow. Due to lack of available connectors, there were three different sized tubing used for the setup. The green line that connects the reservoir to the syringe has a radius of 1.13 mm. The red line indicated a tubing radius of 0.25 mm. To ensure that the gravity pump does not experience back flow the tubing is taut against an acrylic board to keep the system stable and consistent when being moved. The small black lines show the metal connector that is used to connect the two different sized tubing. The blue lines indicate a tubing with a radius of 0.25 mm that is used to connect to the Y connectors and then the microfluidic device. The red and blue lines indicate tubing of the same radius; however, the stiffness of the tubing was different. For the tubing indicated in the schematic as red, the tubing is soft and flexible. For the tubing indicated in the schematic as blue, the tubing is hard and stiff. For our validation process we used the AIM Biotech chip without gel placed inside the center gel chamber and ran water through the system to avoid building waste.

The high shear stress setup had the same structure as the low shear stress setup, however the tubing sizes and lengths were changed, as well as the height of the reservoir. A schematic of the single gravity pump that produces a shear stress of 2.0 Pa is shown below in Figure 47.

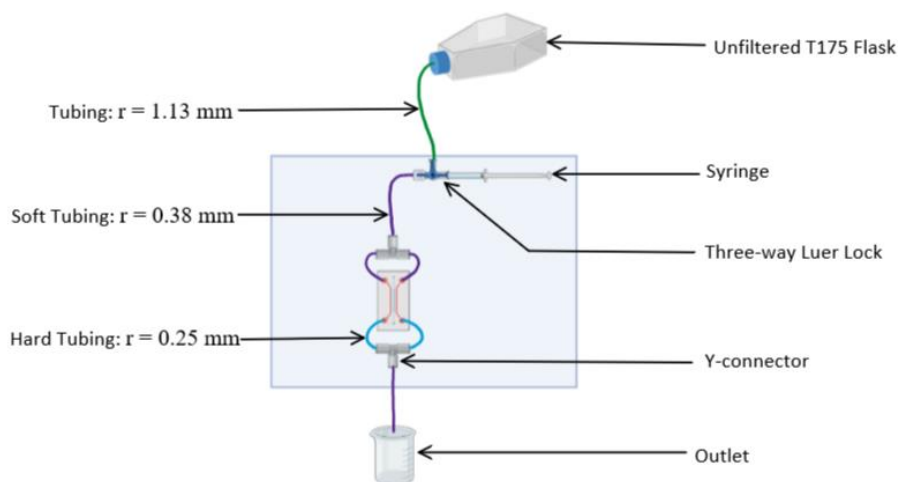


Figure 47. Diagram of gravity pump used for steady flow that produces a shear stress of 2.0 Pa

The diagram in Figure 47 shows the preliminary design for the pumping system that runs at a high shear stress. The setup is similar to our low shear stress setup, however the tubing from the syringe to the microfluidic device was increased in radius to reduce resistance. The length of tubing and height of the reservoir was changed throughout our validation process, which consisted of many trials using water on the AIM Chip.

In order to validate that the flow rate was achieved for both setups, we ran the systems with water and used the AIM Biotech chip as the microfluidic device, recording the outlet volume of water every five minutes with a graduated cylinder. The equation used to calculate flow rate from the experimental trials was:

$$Q = \frac{V}{t} \cdot \frac{1}{2}$$

with Q as flow rate, V as volume of outlet water, and t as time duration of the trial. We divided the flowrate in half, because through the system only half of the water goes through each channel. Therefore, to find an accurate flow rate through one channel of the microfluidic device, the volume would be half of what was collected. The flowrate required to create a shear stress of 0.2 Pa in the AIM Biotech chip was found to be 2.08 microliters per second. This value was found using the equation mentioned in the Theoretical Math section earlier. In the case of validation, we used the viscosity of water which is approximately the same as the viscosity of cell media.

Through trial and error, we ran the gravity system until we got the necessary flow rate that was calculated. In the beginning of the validation process when the flowrate was off by a large amount, we would change the diameter of tubing being used. For example, for the high shear stress setup we changed the radius of the tubing indicated by the purple line in Figure 47 from 0.25 mm to 0.38 mm. By increasing the radius of the tubing, the resistance decreased, ultimately speeding up the flow rate and producing a higher shear stress on the cells. If the trial

had an inaccurate flow rate but was close, two components of the system were changed either the total height of the system from the reservoir to the outlet or the length of the tubing. For example, once we decided to use tubing with a radius of 0.25 mm, the flowrate was found to be approximately 4.17 microliters per second. To get this value closer we increased the length of the tubing before the Y connector that connected to the microfluidic device, indicated on the diagram in Figure 46 as the red line. When the flow rates were achieved for both gravity pumps, they were run multiple times in order to validate its accuracy and determine our final designs. The data collected to validate the setups were conducted over five-minute intervals. For the low shear stress setups, with the reservoir at its highest volume the flow rate achieved was 2.17 $\mu\text{L/s}$ which produced a shear stress in the microfluidic device of 0.208 Pa. However, after approximately 30 minutes of continuously running the system, the flowrate decreased to 1.83 $\mu\text{L/s}$, causing the shear stress to drop to 0.176 Pa which was below our 10% margin of error. Theoretically after 30 minutes, the total amount of fluid collected should be 7.8 mL and the change in height should only be approximately 0.45 mm. Therefore, with this height change the drop in flow rate should have not been as significant, so we determined there must have been a loose connector. For the high shear stress, the flow rate of 20.83 $\mu\text{L/s}$ was achieved which produces a shear stress of 2.0 Pa, which was reproduced multiple times.

To further validate the pumping system, the high shear stress gravity pump was run under sterile conditions in the incubator for two hours. The protocol used to run this validation data is shown in Appendix K. After running the system, the volume collected by the outlet was measured and collected in order to determine the average flow rate. The flow rate was found to be 24.31 $\mu\text{L/s}$ which produced a shear stress on the wall of the microfluidic device to be 2.33 Pa. Data analysis for both gravity pumps were conducted to determine the accuracy of the flow rates produced.

4.9.3 Data Analysis

For the shear stress pumping system to pass validation it must be able to be reproduced and each trial was run within 10% of the target shear stress. The target shear stresses for the pumps were a low of 0.2 Pa and a high of 2.0 Pa. Both pumping systems are able to achieve these metrics. For the low shear stress pump system, three trials were conducted with the average of each trial within 10% of 0.2 Pa, which can be seen in Figure 48. Each data point was collected over a duration of five minutes, taking into account the time between each collection for recording, each trial lasting between 30-45 minutes. The reservoir maintained the pressure head for that duration providing a consistent average flow rate. The average flow rates for the three trials are 2.1 $\mu\text{L/s}$, 1.94 $\mu\text{L/s}$, and 2.03 $\mu\text{L/s}$, respectively.

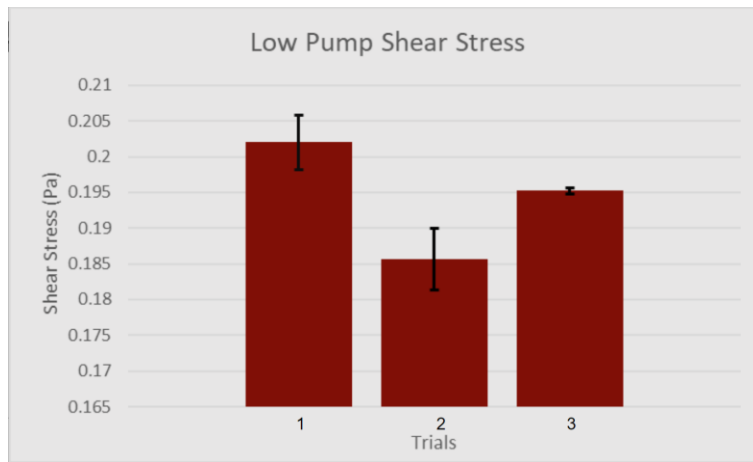


Figure 48. Average shear stress of the low system over three trials (Trial 1: n=4, Trials 2,3: n=5)

The high shear stress system was also able to be reproduced and provide a consistent average flow rate over multiple hours. During the incubator flow test the system was at a height of 60 cm and ran at an average shear stress of 2.33 Pa, which is consistent with the validation data that had an average shear stress of 2.32 Pa. The flow rate for the shear stress of 2.33 Pa is calculated to be 24.2 $\mu\text{L/s}$ theoretically and experimentally was 24.3 $\mu\text{L/s}$. This flow rate was within the 10% margins that was set. Figure 49 is the flow rate data for the high shear stress pumping system at a height of 55.8 cm. There was one outlier, but it can be concluded that the high shear stress pumping system can maintain the needed pressure head and flow rate.

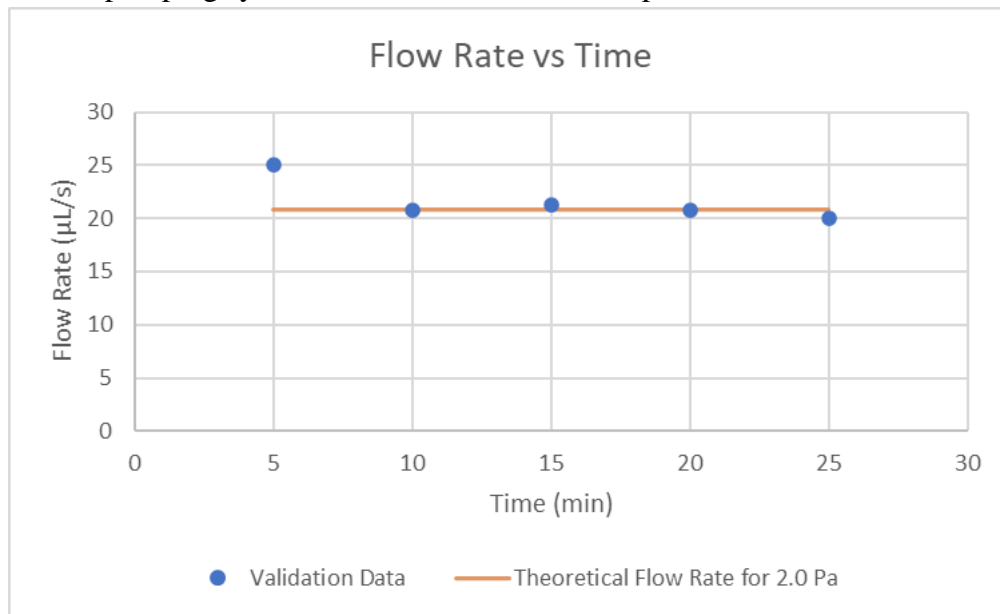


Figure 49. Flow rates of the high shear stress pumping system compared to the theoretical flow rate

6. Final Design

6.1 Microfluidic Designs

All of the device designs were able to retain gel within the gel chamber at some capacity, even those that were modified. In addition, any leakage into the media channels was due to user error during fabrication of the devices or gel placement, causing posts to misshapen or devices to debond from the coverslip, respectively. This means that had there been no user error, all of the devices would have retained gel in some capacity. Given the successes we had with device fabrication and gel retention overall, it is important to narrow down what should be further fabricated and validated.

Breaking it down into success based on design, the AIM Chip, with each modification, performed well. The two designs that performed best were the AIM Chip with an increased spacing of 150 μm and increased post angle to 75°, from 100 μm and 60°, respectively. Both the Polachek and Farahat replicas performed well; however, due to the overwhelming success of the AIM Chip designs, it may be best to not continue these designs. Finally, the Yoon replica and modified version with 100 μm spacing performed well and retained gel. Again, despite its success, moving forward with the AIM Chip designs would be best. Even though these designs should be discontinued in future iterations, there are aspects of the designs that should be incorporated into the AIM Chip designs, the spacing between the posts, in particular. This will aid in maximizing the space between the posts, allowing for an increase of cell migration into the gel chamber.

Focusing on the goal of maximizing space, both post spacing and angle are key. Despite the AIM Chip design with 200 μm post spacing not being entirely successful, the Yoon replica, with a 200 μm post spacing, was successful. This proves that gel can be retained within a chamber with 200 μm spacing between the posts. In addition to the Yoon replica bolstering the results of the AIM Chip with 200 μm spacing, the larger angle in the AIM Chip design proved to retain gel within the gel chamber successfully in all iterations. Given these two successes, with 200 μm post spacing and a 75° post angle, along with the success with devices at a height of 200 μm , it is important to further iterate on and validate these findings. The final set of designs should maintain the base design of the AIM Chip, as it was the most successful base design. Modifications should be made to this base, such as increasing both post spacing and angle; it would be helpful to have replicates of the 200 μm spacing design to ensure that fabrication error is the reason for a lack of gel retention. Testing these iterations of the design with both increased post spacing and post angle would be key to bolstering our findings. This would further validate the findings that gel can successfully be retained in a gel chamber with 200 μm spacing at a height of 200 μm , meaning that the space that cells can migrate through has been increased fourfold compared designs in literature and 1.6 times compared to the plastic AIM Chip. This also means that devices that retain gel can be manufactured in-house, meaning a lower cost per experiment can be more easily achieved.

6.2 Steady Flow Gravity Pumps

At the completion of our project, we designed two steady flow gravity pumps that produce a high and low shear stress similar to the stresses experienced from blood flow through a heart valve. Both gravity pumps consist of an unfiltered T175 flask, a syringe, two Y-connectors, metal connectors, a three-way luer lock, and various tubing. The tubing and Y-connectors are stabilized on a 24 inch by 12 inch acrylic. A recycled pipette tip box cover was attached to the acrylic as well and used to behave as a stand for the microfluidic device. For the low shear stress setup, the tubing connects to the syringe through a blunt-end needle and for the high shear stress setup, the tubing connects to a standard plastic connector. All the tubing dimensions are shown below in Figure 50 and the final high shear stress gravity pump is shown in Figure 51.

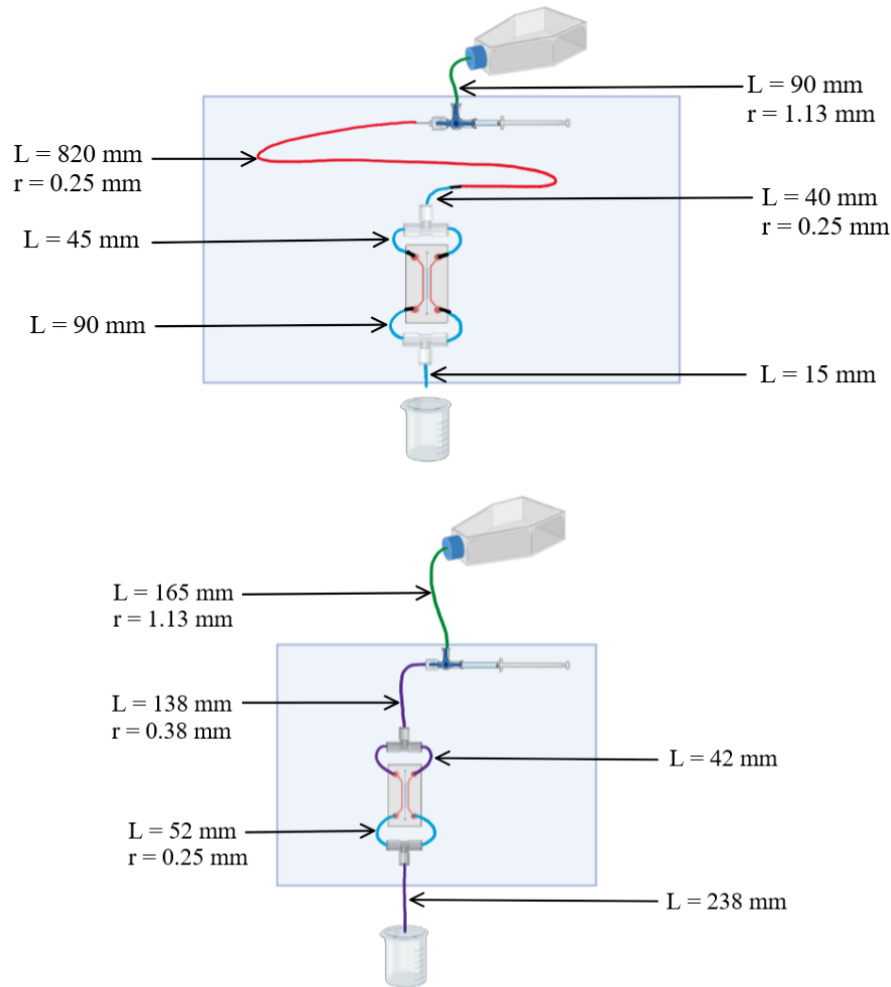


Figure 50. Both final setups for low and high shear stress gravity pumps with tubing dimensions.

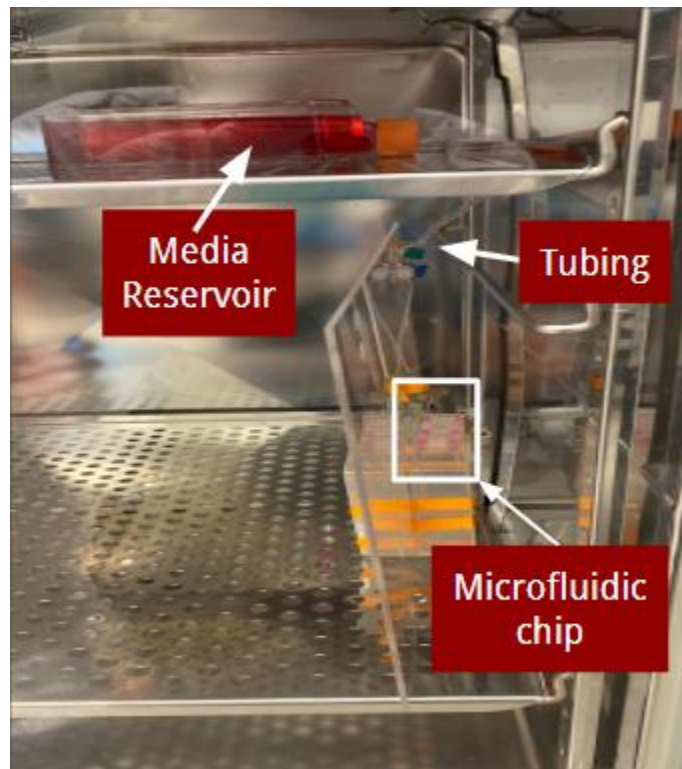


Figure 51. Final setup of high shear stress gravity pump running with the AIM Chip within the incubator.

The height from the reservoir to the outlet was 0.3058 m for the low shear stress and 0.6096 for the high shear stress setup. Both gravity pumps consist of more than one sized tubing as shown in the diagrams in Figure 50. The different colored tubings indicate a different radius or material. The green line indicates a larger silicone tubing used, the red line is a smaller radius of softer silicone tubing, the blue line is the same radius as the red line, however, has a stiffer material, and lastly the purple line is the same material as the softer silicone tubing but has a larger radius. Due to complications when setting up the gravity pump in the incubator the cap was changed to contain a layer of PDMS inside. This helped seal the hole created in the cap and remained sterile. The gravity pumps run for multiple hours within the incubator connected to the AIM Chip and hold the ability to run with our designs made out of PDMS.

6.3 Oscillatory Flow Circuit

The double gravity pump cannot produce oscillatory flow on its own, as it runs on gravity and cannot oscillate media without an external mechanism. To create oscillatory flow using the double gravity pump, four solenoid pinch valves from Clippard (2-Way N.C. Pinch Valve, 0.75" Dia., 0.030" ID-0.065" OD Tubing, 24 VDC) were used. However, these valves need to be programmed to open and close at a rate consistent with 60 to 72 beats per minute, to simulate what cells would experience on the heart valve. To program the valves, an Arduino Uno microprocessor was used. An overview of the circuit is shown in Figure 52, below.

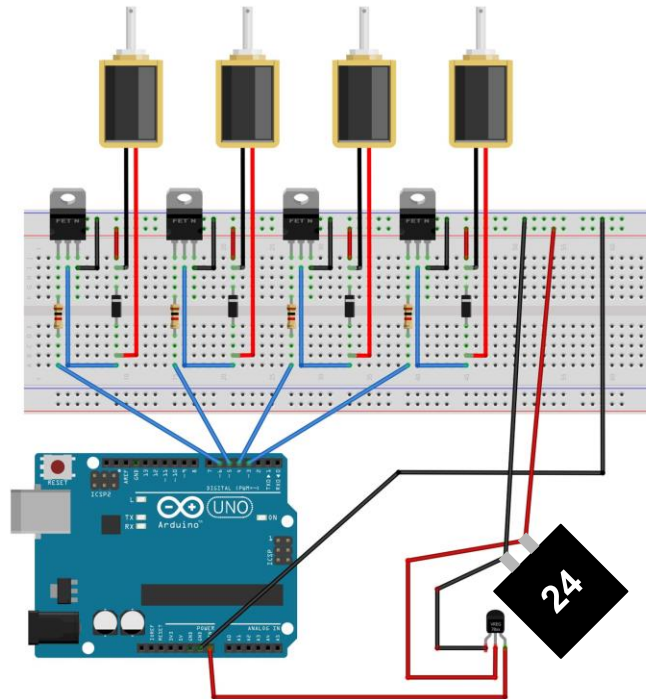


Figure 52: Full Circuit Diagram of Solenoid Pinch Valves in Parallel for Creating Oscillatory Flow

To program the solenoids to open and close at the desired rate, they need to be wired to receive signals from the Arduino Uno and power from a Class Two power supply, which has an input of 120V AC and output of 24 V DC (3Com® 7900-000-044-1.00). They all need to be turned on and off individually, meaning they can be connected in parallel on a breadboard without interference from one another. To turn the valves off, the solenoids are short-circuited, which can damage the rest of the circuit if precautions are not taken. The solenoid is connected directly to the two ends of a 1N4007 Rectifier Diode, to allow for the solenoid valve to be opened and closed without harming the circuit. A diagram of the circuit used for an individual solenoid is shown in Figure 53, below.

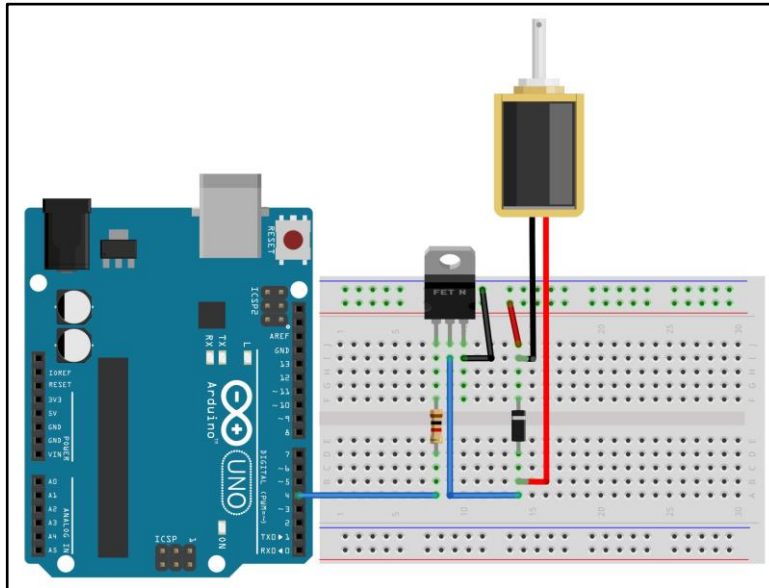


Figure 53: Circuit Diagram for one Solenoid Pinch Valve

The four solenoid valves are set up in parallel and powered by a 24 VDC power source. This power source is split to go into the breadboard and a voltage regulator, which is connected to the Arduino Uno, to ensure that both the solenoid valves and Arduino are powered by the same source. This power source can be plugged into the wall behind the incubator, allowing the solenoid valves to operate and create oscillatory flow while the microfluidic chip is in the incubator. To further explain the power supply, a diagram of the circuit is shown in Figure 54, below. The 24 VDC power source is connected directly into the breadboard, to deliver 20 to 24 V of power to the solenoids. It is also connected to a 7806 6V voltage regulator, which has an input maximum of 35 V. This regulator helps power the Arduino Uno without sending all 20 to 24 V into it.

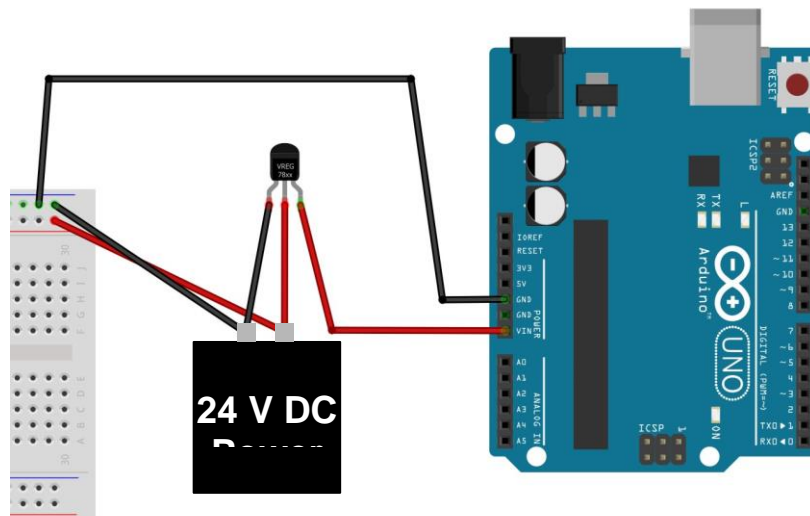


Figure 54: Circuit Diagram for Powering the Breadboard and Arduino Uno

The circuit safely powers all of the solenoid valves, and they operate as expected, turning on and off at a rate of 60 to 72 beats per minute. We discovered that the circuit may need parts

replaced as a result of running it for longer periods of time. The diodes and N-Channel Power MOSFETs are the two parts that may need to consistently be replaced. This may change once a custom circuit is made for the double gravity pump, but using the breadboard, there will need to be parts replaced during its lifetime. Due to this replacement, as well as how the solenoid pinch valves are short-circuited to turn them off, the circuit will need to be monitored to ensure that no issues occur during incubation.

7. Ethical Consideration

We considered all ethical concerns of our project, which we have broken down into eight different categories that can impact our research and outcomes. The categories are economic, environmental, social, global, ethical, health and safety, manufacturability, and sustainability for in vitro studies. Our research aims to aid the improvement of TEHVs; therefore, we considered our own device and its future implications.

7.1 Economic Factors

The majority of the materials used to construct our gravity pump were common materials found around a biological laboratory, but we understand that the total cost of the materials can be expensive. An example of one of the expensive materials was the PDMS kit, which was \$177. We used the following materials to build our gravity pump, Y connectors, solenoid pinch valves, tubing of varying diameters, a breadboard, and an Arduino Uno microprocessor with the necessary circuitry. The creation of the microfluidic device was a two-step process that we outsourced the first step, the photomask, and produced, the second step, the wafer, in-house using photolithography. We understand not everyone has access to photolithography equipment, which would increase the cost of manufacturing. These processes and materials can be costly, and inflation can increase the pricing of tubing, flasks, cell media, etc. Therefore, the cost to create the gravity pump could make this design inaccessible to others. Our reagents, such as cell media, endothelial cells, and PDMS cannot be supplemented for cheaper materials, however the tubing, T175 flasks, and connectors that were used for constructing the gravity pump could be. These materials were chosen because they were readily available and could maintain sterility to house cells and be placed in the incubator. We understand that other labs may use other materials, but these materials met the requirements of our project. We encourage the development of the gravity pump to use cheaper and more accessible equipment for the laboratories that do not have a surplus of extra materials, such as syringes and reservoirs that can be sterilized and reused instead of discarded after each experiment. The results of our project could lead to TEHVs to be further advanced and put on the market for a replacement valve. This would limit the number of surgeries pediatric patients need to undergo and in comparison, reduce the costs of treatment for those families.

7.2 Environmental Impact

The microfluidic chip device used to house the cells is not reusable, causing a small amount of waste after each experiment. Our devices are made of PDMS, and a glass coverslip, utilizing a silicon wafer as a mold. The microfluidic chip device needs to be discarded after one use, since the PDMS cannot be sterilized after injecting cells into the small features. Another device used in this project, the AIM Biotech chip, is made out of plastic which cannot be reused and therefore also needs to be disposed of after one use. However, the silicon wafer used to produce the microfluidic devices can be reused and cast with new PDMS to make more devices.

For the gravity pump, many of the parts can be autoclaved and therefore reused, due to maintaining sterility. The tubing, tubing connectors, Y connectors, reservoir caps, syringes, and the acrylic board can be reused. However, the T175 flasks cannot be reused, therefore after running the experiment, they would need to be disposed of. The Arduino Uno microprocessor and wires would not need to be changed after initial setup. All of these components may need to be replaced after some time, however not often. However, a significant number of materials are in single use therefore everything should be used with proper care to limit the amount of waste. Additionally, all products that do result in waste need to be disposed of properly using the correct guidelines. Such as, all biological waste, which needs to be disposed of properly in the correct hazardous waste containers.

Since our project functions on a microscopic scale the quantity of waste is small, even with multiple components being single use. We use fibrin, which is the result of bleeding of a cow, therefore even though our project does not include animal testing we recognize the concerns of animal cruelty and follow all correct procedures of care and try to limit the use of fibrin waste.

7.3 Social Influence

The research of TEHV can be improved by utilizing this gravity pump and microfluidic device. The system as a whole aims to help understand the migration of cells and how stress from flow affects them. By determining how cells repopulate TEHV, it can help these valves become a safe replacement heart valve for children and adults in the future. Even though TEHV are primarily more favored for use in children, they will be available for adults as well. Since current replacements require the use of blood thinners, and it is not ideal for adults with normal to low blood pressure to take that particular medication, therefore TEHVs will be ideal for adults with a stable blood pressure. TEHV could also be used for heart disease treatment in adults. The result of our project can help limit the amount of valve replacement surgeries, therefore providing more opportunity for other surgeries. By reducing the amount of surgeries, there is a smaller amount of donated blood being used as well. Our project does not directly cost patients, however in the future it is anticipated that TEHV replacements may be expensive, making them inaccessible for some marginalized population. More research about how to improve TEHV replacements could potentially lower the cost and increase the accessibility of TEHV due to larger supply. The development of our microfluidic device and gravity pump followed all the

rules and regulations set for PDMS models and fluidic devices. Overall, this project can help further the research of TEHV and improve the treatment for heart disease of all ages.

7.4 Global Ramifications

Our microfluidic device and gravity pump are designed so that all laboratories that study TEHVs can recreate the system. With this research, TEHVs can be improved so that people with heart disease will undergo less invasive surgeries. Our project could lead to TEHV replacements becoming more accessible to those in poorer communities, especially children, limiting the number of surgeries a person needs. In addition, with the idea that blood thinners will not be required, a reduced cost of medication can help a wider population to have a successful heart valve replacement for a longer period of time. There is a chance different materials or parts of the procedure of making the microfluidic device may need to be delivered or outsourced, however with our procedure that is posted online, all parts of the system can be constructed. Any computer aided design (CAD) drawings were done with ISO standards to ensure accessibility outside of the United States. Since the pumping system is a gravity pump, as long as the user can accommodate the needed height to maintain flow in their incubator, the temperature and environment can be controlled in the same way that our project was designed for. Also, for our design we focused on endothelial cells of humans, which is globally what has been used to study EndMT.

A. Ethical Concerns

The result of our project can address a good and satisfying life for those that need heart valve replacements. By using our microfluidic bioreactor, TEHV can be studied and improved upon until it can be put on the market. After TEHVs are considered a viable option for valve replacements, there is possibility that these patients will undergo less invasive surgeries in a lifetime. In addition, the patients would not need to be on blood thinners and could continue to live an active lifestyle without concerns. With the possibility of TEHVs, it could improve many lives of adults and children that need to undergo a heart valve replacement.

B. Health and Safety Issues

The personal health and safety of patients would be improved with the result of our project. TEHVs should limit the amount of possible blood clots even without the patients needing to be on blood thinners. Also, patients with healthy blood pressure do not necessarily need to be on blood thinner medications, so when they are forced to due to valve replacement surgery, it can cause possible complications. In addition, further research for TEHV holds the possibility for these patients to undergo less surgeries and increase their quality of life, such as being able to exercise on a regular basis.

C. Manufacturability

Overall, our microfluidic bioreactor is fairly easy to reproduce in other laboratories. For the gravity pumps, the materials are all commonly found in a laboratory, such as the tubing, tubing connectors, syringe, unfiltered T175 flasks, and Y connectors. Since our product is not strict on what kind of tubing is needed, it allows more variability to reuse tubing from the place

of work that will be creating the pump. The photomask and wafer could be a little more difficult to reproduce, as not every lab has access to companies that can manufacture a photomask or access to photolithography. However, with time it is possible to outsource these things to be made as well as order online anything that may be missing, therefore our design is reproducible.

D. Sustainability

Currently, the steady flow gravity pumps and microfluidic devices do not require energy, however, to produce oscillatory flow a DC power supply is used. In the future, to address this, the power could come from a different method, such as solar or possible fluid flow, in order to use renewable energy to run the bioreactor.

8. Discussion

8.1 Imaging

An important parameter for the microfluidic device is the ability to image cell infiltration from the fluid channels into the gel matrix. The ability to image this cell infiltration is of paramount importance as it allows the user of this device to examine and observe the effect that shear stresses have on cell infiltration and migration. The imaging ability allows the user to observe how cell behavior changes after being exposed to various mechanical forces. The microfluidic devices that were designed possess the ability to image cell infiltration and migration, however we did not validate this.

8.2 Accuracy and Reproducibility

To maintain consistency between experiments each component of the bioreactor needed to be able to reproduce our target parameters. Both the high and low shear stress systems must be able run within 10% of the shear stresses of 0.2 Pa and 2.0 Pa for the entirety of the experiment. The low and high shear stress systems were validated to be able to run at the needed flow rates to achieve being within the goal shear stresses. The systems were run for multiple trials and were within 10% of 0.2 Pa and 2.0 Pa. The microfluidic devices are accurate and reproducible as well, as the wafer has been made and can create devices that retain the gel. If the protocols are followed properly then the microfluidic devices can be recreated with the same degree of accuracy every time. Therefore, the microfluidic bioreactor can run tests that are accurate and reproducible.

8.3 High Throughput

One of the parameters that apply to both the pump and microfluidic device is high throughput. Considering this parameter for the pump, high throughput is whether the pump can push media through multiple microfluidic devices. In its current state, the pump can only push media through one microfluidic device, as it has enough connectors to connect to each inlet and

outlet of the media channels in one device, four. The addition of more tubing and connectors would allow for more throughput; however, the reservoir may not be able to support the throughput, as the pump goes through media quickly, and the media cannot be recycled.

The microfluidic device itself would be considered high throughput if a multitude of replicates can be done within one device. As of right now, this is not the case. Only one replicate can be done per device. However, given what we had learned about gel retention, devices can be further validated and modified to fit this parameter in the future. In addition, once the devices have been validated, soft lithography will have high throughput, as up to nine devices can be manufactured. The work done here may not have provided high throughput for the pump and microfluidic device, but a foundation has been put in place for accomplishing the creation of a high throughput pump and microfluidic device.

8.4 Shear Stresses

Two shear stress pumping systems were created to achieve the goal of being able to produce a range of shear stress between 0.2 Pa and 2.0 Pa, with those being our target shear stresses. The low pumping system produces low shear stresses and is designed to produce a shear stress that is within 0.18 Pa and 0.22 Pa. The high pumping system is designed to produce a shear stress that is within 1.8 Pa and 2.2 Pa, but has achieved shear stresses as large as 2.5 Pa. We concluded that we have designed a system that can achieve a wide range of shear stress.

8.5 Compact and Contained

The microfluidic bioreactor was able to fit within the incubator without taking up more than half of the space. The shear stress pumping system tubing fits on a ¼ inch thick and 12 inches high piece of acrylic. The entire system can be placed in the incubator in two pieces with the reservoir, acrylic, tubing, and microfluidic chip being one section and a collection reservoir as the second piece to be placed in the incubator. Due to the system taking up minimal space within the incubator and a small number of sections the microfluidic bioreactor met the parameter of being compact.

8.6 Ease of Use

The microfluidic bioreactor designed achieved many parameters, however we determined that the ease of use needs to be improved on. The gravity pumps have many factors involved during setup to ensure a successful experiment, including making sure all the connectors are tight, the reservoir cap is secured, and everything is completely sterile. In addition, the fabrication of the microfluidic devices requires many days of work, such as photolithography, soft lithography, and plasma bonding. The gel placement in our devices also requires a lot of attention and focus as too much pressure can cause the gel to spill into the media channels or cause the devices to debond from the glass coverslip. Due to the required careful attention and multiple steps to producing and setting up the microfluidic bioreactor we determined that the designs do not meet the criteria for ease of use.

8.7 Overall Cost

Overall, the gravity pumps were inexpensive, due to the use of reusing various materials around the laboratory and being able to autoclave nearly everything. By being able to autoclave the materials everything can be used multiple times for more than one experiment under sterile conditions. However, the microfluidic device is not as cheap to produce. The cost of fabricating the photomask is fairly expensive, however should only be required once as the photomask can be reused many times. Photolithography and the use of SU-8 is also quite expensive, however if fluorinated the silicon wafer can be reused and if the photomask is improved upon three of each design could be produced using the wafer. If done correctly the amount of PDMS required to perform soft lithography on the wafer is not a raise for concern especially if the wafer consists of three devices for each design. To fully run the microfluidic bioreactor, 600 mL of cell media is necessary to run for many hours, which can add up in price, however if used responsibly not much waste is necessary, as the leftover cell media should be able to be saved if all precautions are taken. Overall, the pricing of the microfluidic bioreactor is fairly expensive, however most of the materials can be reused.

8.8 Cost Breakdown

The total cost to complete our project was \$1,089.43. The largest cost was the supplies and space to manufacture the wafer, billed at \$685. The two replacement solenoids cost \$118.78, which were purchased from Clippard. Additional tubing was also purchased from Clippard for \$30.30. To create the microfluidic chip, we used PDMS that cost \$177.50 from Ellsworth Adhesive. Parts for the circuit were purchased from Digikey and Amazon for a total of \$64.85. The final cost was for the acrylic, which was bought from the Innovation Studio makerspace, for \$13.

8.9 Future Research Impacts

We hope this project helps further the research in tissue-engineered heart valves. By running our gravity pumps through our seeded microfluidic devices, the study of how cells repopulate the matrix of a decellularized TEHV can be observed. By understanding the process of repopulation as well as how blood flow affects the cellular response within the device, TEHVs can be further advanced and improved in order to take a step closer to being successfully implanted into patients.

9. Future Considerations

To advance this project for the study of cell migration under shear fluid flow, additional steps are needed. For the microfluidic bioreactor design, the next steps include further validation of both the PDMS microfluidic devices and the double gravity pump for oscillatory flow.

The microfluidic devices need further testing for reproducibility for reliably containing the gel as well as allowing for cells to be seeded on the gel surface. These steps also need validation with aseptic technique. Modifications to the silicon wafer design is recommended, as the three designs that were successful at retaining gel should be recreated so that there are three copies of each design on the wafer. This will improve the throughput of the process and decrease the amount of waste and time spent on creating the devices. Including decellularized matrix rather than a fibrin gel into the gel chamber will create a more accurate model of a TEHV, where cells can be seeded into the media channels and then introduced to fluid flow.

The double gravity pump also needs further validation, especially running it within the incubator for over 12 hours. This would be advantageous to the overall validation process of the project, as this can test the sterility. A full experiment of cell migration can be also be conducted. Also, after validating the double gravity pump, the cells could be introduced to both steady and oscillatory flow similar to the environment of a heart valve.

10. Conclusions

We were able to create a microfluidic bioreactor that produced a high range of shear stresses and maximized the space to observe cellular migration. To achieve the low shear stress of 0.2 Pa and the high shear stress of 2.0 Pa, two gravity pumps that produce steady flow were created that met the dimension constraints of the incubator, while maintaining an accurate and consistent flow rate. The microfluidic chip was able to contain the gel matrix within the central gel chamber at a height of 200 μm and a post spacing of 200 μm . These features exceeded the other microfluidic chips found in literature that are used for other applications. The previous designs found were not ideal for our project, as we needed to maximize the space for cell infiltration. We successfully increased the space within the gel chamber, while retaining the gel, to maximize the area four times compared to the literature that has been published. This increase in the space, in addition to the production of the steady flow gravity pumpes, allowed us to use the microfluidic device to achieve our project goal of being able to observe cell migration under fluid flow conditions.

References

- Ahmed, M. (2017, August 21). Heart Valve Surgery - Mechanical Vs. Bioprosthetic – Which Is Better? • MyHeart. MyHeart. <https://new.myheart.net/articles/heart-valve-surgery-mechanical-vs-bioprosthetic-which-is-better/>
- Aikawa, E., Whittaker, P., Farber, M., Mendelson, K., Padera, R. F., Aikawa, M., & Schoen, F. J. (2006). Human semilunar cardiac valve remodeling by activated cells from fetus to adult: implications for postnatal adaptation, pathology, and tissue engineering. *Circulation*, *113*(10), 1344–1352. <https://doi.org/10.1161/CIRCULATIONAHA.105.591768>
- AIM Biotech. (2022, May 12). <https://aimbiotech.com/>
- Blackman , B. R., García-Cardena , G., and Gimbrone, M. A., Jr. (July 30, 2002). "A New In Vitro Model to Evaluate Differential Responses of Endothelial Cells to Simulated Arterial Shear Stress Waveforms ." *ASME. J Biomech Eng. August 2002; 124*(4): 397–407. <https://doi.org/10.1115/1.1486468>
- Blum, K. M., Drews, J. D., & Breuer, C. K. (2018). Tissue-Engineered Heart Valves: A Call for Mechanistic Studies. *Tissue Engineering. Part B, Reviews*, *24*(3), 240-253. <https://doi.org/10.1089/ten.teb.2017.0425>
- Brown, K. N., & Kanmanthareddy, A. (2022). Aortic Valve Ross Operation. In, *StatPearls*. StatPearls Publishing.
- Butcher, J. T., Mahler, G. J., & Hockaday, L. A. (2011). Aortic valve disease and treatment: The need for naturally engineered solutions. *Advanced Drug Delivery Reviews*, *63*(4), 242–268. <https://doi.org/10.1016/j.addr.2011.01.008>
- Chen, M. B., Whisler, J. A., Jeon, J. S., & Kamm, R. D. (2013). Mechanisms of tumor cell extravasation in an in vitro microvascular network platform. *Integrative biology : quantitative biosciences from nano to macro*, *5*(10), 1262–1271. <https://doi.org/10.1039/c3ib40149a>
- Centers for Disease Control and Prevention, National Center for Health Statistics. Underlying Cause of Death 1999-2017 on CDC WONDER Online Database, released December, 2018. Accessed at <http://wonder.cdc.gov/ucd-icd10.html> on Oct 24, 2019.
- Cukierman, E., Pankov, R., Stevens, D. R., & Yamada, K. M. (2001). Taking cell-matrix adhesions to the third dimension. *Science (New York, N.Y.)*, *294*(5547), 1708–1712. <https://doi.org/10.1126/science.1064829>
- Dai, G., R., M., Natarajan, S., Zhang, Y., Vaughn, S., Blackman, B. R., Kamm, R. D., & Gimbrone, M. A. (2004). Distinct endothelial phenotypes evoked by arterial waveforms derived from atherosclerosis-susceptible and -resistant regions of human vasculature.

Proceedings of the National Academy of Sciences, 101(41), 14871-14876.
<https://doi.org/10.1073/pnas.0406073101>

- Duraiyan, J., Govindarajan, R., Kaliyappan, K., & Palanisamy, M. (2012). Applications of immunohistochemistry. *Journal of Pharmacy & Bioallied Sciences*, 4(Suppl 2), S307.
<https://doi.org/10.4103/0975-7406.100281>
- Evrard, S. M., Lecce, L., Michelis, K. C., Nomura-Kitabayashi, A., Pandey, G., Purushothaman, K.-R., d'Escamard, V., Li, J. R., Hadri, L., Fujitani, K., Moreno, P. R., Benard, L., Rimmele, P., Cohain, A., Mecham, B., Randolph, G. J., Nabel, E. G., Hajjar, R., Fuster, V., ... Kovacic, J. C. (2016). Endothelial to mesenchymal transition is common in atherosclerotic lesions and is associated with plaque instability. *Nature Communications*, 7(1). <https://doi.org/10.1038/ncomms11853>
- Farahat, W. A., Wood, L. B., Zervantonakis, I. K., Schor, A., Ong, S., Neal, D., Kamm, R. D., & Asada, H. H. (2012). Ensemble Analysis of Angiogenic Growth in Three-Dimensional Microfluidic Cell Cultures. *PLOS ONE*, 7(5), e37333.
<https://doi.org/10.1371/journal.pone.0037333>
- Fioretta, E. S., Motta, S. E., Lintas, V., Loerakker, S., Parker, K. K., Baaijens, F. P. T., Falk, V., Hoerstrup, S. P., & Emmert, M. Y. (2021). Next-generation tissue-engineered heart valves with repair, remodelling and regeneration capacity. *Nature Reviews Cardiology*, 18(2), Article 2. <https://doi.org/10.1038/s41569-020-0422-8>
- Fishbein, G. A., & Fishbein, M. C. (2019). Tricuspid and pulmonic valve pathology. *Current Cardiology Reports*, 21(7). <https://doi.org/10.1007/s11886-019-1143-7>
- Gandaglia, A., Bagno, A., Naso, F., Spina, M., & Gerosa, G. (2011). Cells, scaffolds and bioreactors for tissue-engineered heart valves: A journey from basic concepts to contemporary developmental innovations. *European Journal of Cardio-Thoracic Surgery*, 39(4), 523–531. <https://doi.org/10.1016/j.ejcts.2010.07.030>
- Girard, P.R. and Nerem, R.M. (1995), Shear stress modulates endothelial cell morphology and F-actin organization through the regulation of focal adhesion-associated proteins. *J. Cell. Physiol.*, 163: 179-193. <https://doi.org/10.1002/jcp.1041630121>
- Gopal S, Hauser JM, Mahboobi SK. (2022) Mechanical Aortic Valve Replacement. StatPearl publishing. <https://www.ncbi.nlm.nih.gov/books/NBK564339/>
- Hajal, C., Ibrahim, L., Serrano, J. C., Offeddu, G. S., & Kamm, R. D. (2021). The effects of luminal and trans-endothelial fluid flows on the extravasation and tissue invasion of tumor cells in a 3D in vitro microvascular platform. *Biomaterials*, 265, 120470.
<https://doi.org/10.1016/j.biomaterials.2020.120470>

- Hari Priya, C., Divya, M., & Ramachandran, B. (2020). Recent investigation on biomaterial based tissue engineered heart valve (TEHV). *Materials Today: Proceedings*, 33, 4467–4478. <https://doi.org/10.1016/j.matpr.2020.07.712>
- Harris, C., Croce, B., & Coa, C. (2015). Tissue and mechanical heart valves. *Annals of Cardiothoracic Surgery*, 4(4), 399. <https://doi.org/10.3978%2Fj.issn.2225-319X.2015.07.01>
- Hasan, A., Ragaert, K., Swieszkowski, W., Selimović, Š., Paul, A., Camci-Unal, G., Mofrad, M. R. K., & Khademhosseini, A. (2014). Biomechanical properties of native and tissue engineered heart valve constructs. *Journal of Biomechanics*, 47(9), 1949–1963. <https://doi.org/10.1016/j.jbiomech.2013.09.023>
- Hinton, R. B., & Yutzey, K. E. (2011). Heart valve structure and function in development and disease. *Annual Review of Physiology*, 73(1), 29–46. <https://doi.org/10.1146/annurev-physiol-012110-142145>
- Kaushik, R., Mani, A., Ganapathi, S., Pillai, V. V., Jayakumar, K., & S, H. (2022). Clinical outcomes of Bileaflet St. Jude Medical and tilting disc ttk Chitra mechanical heart valve prosthesis: A comparative study. *Journal of Cardiac Surgery*, 37(8), 2367–2374. <https://doi.org/10.1111/jocs.16605>
- Kodigepalli, K. M., Thatcher, K., West, T., Howsmon, D. P., Schoen, F. J., Sacks, M. S., Breuer, C. K., & Lincoln, J. (2020). Biology and biomechanics of the heart valve extracellular matrix. *Journal of Cardiovascular Development and Disease*, 7(4), 57. <https://doi.org/10.3390/jcdd7040057>
- Kostyunin, A., Yuzhalin, A., Rezvova, M., Ovcharenko, E., Glushkova, T., Kutikhin, A., (2020). Degeneration of Bioprosthetic Heart Valves. *Journal of the American Heart Association*. 9(19). <https://doi.org/10.1161/JAHA.120.018506>
- Kovacic, J. C., Dimmeler, S., Harvey, R. P., Finkel, T., Aikawa, E., Krenning, G., & Baker, A. (2019). Endothelial to Mesenchymal Transition in Cardiovascular Disease. *Journal of the American College of Cardiology*, 73(2), 190. <https://doi.org/10.1016/j.jacc.2018.09.089>
- Kovacic, J. C. (2018). The endothelial-metabolic axis: a novel cardiometabolic disease target. *Trends in endocrinology and metabolism: TEM*, 29(8), 527. <https://doi.org/10.1016/j.tem.2018.03.015>
- Krenning, G., Moonen, J.-R. A. J., van Luyn, M. J. A., & Harmsen, M. C. (2008). Vascular smooth muscle cells for use in vascular tissue engineering obtained by endothelial-to-mesenchymal transdifferentiation (ENMT) on collagen matrices. *Biomaterials*, 29(27), 3703–3711. <https://doi.org/10.1016/j.biomaterials.2008.05.034>
- Lincoln, J., & Garg, V. (2014). Etiology of Valvular Heart Disease. *Circulation Journal*, 78(8), 1801–1807. <https://doi.org/10.1253/circj.CJ-14-0510>

- Maganti, K., Rigolin, V. H., Sarano, M. E., & Bonow, R. O. (2010). Valvular heart disease: Diagnosis and management. *Mayo Clinic Proceedings*, 85(5), 483–500. <https://doi.org/10.4065/mcp.2009.0706>
- Mahler, G.J., Frenzl, C.M., Cao, Q. & Butcher, J.T. (2014). Effects of shear stress pattern and magnitude on mesenchymal transformation and invasion of aortic valve endothelial cells. *Biotechnology & Bioengineering*, 111(11), 2326-2337. <https://doi.org/10.1002/bit.25291>
- Manji, R. A., & Manji, J. S. (2020). Studying xenograft rejection of bioprosthetic heart valves. *Xenotransplantation*, 227–243. https://doi.org/10.1007/978-1-0716-0255-3_15
- Mendelson, K., & Schoen, F. J. (2006). Heart valve tissue engineering: Concepts, approaches, progress, and challenges. *Annals of Biomedical Engineering*, 34(12), 1799–1819. <https://doi.org/10.1007/s10439-006-9163-z>
- Meng, F., Cheng, H., Qian, J., Dai, X., Huang, Y., & Fan, Y. (2022). In vitro fluidic systems: Applying shear stress on endothelial cells. *Medicine in Novel Technology and Devices*, 15, 100143. <https://doi.org/10.1016/j.medntd.2022.100143>
- Mohammadi, H., & Fradet, G. (2017). Oval housing for the St. Jude Medical bileaflet mechanical heart valve. *Proceedings of the institution of mechanical engineers, part H: journal of engineering in medicine*, 231(10), 982-986. <https://doi.org/10.1177/0954411917719742>
- Moonen, J.-R. A. J., Krenning, G., Brinker, M. G. L., Koerts, J. A., van Luyn, M. J. A., & Harmsen, M. C. (2010). Endothelial progenitor cells give rise to pro-angiogenic smooth muscle-like progeny. *Cardiovascular Research*, 86(3), 506–515. <https://doi.org/10.1093/cvr/cvq012>
- Motta, S. E., Fioretta, E. S., Lintas, V., Dijkman, P. E., Hilbe, M., Frese, L., Cesarovic, N., Loerakker, S., Baaijens, F. P. T., Falk, V., Hoerstrup, S. P., & Emmert, M. Y. (2020). Geometry influences inflammatory host cell response and remodeling in tissue-engineered heart valves in-vivo. *Scientific Reports*, 10, 19882. <https://doi.org/10.1038/s41598-020-76322-9>
- Neuenschwander, S., & P. Hoerstrup, S. (2004). Heart valve tissue engineering. *Transplant Immunology*, 12(3), 359–365. <https://doi.org/10.1016/j.trim.2003.12.010>
- Nishimura, R. A. (2002). Aortic valve disease. *Circulation*, 106(7), 770–772. <https://doi.org/10.1161/01.cir.0000027621.26167.5e>
- O'Donnell, A., & Yutzey, K. E. (2020). Mechanisms of heart valve development and disease. *Development*, 147(13). <https://doi.org/10.1242/dev.183020>
- Otto, C. M., & Bonow, R. O. (2021). Valvular heart disease: A companion to braunwald's heart disease. Elsevier.

- Polacheck, W. J., German, A. E., Mammoto, A., Ingber, D. E., & Kamm, R. D. (2014). Mechanotransduction of fluid stresses governs 3D cell migration. *Proceedings of the National Academy of Sciences*, *111*(7), 2447–2452. <https://doi.org/10.1073/pnas.1316848111>
- Polacheck, W. J., Kutys, M. L., Tefft, J. B., & Chen, C. S. (2019). Microfabricated blood vessels for modeling the vascular transport barrier. *Nature protocols*, *14*(5), 1425. <https://doi.org/10.1038/s41596-019-0144-8>
- Rosenthal, N., & Harvey, R. P. (Eds.). (2010). *Heart Development and Regeneration (Vol. 1)*. Elsevier/Academic Press.
- Scott, S. M., & Ali, Z. (2021). Fabrication Methods for Microfluidic Devices: An Overview. *Micromachines*, *12*(3). <https://doi.org/10.3390/mi12030319>
- Syedain, Z. H., Haynie, B., Johnson, S. L., Lahti, M., Berry, J., Carney, J. P., Li, J., Hill, R. C., Hansen, K. C., Thiruvikraman, G., Bianco, R., & Tranquillo, R. T. (2021). Pediatric tri-tube valved conduits made from fibroblast-produced extracellular matrix evaluated over 52 weeks in growing lambs. *Science Translational Medicine*, *13*(585), eabb7225. <https://doi.org/10.1126/scitranslmed.abb7225>
- Vesely, I. (2003). The evolution of bioprosthetic heart valve design and its impact on durability. *Cardiovascular Pathology*, *12*(5), 277-286. [https://doi.org/10.1016/s1054-8807\(03\)00075-9](https://doi.org/10.1016/s1054-8807(03)00075-9)
- Vlaming, A. D., Sauls, K., Hajdu, Z., Visconti, R., Mehesz, A. N., Levine, R. A., Slaughaupt, S. A., Hagege, A., Chester, A., Markwald, R. R., & Norris, R. A. (2012). Atrioventricular Valve Development: New Perspectives on an Old Theme. *Differentiation; Research in Biological Diversity*, *84*(1), 103. <https://doi.org/10.1016/j.diff.2012.04.001>
- Xue, Y., Sant, V., Phillippi, J., & Sant, S. (2017). Biodegradable and biomimetic elastomeric scaffolds for tissue-engineered heart valves. *Acta Biomaterialia*, *48*, 2–19. <https://doi.org/10.1016/j.actbio.2016.10.032>
- Yoon, D., Kim, H., Lee, E., Park, M. H., Chung, S., Jeon, H., Ahn, C.-H., & Lee, K. (2016). Study on chemotaxis and chemokinesis of bone marrow-derived mesenchymal stem cells in hydrogel-based 3D microfluidic devices. *Biomaterials Research*, *20*(1), 25. <https://doi.org/10.1186/s40824-016-0070-6>
- Yun, B. M., Aidun, C. K., & Yoganathan, A. P. (2014). Blood Damage Through a Bileaflet Mechanical Heart Valve: A Quantitative Computational Study Using a Multiscale Suspension Flow Solver. *Journal of Biomechanical Engineering*, *136*(10), 1010091-10100917. <https://doi.org/10.1115/1.4028105>

Zhu, A. S., & Grande-Allen, K. J. (2018). Heart valve tissue engineering for valve replacement and disease modeling. *Current Opinion in Biomedical Engineering*, 5, 35– 41.
<https://doi.org/10.1016/j.cobme.2017.12.006>

Appendices

Appendix A: Contact Angle Study Protocol

Purpose: Determine the contact angle of the gel being placed into the microfluidic devices to inform the angles of the trapezoidal posts within the gel channel

Materials:

- DI Water
- PDMS Squares
- Petri dishes
- Glass coverslips
- Fibrinogen
 - Stock is 16.7 mg/mL
 - Stored in -20, keep on ice
- Thrombin
 - Stock is 25 units/mL
 - Stored in -80, keep on ice, most temp sensitive
- Gel
 - 4 mg/mL fibrinogen
 - 0.38 U/mL thrombin
 - Cell media
 - Total 300 μ L needed

Methods:

Optimizing Procedure: [No Hood]

1. Obtain 300 μ L of DI Water, a coverslip, a cell culture plate, and a PDMS square
2. Practice pipetting 10 μ L of water onto each surface
3. Practice taking photos with a phone and camera
4. Update values in the following procedure with what works best for the purpose of this experiment

Gel Solution: [In Hood]

1. Make 150 μ L of 8 mg/mL fibrinogen solution $(16.7\text{mg/mL})X=(8\text{mg/mL})(150\text{uL})$
 - a. Combine 71.86 μ L fibrinogen stock solution with 78.14 μ L DPBS.
2. Make 75 μ L of 1.52 U/mL thrombin solution $(25\text{U/mL})X=(1.52\text{U/mL})(75\text{uL})$
 - a. Combine 4.56 μ L thrombin stock solution with 70.44 μ L DPBS.
3. Add 75 μ L of cell media to thrombin solution

Contact Angle: [In Hood until Step 5]

1. Obtain PDMS squares, cell culture plates, glass coverslips, gel components

2. Take 5 μL of fibrinogen solution and 5 μL of thrombin solution and mix quickly in microcentrifuge tube
3. Place droplet on surface
4. Trials should be set up as follows:

	Cell Culture Plate	Coverslip	PDMS Square
<u>No Incubation</u>	Break in half; 2-3 drops per half	Place in cell culture plate; 4 drops on slip	Place in cell culture plate; 2 drops per square
<u>Incubation</u>	4 drops on plate	Place in cell culture plate; 4 drops on slip	Place in cell culture plate; 2 drops per square

- a. $\sim 10 \mu\text{L}$ for each droplet
 - b. 1 set of conditions will be immediately after droplets placed
 - c. 1 set of conditions will be after 1 hour of incubation
 - d. For each condition, 5 droplets will be placed for examination
5. Take a photo of the droplet (phone or camera)
- Examine it using imageJ (contact angle between droplet and surface)

Appendix B: Contact Angle Datasheet

Contact Angle Data							
Trial	Condition	Before/After Incubation	Angle of Droplet 1 (°)	Angle of Droplet 2 (°)	Angle of Droplet 3 (°)	Average	Standard Deviation
1	Petri Dish	Before	130	138	145	138	8
2	Coverslip	Before	135	146	132	138	7
3	PDMS	Before	104	110	105	106	3
4	Petri Dish	After	147	141	138	142	5
5	Coverslip	After	144	142	141	142	2
6	PDMS	After	85	85	89	86	2
Differences b/w Conditions		Recommended Angle of Posts					
After Angle [°] - Before Angle [°] = Δ [°]		$180^\circ - \text{Contact Angle } (\theta_c) [^\circ] = \text{Recommended Angle } (\theta_r) [^\circ]$					
Petri	5		1	2	3	Average	Standard Deviation
Coverslip	5	PDMS Before	76	70	75	74	3
PDMS	-52	PDMS After	95	95	91	94	2
Overall Avg						84	

Appendix C: Gravity Pump Validation Procedure

Purpose: Validate the gravity pump system for desired BPM and flow rates

Materials:

1. Gravity Pump
 - a. 2 30 mL syringes
 - i. With plunger removed (used as pressure wells)
 - b. Priming syringes
 - c. 2 3-way valves
 - d. 2 solenoid valves
 - e. 2 y connectors
 - f. Tubing of various sizes
 - g. Metal fittings
2. Timer
3. Graduated Cylinder
4. Water

Methods:

1. Prime the entirety of the gravity pump
 - a. See Appendix K for Steady Flow Gravity Pump SOP
2. Modify Arduino code to maintain desired BPM
 - a. To change the code modify $x = \#$ milliseconds
 - b. Range of BPM (within 10% of desired)
 - i. For lowest: 60 BPM [54-66]
 - ii. For highest: 72 BPM [65-79]
3. Open three-way valves
4. Power the Arduino for the solenoid valves to start
5. Start timer
6. Allow gravity pump to run for 5 minutes
7. Collect outlet volume using a graduated cylinder
8. Calculate the flow rate and shear stress
9. Repeat steps 2-8, if starting after considerable time following previous experiment, reprime system if issues occur

Appendix D: Pump Calculations

Flow rate calculation for the theoretical shear stresses of 0.2 Pa and 2.0 Pa on the wall of the microfluidic device in the AIM Biotech Chip:

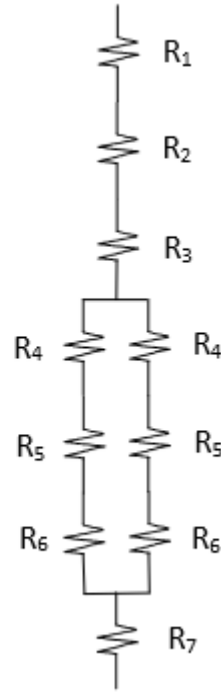
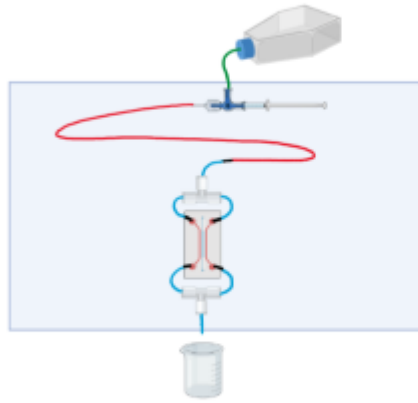
Variable	Symbol	Value
Flow rate	Q	Unknown
Shear stress	τ	0.2 Pa or 2.0 Pa
Width of media channel	w	0.5 mm
Height of microfluidic device	h	0.25 mm
Dynamic viscosity of fluid	μ	0.001 Pa*s

$$Q = \frac{\tau h^2 w}{6\mu} \rightarrow Q = \frac{\tau w^2 h}{6\mu} \rightarrow \frac{(0.2 \text{ Pa}) * (0.5 \text{ mm})^2 * (0.25 \text{ mm})}{6 * (0.001 \text{ Pa} * \text{s})} = 2.08 \frac{\text{mm}^3}{\text{s}} = 2.08 \frac{\mu\text{L}}{\text{s}}$$

$$Q = \frac{\tau h^2 w}{6\mu} \rightarrow Q = \frac{\tau w^2 h}{6\mu} \rightarrow \frac{(2.0 \text{ Pa}) * (0.5 \text{ mm})^2 * (0.25 \text{ mm})}{6 * (0.001 \text{ Pa} * \text{s})} = 20.8 \frac{\text{mm}^3}{\text{s}} = 20.8 \frac{\mu\text{L}}{\text{s}}$$

Resistance calculations for low shear stress gravity pump:

Variable	Symbol	Value
Resistance	R	Unknown
Dynamic viscosity of fluid	μ	0.001 Pa*s
Length of tubing/channel	L	Dependent
Inner radius of tubing	r	Dependent
Height of pumping system from output	h	0.3048 m
Density of fluid	ρ	997 kg/m ³
Acceleration of gravity	g	9.81 m/s ²



R_1 = Clear tubing from reservoir to syringe ($r = 1.13$ mm)

$$R_1 = \frac{8 * \mu * L}{\pi * r^4} \rightarrow \frac{8 * (0.001 \text{ Pa} * \text{s}) * (90 \text{ mm})}{\pi * (1.13 \text{ mm})^4} = 0.141 \frac{\text{Pa} * \text{s}}{\text{mm}^3}$$

$$R \text{ per mm} = \frac{R}{L} \rightarrow \frac{0.141 \frac{\text{Pa} * \text{s}}{\text{mm}^3}}{90 \text{ mm}} = 0.00156 \frac{\text{Pa} * \text{s}}{\text{mm}}$$

R_2 = Soft tubing from syringe ($r = 0.25$ mm)

$$R_2 = \frac{8 * \mu * L}{\pi * r^4} \rightarrow \frac{8 * (0.001 \text{ Pa} * \text{s}) * (820 \text{ mm})}{\pi * (0.25 \text{ mm})^4} = 534.6 \frac{\text{Pa} * \text{s}}{\text{mm}^3}$$

$$R \text{ per mm} = \frac{R}{L} \rightarrow \frac{534.6 \frac{\text{Pa} * \text{s}}{\text{mm}^3}}{820 \text{ mm}} = 0.652 \frac{\text{Pa} * \text{s}}{\text{mm}}$$

R_3 = Hard tubing before Y connector ($r = 0.25$ mm)

$$R_3 = \frac{8 * \mu * L}{\pi * r^4} \rightarrow \frac{8 * (0.001 \text{ Pa} * \text{s}) * (40 \text{ mm})}{\pi * (0.25 \text{ mm})^4} = 26.1 \frac{\text{Pa} * \text{s}}{\text{mm}^3}$$

$$R \text{ per } mm = \frac{R}{L} \rightarrow \frac{26.1 \frac{Pa * s}{mm^3}}{40 mm} = 0.652 \frac{Pa * s}{mm}$$

R₄ = Hard tubing after Y connector split into the microfluidic device (r = 0.25 mm)

$$R_4 = \frac{8 * \mu * L}{\pi * r^4} \rightarrow \frac{8 * (0.001 Pa * s) * (90 mm)}{\pi * (0.25 mm)^4} = 58.7 \frac{Pa * s}{mm^3}$$

$$\frac{1}{R} = \frac{1}{R_1} + \frac{1}{R_2} \dots$$

$$\frac{1}{R} = \frac{1}{58.7 \frac{Pa * s}{mm^3}} + \frac{1}{58.7 \frac{Pa * s}{mm^3}} = 29.3 \frac{Pa * s}{mm^3}$$

$$R \text{ per } mm = \frac{R}{L} \rightarrow \frac{29.3 \frac{Pa * s}{mm^3}}{45 mm} = 0.652 \frac{Pa * s}{mm}$$

R₅ = Microfluidic channel

$$R_5 = \frac{12 * \mu * L}{w * h^3} * \frac{1}{1 - (0.63 * \frac{h}{w})}$$

$$\rightarrow \left| \frac{12 * (0.001 Pa * s) * (10.5 mm)}{(0.25 mm) * (0.5 mm)^3} * \frac{1}{1 - (0.63 * \frac{0.5 mm}{0.25 mm})} \right|$$

$$= 15.5 \frac{Pa * s}{mm^3}$$

R₆ = Hard tubing after the microfluidic device split before the Y connector (r = 0.25 mm)

$$R_6 = \frac{8 * \mu * L}{\pi * r^4} \rightarrow \frac{8 * (0.001 Pa * s) * (180 mm)}{\pi * (0.25 mm)^4} = 117.3 \frac{Pa * s}{mm^3}$$

$$\frac{1}{R} = \frac{1}{R_1} + \frac{1}{R_2} \dots$$

$$\frac{1}{R} = \frac{1}{117.3 \frac{Pa * s}{mm^3}} + \frac{1}{117.3 \frac{Pa * s}{mm^3}} = 58.7 \frac{Pa * s}{mm^3}$$

$$R \text{ per } mm = \frac{R}{L} \rightarrow \frac{58.7 \frac{Pa * s}{mm^3}}{90 mm} = 0.652 \frac{Pa * s}{mm}$$

R_7 = Hard tubing after the Y connector ($r = 0.25$ mm)

$$R_7 = \frac{8 * \mu * L}{\pi * r^4} \rightarrow \frac{8 * (0.001 \text{ Pa} * \text{s}) * (40 \text{ mm})}{\pi * (0.25 \text{ mm})^4} = 26.1 \frac{\text{Pa} * \text{s}}{\text{mm}^3}$$

$$R \text{ per mm} = \frac{R}{L} \rightarrow \frac{26.1 \frac{\text{Pa} * \text{s}}{\text{mm}^3}}{40 \text{ mm}} = 0.652 \frac{\text{Pa} * \text{s}}{\text{mm}}$$

Total resistance of system:

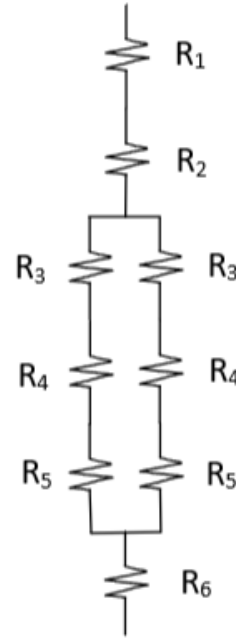
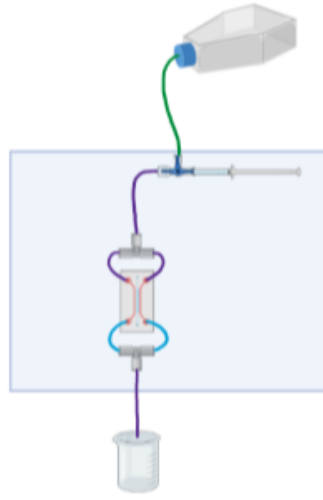
$$\begin{aligned} R_{total} &= R_t + R_c = R_1 + R_2 + R_3 + R_4 + R_5 + R_6 + R_7 \\ \rightarrow &0.141 \frac{\text{Pa} * \text{s}}{\text{mm}^3} + 534.6 \frac{\text{Pa} * \text{s}}{\text{mm}^3} + 26.1 \frac{\text{Pa} * \text{s}}{\text{mm}^3} + 29.3 \frac{\text{Pa} * \text{s}}{\text{mm}^3} + 15.5 \frac{\text{Pa} * \text{s}}{\text{mm}^3} \\ &+ 58.7 \frac{\text{Pa} * \text{s}}{\text{mm}^3} + 26.1 \frac{\text{Pa} * \text{s}}{\text{mm}^3} \\ &= 690.4 \frac{\text{Pa} * \text{s}}{\text{mm}^3} \end{aligned}$$

Total resistance based on flow rate:

$$\begin{aligned} P &= \Delta h * \rho * g \rightarrow 0.3048 \text{ m} * 997 \frac{\text{kg}}{\text{m}^3} * 9.81 \frac{\text{m}}{\text{s}^2} = 2981.1 \frac{\text{kg}}{\text{m} * \text{s}^2} = 2981.1 \text{ Pa} \\ R &= \frac{P}{Q} \rightarrow \frac{2981.1 \text{ Pa}}{2.08 \frac{\text{mm}^3}{\text{s}}} = 1433.2 \end{aligned}$$

Resistance calculations for high shear stress gravity pump:

Variable	Symbol	Value
Resistance	R	Unknown
Dynamic viscosity of fluid	μ	0.001 Pa*s
Length of tubing/channel	L	Dependent
Inner radius of tubing	R	Dependent
Height of the microfluidic device	H	0.25 mm
Width of the channel	W	0.5 mm
Height of pumping system from output	Δh	0.6096 m
Density of fluid	P	997 kg/m ³
Acceleration of gravity	G	9.81 m/s ²



R_1 = Clear tubing from reservoir to syringe ($r = 1.13 \text{ mm}$)

$$R_1 = \frac{8 * \mu * L}{\pi * r^4} \rightarrow \frac{8 * (0.001 \text{ Pa} * \text{s}) * (165 \text{ mm})}{\pi * (1.13 \text{ mm})^4} = 0.258 \frac{\text{Pa} * \text{s}}{\text{mm}^3}$$

$$R \text{ per mm} = \frac{R}{L} \rightarrow \frac{0.258 \frac{\text{Pa} * \text{s}}{\text{mm}^3}}{165 \text{ mm}} = 0.00156 \frac{\text{Pa} * \text{s}}{\text{mm}}$$

R_2 = Soft tubing from syringe to first Y connector ($r = 0.38 \text{ mm}$)

$$R_2 = \frac{8 * \mu * L}{\pi * r^4} \rightarrow \frac{8 * (0.001 \text{ Pa} * \text{s}) * (138 \text{ mm})}{\pi * (0.38 \text{ mm})^4} = 16.9 \frac{\text{Pa} * \text{s}}{\text{mm}^3}$$

$$R \text{ per mm} = \frac{R}{L} \rightarrow \frac{16.9 \frac{\text{Pa} * \text{s}}{\text{mm}^3}}{138 \text{ mm}} = 0.122 \frac{\text{Pa} * \text{s}}{\text{mm}}$$

R_3 = Soft tubing after Y connector split into microfluidic device ($r = 0.38 \text{ mm}$)

$$R_3 = \frac{8 * \mu * L}{\pi * r^4} \rightarrow \frac{8 * (0.001 \text{ Pa} * \text{s}) * (84 \text{ mm})}{\pi * (0.38 \text{ mm})^4} = 10.3 \frac{\text{Pa} * \text{s}}{\text{mm}^3}$$

$$\frac{1}{R} = \frac{1}{R_1} + \frac{1}{R_2} \dots$$

$$\frac{1}{R} = \frac{1}{10.3 \frac{Pa \cdot s}{mm^3}} + \frac{1}{10.3 \frac{Pa \cdot s}{mm^3}} = 5.13 \frac{Pa \cdot s}{mm^3}$$

$$R \text{ per mm} = \frac{R}{L} \rightarrow \frac{5.13 \frac{Pa \cdot s}{mm^3}}{42 \text{ mm}} = 0.122 \frac{Pa \cdot s}{mm}$$

R₄ = Microfluidic channel

$$R_4 = \frac{12 * \mu * L}{w * h^3} * \frac{1}{1 - (0.63 * \frac{h}{w})} \rightarrow R_5 = \frac{12 * \mu * L}{h * w^3} * \frac{1}{1 - (0.63 * \frac{w}{h})}$$

$$\rightarrow \left| \frac{12 * (0.001 Pa \cdot s) * (10.5 \text{ mm})}{(0.25 \text{ mm}) * (0.5 \text{ mm})^3} * \frac{1}{1 - (0.63 * \frac{0.5 \text{ mm}}{0.25 \text{ mm}})} \right| = 15.5 \frac{Pa \cdot s}{mm^3}$$

R₅ = Hard tubing after the microfluidic device split before the Y connector (r = 0.25 mm)

$$R_5 = \frac{8 * \mu * L}{\pi * r^4} \rightarrow \frac{8 * (0.001 Pa \cdot s) * (104 \text{ mm})}{\pi * (0.25 \text{ mm})^4} = 67.8 \frac{Pa \cdot s}{mm^3}$$

$$\frac{1}{R} = \frac{1}{R_1} + \frac{1}{R_2} \dots$$

$$\frac{1}{R} = \frac{1}{67.8 \frac{Pa \cdot s}{mm^3}} + \frac{1}{67.8 \frac{Pa \cdot s}{mm^3}} = 33.9 \frac{Pa \cdot s}{mm^3}$$

$$R \text{ per mm} = \frac{R}{L} \rightarrow \frac{33.9 \frac{Pa \cdot s}{mm^3}}{52 \text{ mm}} = 0.652 \frac{Pa \cdot s}{mm}$$

R₆ = Soft tubing after the Y connector (r = 0.38 mm)

$$R_6 = \frac{8 * \mu * L}{\pi * r^4} \rightarrow \frac{8 * (0.001 Pa \cdot s) * (238 \text{ mm})}{\pi * (0.38 \text{ mm})^4} = 29.1 \frac{Pa \cdot s}{mm^3}$$

$$R \text{ per mm} = \frac{R}{L} \rightarrow \frac{29.1 \frac{Pa \cdot s}{mm^3}}{238 \text{ mm}} = 0.122 \frac{Pa \cdot s}{mm}$$

Total resistance of system:

$$\begin{aligned}
 R_{total} &= R_t + R_c = R_1 + R_2 + R_3 + R_4 + R_5 + R_6 \\
 \rightarrow 0.258 \frac{Pa * s}{mm^3} &+ 16.9 \frac{Pa * s}{mm^3} + 5.13 \frac{Pa * s}{mm^3} + (15.5 \frac{Pa * s}{mm^3} * 2) + 67.8 \frac{Pa * s}{mm^3} \\
 &+ 29.1 \frac{Pa * s}{mm^3} \\
 &= 149.7 \frac{Pa * s}{mm^3}
 \end{aligned}$$

Total resistance based on flow rate:

$$\begin{aligned}
 P &= \Delta h * \rho * g \rightarrow 0.6096 m * 997 \frac{kg}{m^3} * 9.81 \frac{m}{s^2} = 5962 \frac{kg}{m * s^2} = 5962 Pa \\
 R &= \frac{P}{Q} \rightarrow \frac{5962 Pa}{20.8 \frac{mm^3}{s}} = 286.6 \frac{Pa * s}{mm^3}
 \end{aligned}$$

Appendix E. MATLAB Code of Calculations

```
%Variables based on the sideways orientation
Tau=200; %mPa
h_w=.5; %mm
w_w=.25; %mm
mu=1; %mPa*s
r_o=.25; %mm
L_t=350; %mm
L_c=10.5; %mm
rho=997; %kg/m^3
g=9.8; %m/s^2
%All answers are in mm, unless denoted
%Volumetric flow rate on the wall based on shear stress
%tau = mu * (6Q/wh^2)
Q_w=(Tau*w_w*(h_w^2))/(mu*6)
%Volumetric flow rate on the floor based on shear stress
%tau=mu *(6Q/wh^2)
Q_f=(Tau*h_w*(w_w^2))/(mu*6)
%linear flow velocity
%v=Q/A
A=r_o^2*pi
v=Q_w/A
%Tubing resistance
%R_t= 8*mu*L/pi*r_o^4
R_t=(8*mu*L_t)/(pi*r_o^4)
%Channel resistance
%R_c=((12*mu*L_c)/((w_w*h_w^3)))*(1/((1-(.63*(h_w/w_w))))
R_c=((12*mu*L_c)/(w_w*h_w^3))*(1/((1-(.63*(h_w/w_w))))*(-1))
%Total Pressure in system (change in pressure)
%P=(R_t+R_c)*Q_w
P=(R_t+R_c)*Q_w
%Determining Height based on the change in pressure
%h=p/rho*g
%m for units
h=((P/1000)/(rho*g))%height in m
h_in= 39.37*h %height in inches
RP=516*rho*g %Pressure which its currently operating under (the
number is the height in mm)
QW=RP/(R_t+R_c) %Current flow rate
tau_2 = (mu *((6*2.0))/(w_w*h_w^2))
```

Appendix F. MATLAB Code of Resistance Calculations

```
%resistance of the system
%Tubing resistance  $(8*\mu*L_t)/(pi*r^4)$ 
%L_t in mm
%Flow Rate
Q_st= 19.33 %ul/s %flow rate out of syringe+tubing
Q_s= 31.67 %ul/s %flow rate out of Syringe
rho=997; %kg/m^3
g=9.8; %m/s^2
mu=1; %mPa*s
h_w=.5; %mm
w_w=.25; %mm
L_c=10.5; %mm
%length of tubing 15 cm coming out of syringe no metal connector
r_ht=  $(8*\mu*150)/(pi*.25^4)$  %mpa*s/mm^3
%resistance of hard tubing with r: .25mm / mm
R_mmht= r_ht/(150 *pi*.25^4) %mpa*s/mm
%resistance of tubing coming out of the Y connector in and out
of the device
R_3=(1/(R_mmht*95))+(1/(R_mmht*95))
R_4=(1/(R_mmht*95))+(1/(R_mmht*95))
%Pressure of the system from the syringe
P_s=101.6*rho*g
%resistance based on the flow rate
%Q=P/R
%R=P/Q
%Clear tubing from Reservoir
R_ct=(8*\mu*305)/(pi*1.13^4) %need to get diameter it was a guess
R_mmct=R_ct/(305*pi*1.13^4)
%Grey tubing from reservoir
R_g=(8*\mu*410)/(pi*1.3^4) %need to get diameter it was a guess
R_mmg=R_g/(410*pi*1.3^4)
%resistance from reservoir out of syringe
R_1=((P_s/Q_st)-r_ht) %mpa*s/mm^3
R_12=(P_s/Q_s) %mpa*s/mm^3
%resistance of the larger squishy tubing
R_ls=(8*\mu*150)/(pi*.381^4) %mpa*s/mm^3
R_mmls=R_ls/(150*pi*.381^4) %mpa*s/mm
%resistance of the smaller squishy tubing
R_ss=(8*\mu*609.6)/(pi*.2^4) %mpa*s/mm^3 %unknown on the exact
tubing diameter
R_mmss=R_ss/(609.6*pi*.2^4)
```



```
%resistance of the whole system tubing based on flow rate (h in
meter)
P_ws=.3556*rho*g
R_ws=P_ws/5.5
%channel resistance
R_c=((12*mu*L_c)/(w_w*h_w^3))*(1/((1-(.63*(h_w/w_w))))*(-1))
%Total system Resistance
R_tot=R_ws+R_c
```

Appendix G. Arduino Code for Circuit

```
int x=1111;
int b1=0;
int g1=2;
int b2=8;
int g2=10;
void setup() {
    // put setup code here, to run once:
    pinMode(b1, OUTPUT);
    pinMode(b2, OUTPUT);
    pinMode(g1, OUTPUT);
    pinMode(g2, OUTPUT);
}
void loop () {
    // put your main code here, to run repeatedly:
    // activate solenoids 1 & 4
    digitalWrite(b1, HIGH);
    digitalWrite(b2, HIGH);
    // deactivate 2 & 3
    digitalWrite(g1, LOW);
    digitalWrite(g2, LOW);
    // hold for x secs
    delay(x); // 2 steps ahead
    // deactivate 1 & 4
    digitalWrite(b1, LOW);
    digitalWrite(b2, LOW);
    // activate 2 & 3
    digitalWrite(g1, HIGH);
    digitalWrite(g2, HIGH);
    // hold for x secs
    delay(x/2); // 1 step back
}
```

Appendix H. Making and Placing Gels in PDMS Devices

Making Gels [20 min]

Materials:

- Fibrinogen
 - Stock 16.7 mg/mL
 - Desired concentration 4 mg/mL
 - Stored in -20 °C, keep on ice
- Thrombin
 - Stock 25 U/mL
 - Desired concentration 0.38 U/mL thrombin
 - Stored in -80 °C, keep on ice
- PDMS Devices
 - 10 µL per gel chamber
 - Total of 18 gel chambers (180 µL)
- Complete Medium
 - Dulbecco's Modified Eagle Medium (DMEM)
 - 10% FBS
 - 1% Anti-Anti
 - 50 U/mL Heparin
- Phosphate-buffered saline (DPBS)

Methods:

1. Make 100 µL of 8 mg/mL fibrinogen solution
 - a. Combine 50 µL of fibrinogen stock and 50 µL of DPBS
2. Make 50 µL of 1.52 U/mL thrombin solution
 - a. Combine 3 µL of thrombin and 47 µL of DPBS
3. Add 50 µL of complete media to the thrombin solution

Calculations:

- $(8 \text{ mg/mL} \times 0.1 \text{ mL}) / 16 \text{ mg/mL} = 0.050 \text{ mL}$ or 50 µL of fibrinogen
- $(1.52 \text{ U/mL} \times 0.050 \text{ mL}) / 25 \text{ U/mL} = 0.003 \text{ mL}$ of 3 µL of thrombin

Placing Gels [45 min]

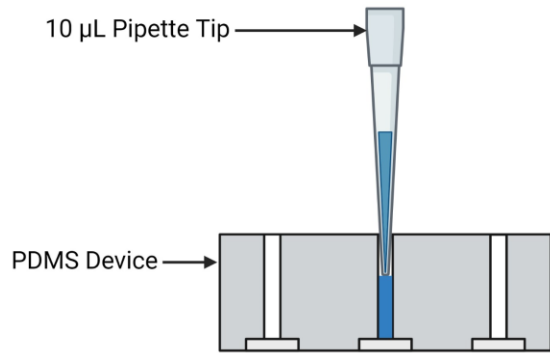
Materials:

- Fibrinogen solution
- Thrombin solution
- PDMS devices
- Pipette and pipette tips

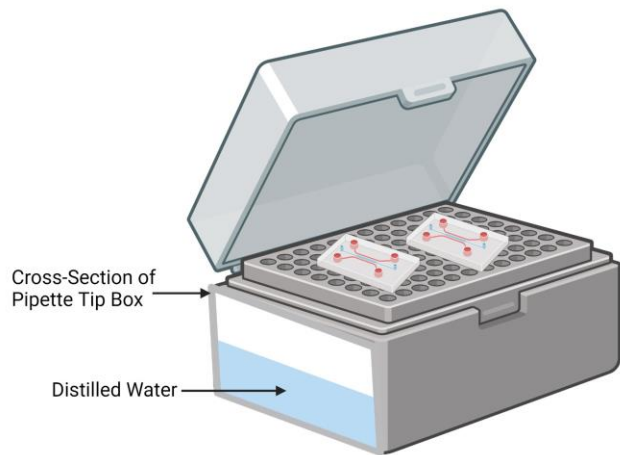
Methods:

1. Keep solutions on ice for the duration, as they are temperature sensitive
2. Prepare to pipette gels quickly following mixing
3. Combine 5 µL of thrombin solution and 5 µL of fibrinogen solution
4. Take 10 µL of solution and place half of the gel in each inlet

- a. Use a 10 μL pipette tip and make sure not to push too deep into the inlet



5. Examine gels to ensure that they remained within the gel chamber
6. Once all gels are imaged, place device in the incubator for 1 hour
 - a. Use a pipette tip box filled halfway with water to increase humidity around the gel



7. Following incubation, fill media channels with 20 μL of media in inlet to maintain a hydrated gel

Appendix I. Seeding Cells in Microfluidic Devices

Seeding Cells [40 min]

Materials:

- Cell Media
- Gelated AIM Chips

Methods:

1. Add an additional 20 uL of cell media to the channel where cells will be seeded
 - a. Ports should be filled with media before seeding cells
2. Take 10 uL of cell suspension and inject into one side of a media channel
 - a. Position it in inlet, but not completely into inlet, may result in uneven distribution
3. Wait two minutes, then inject 10 uL of cell suspension into the other connected end
 - a. Mix cell suspension well
4. Inspect under microscope to ensure cells are present
5. Incubate devices after for two to four hours
 - a. Follow same volumes for gel placing procedure

Appendix J: Soft Lithography Protocol

Soft lithography: PDMS fabrication from a mold master

Step 1

Time: 1-3 hrs depending on vacuum used and level of degassing needed

1. Weigh a 10:1 (w/w) ratio of Sylgard 184 PDMS base to curing agent into a large weigh boat
 - Aim for 100-120g PDMS base
2. Mix PDMS base and curing agent thoroughly until many air bubbles are visible
 - Use a plastic fork
3. Degas the mixture in the vacuum desiccator for 30 min to 1 h to eliminate bubbles
 - **Can do this twice to accelerate process. Normally we degass for about 20 mins here and then pour it into the mold and degas again for 30mins – 1 hour**
4. Clean the mold master in an air stream if dust is visible
5. Pour the PDMS mixture onto the mold master in a large (150 mm diameter) Petri dish and fill to the desired device thickness, approximately 4–5 mm
 - Avoid forming bubbles
6. As mentioned in step 3, degas the PDMS mixture again
 - Then inspect the poured PDMS and remove bubbles or dust if needed
7. Bake at 65°C on a level shelf for between 3 h to overnight

****Potential stopping point: Can do the remaining steps on a different day***

Step 2

Time: 2-5 hrs depending on number of devices needed

8. Remove the PDMS casting:
 - Cut along the mold master perimeter with a scalpel, gently peel up, and remove the PDMS
9. Cut individual devices from the PDMS casting with a single-edge razor blade
10. Punch inlet and outlet holes using a sharp 1 mm diameter dermal punch
 - Start punching from the non-patterned side since the PDMS will taper at the end
 - Can mark the inlet with a marker to make viewing easier
 - Clean any remaining in the holes
11. Clean the cut-out devices by spraying with 70% ethanol, wiping down with a Kim Wipe, spraying again with ethanol, blowing dry with compressed nitrogen. Wrap the devices with Scotch tape to remove any remaining dust

12. Clean out coverslips similarly

- Make sure that the coverslip is large enough to cover the channels and inlets and outlets of the device

13. Carefully remove the tape only from the pattern side of the device and one side of a coverslip.

- Be careful not to touch the un-taped side – it should face up

14. Carefully place a PDMS device and coverslip side-by-side into the plasma cleaner making sure not to touch their un-taped sides.

15. Plasma treat the PDMS and glass coverslips. clean the device

- Place cover on opening
- Turn on device
- Turn on vacuum pump. Wait about 30s before closing the knob on the cover. The seal should be shut
- Wait another 30 – 60s before turning the dial to “high”
- Allow to treat for 1 min (set a timer). Check to make sure it is working – should turn purple
- Turn dial to “off” and turn off vacuum
- Slowly and carefully open the knob on the cover. Be careful when you hear hissing
- Lift away cover

16. Carefully remove the devices and flip the coverslip onto the PDMS to bond. Use your fingers to apply light even pressure for a few seconds to encourage bonding. Don't push too hard – might break coverslip or seal the channels.

17. Allow to rest for 1 hour or more before further manipulation

Appendix K: Steady Flow Gravity Pump SOP

Standard Operating Procedure for Steady Flow Gravity Pump with Microfluidic Device

Purpose/Background

This procedure is step by step to ensure successful data collection of cell response under fluid flow conditions with limited amount of user error. The system is designed to behave similar to the blood flow through a heart valve consisting of steady flow in one direction through a microfluidic device.

Scope

Use this procedure while running an experiment with the Fluid Flow Simulation of a Heart Valve MQP team's gravity pumping system for steady flow under both high and low shear stresses.

Prerequisites

No additional training is needed to run this equipment. Proper handling of the AIM Biotech chip however should be understood and can be found in https://aimbiotech.com/wp-content/uploads/2021/02/general_protocol_v5.4.pdf . All disposable materials should be replaced prior to starting the experiment and all reusable materials should be autoclaved.

Disposable Materials Used

- T175 flask
- Syringe
- Blunt-end *Insert size* needle
- DMEM Cell Media w/ 10% FBS, 1% Anti-Anti, and 50 U/mL Heparin
- Microfluidic device
- If using AIM Biotech chip, respective connectors and rubber stoppers

Reusable Materials

- All tubing in the system
- Y connectors
- Metal connectors
- Acrylic board

The microfluidic device should be prepared to be connected to the gravity pump before starting the priming procedure, such as gel insertion and cell seeding procedures.

Procedure

Preparing the Microfluidic Device

- a. Make sure the microfluidic is filled with gel and seeded with cells before beginning
- b. Place two rubber stoppers in the inlet and outlet of the gel chamber as tightly as possible
- c. If using the AIM Biotech chip...
 - i. Cut the top of the AIM connectors to allow easier connection to the tubing on the system
 - ii. In all cell media channel inlet and outlets place one AIM connector so that they click in
- d. If using the MQP microfluidic device made of PDMS do not use the AIM connectors as the metal connectors on the pump should be a perfect fit

Preparing Cell Media

- e. Media Preparation is found on page 4 of the Lab Notebook [Protocol/Lab Notebook](#)

Creating the T175 Flask Cap

- f. Poke a hole in the top and center of an unfiltered T175 flask cap
- g. Insert the respective tubing connector into the top from the inside of the cap using the smaller end, so that the smaller end of the connector is poking out of the outside of the cap where the tubing will be connected

Preparing the System and T175 Flask

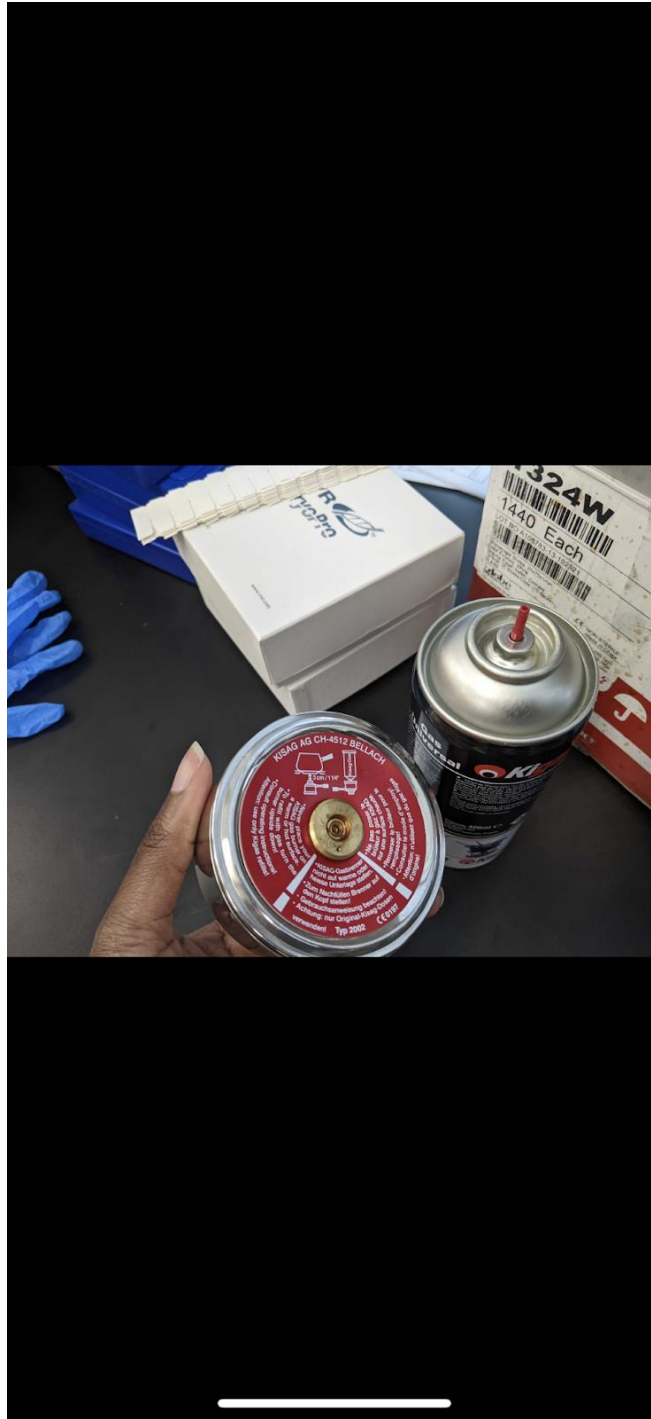
- a. Add a box (we used two boxes) to the back of the hood so that the top is over 14 inches tall
- b. Add the acrylic board to the hood in front of the box stand
- c. Place both three-way luer locks in a beaker filled with 20 mL of ethanol and leave for 5 minutes
- d. Remove both three-way luer locks from ethanol and allow them to dry while preparing the T175 flasks
- e. Take 2 sterile unfiltered T175 flasks
- f. Replace unfiltered cap on both flasks with autoclaved cap with connector attached
- g. Place both flasks upside down with cap tilted downwards
- h. Turn on bunsen burner by turning the knob clockwise until you hear a whistle noise
- i. Light bunsen burner using a lighter outside the hood

i. Make sure all flammable items are removed from the area

ii. If there is no gas coming from the bunsen burner refill it using the respective gas can

1. To refill the Bunsen burner first remove the top and then turn the whole piece over
2. Insert the gas can into the bottom of the Bunsen burner and push down to insert more gas





- j. Heat the head of a screw holding the edge with large forceps with rubber handles for 15 seconds



k. Press the screw at the top of the T175 flask until a hole is formed

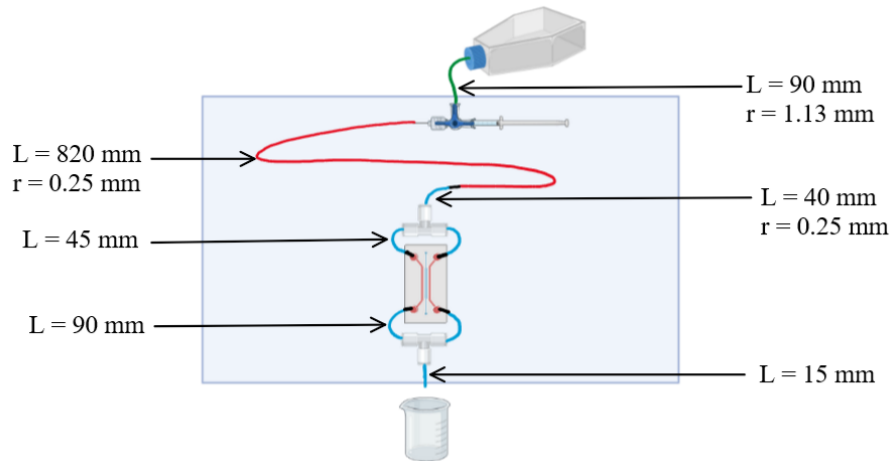
i. Be sure to put force into pushing the screw downwards to make a clean hole

1. Once both holes are formed place the screw on a black benchtop outside of the lab
1. Place a petri dish on top of the T175 flasks so that the hole is covered.
1. Allow 2 minutes for the T-175 flasks to cool down
1. Check to see if the three-way luer locks are completely dry

Setting Up the Pump

- a. Take 2 new syringes and attach the three-way luer lock
- b. Tape the syringe with the needle for the low shear stress setup to the top left of the acrylic so that the tip of the syringe is in between the two holes on the acrylic
- c. Tape the syringe with the luer lock for the high shear stress to the top right of the acrylic so that the tip of the syringe is in between the two holes on the acrylic
- d. Place the shorter large clear tubing on the top of the three-way luer lock on the syringe to the left (syringe with blunt end needle) and the longer clear tubing on the top of the three-way luer lock on the syringe to the right (syringe with luer lock)
- e. Begin setting up low shear stress tubing
 - i. Start with the long, small squishy tubing, by placing one end on the blunt tip needle
 1. **While taping the tubing ensure to not restrict flow and ensure that all tubing is downwards**
 - ii. Snake the long tubing across the entire width of the acrylic taping at each turning point for the tubing
 - iii. Tape the Y connector to the acrylic to add stability
 1. **Make sure the Y connector is taped so that both ends are at the same level to ensure that the flow will be evenly split**
 - iv. Once the first Y connector is stabilized on the acrylic begin the priming system of the top half of the system

Low Shear Stress Setup with Dimensions



f. Begin setting up high shear stress tubing

i. Start with the squishy tubing by placing one end to connect to the syringe

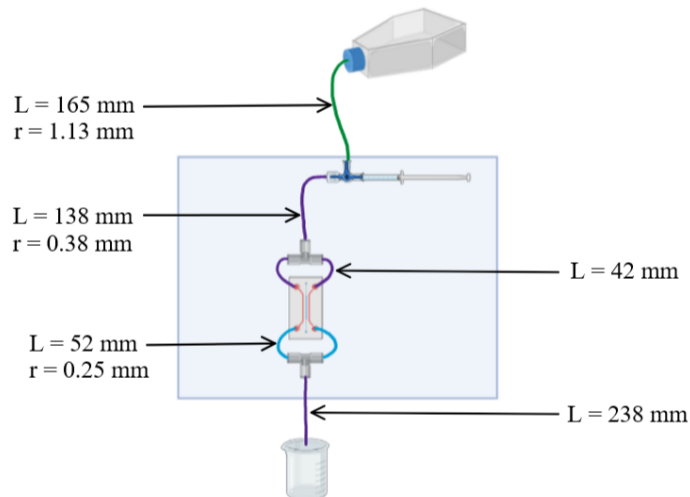
1. There should be no need to tape this tubing section due to the shorter length

ii. Tape the Y connector to the acrylic to add stability

1. **Make sure the Y connector is taped so that both ends are at the same level to ensure that the flow will be evenly split**

iii. Once the first Y connector is stabilized on the acrylic begin the priming system of the top half of the system

High Shear Stress with Dimensions



F. Priming/Starting the Experiment

- a. Fill the T175 flask reservoir with 600 mL of cell media
- b. In the hood, with the cap attached to the tubing connected to the syringe, twist on the cap to the reservoir

i. Be careful to not spill the cell media

- c. Once the reservoir is filled and connected, turn the three-way luer lock so that the “off” label is to the left

- d. Begin to fill the syringe with cell media by pulling the plunger to the right and then push the plunger back to the left, forcing the air bubbles to escape from both the tubing and the syringe
- e. Repeat the step above until there are no air bubbles in the syringe or the tubing connecting the syringe and reservoir
- f. Once all the bubbles are removed, pull the plunger to the right as much as possible filling the syringe with cell media
- g. Turn the three-way luer lock so that the “off” label is up
- h. Push the cell media slowly through the first section of tubing, collecting the cell media through the two connectors that will be placed in the microfluidic device
- i. If there are still air bubbles in the tubing repeat the steps above starting with step f, first moving the three-way luer lock back to its first position with the “off” label to the left
- i. When filling the syringe with cell media the “off” label on the three-way luer lock should always be to the left**
- ii. When pushing cell media through the tubing the “off” label on the three-way luer lock should always be up**
- j. Once all the air bubbles are removed from the first section of tubing, turn the three-way luer lock so that the “off” label is to the left
- i. This keeps the system from allowing air bubbles in without running the system and wasting cell media**
- k. For both high and low shear stress setup after all the air bubbles are removed from the top section of the tubing, attach the microfluidic device by placing the metal connectors from one Y connector (the Y connector that has already been filled with cell media) into the two inlets on one end of the microfluidic device and then the other two metal connectors from the other Y connector into the two outlets on the other end of the microfluidic device
- i. Make sure all connectors are tightly in place as well as the rubber stoppers in the gel inlet and outlet**
- ii. If a rubber stopper comes out of the microfluidic device stop the pump immediately and restart the priming process after it has been replaced**
- l. Once the microfluidic device is attached to the system as well as the rest of the tubing, place a collection beaker underneath the outlet of the system
- m. Keeping the three-way luer lock where it is (“off” label to the left) fill the syringe with cell media by pulling the plunger to the right
- n. Move the three-way luer lock so that the “off” label is up and then push the cell media through the tubing
- o. Repeat this step until all air bubbles are removed from the tubing
- i. When filling the syringe with cell media the “off” label on the three-way luer lock should always be to the left**
- ii. When pushing cell media through the tubing the “off” label on the three-way luer lock should always be up**
- p. After all air bubbles are removed, keep the plunger of the syringe to the left with no cell media in the syringe and turn the three-way luer lock all the way to the right
- q. The system should be on now and cell media should be dripping from the outlet into the collection beaker
- i. If there is no visible cell media dripping from the system stop the system by turning the three-way luer lock so that the “off” label is up and repeat the priming process**

F. Moving the System to the Incubator

- r. First check the top shelf placement

- i.If running the low shear stress setup make sure the shelf is at its lower level
- ii.If running the high shear stress setup make sure the shelf is at its higher level
- iii.If running both at the same time make sure the shelf is at its lower level same as the low shear stress setup

Refilling the Reservoir

- s. When running the experiment for longer than 8 hours, the T175 flask must be refilled to maintain the correct pressure head for the experiment
- t. If only filling the flask twice a day, morning and night, 200 mL should be added
- u. Keeping the system in the incubator and continuously running, in the hood, fill a graduated cylinder with the approximate volume of cell media to get the volume back to its original position
- v. Bring the cell media to the incubator and remove the protective petri dish top from the reservoir and place the previously autoclaved funnel onto the open hole in the T175 flask
- w. Fill the T175 flask back to its original volume using the measured cell media
- x. Place the petri dish top back on the reservoir and check for any leaks in the system and ensure there is still cell media flowing through
- y. Close the incubator and continue the test

Roles and Responsibilities

This system was designed by the 2022-2023 Fluid Flow Simulation of a Heart Valve MQP team, if there are any questions about the system contact a member of this team, their advisor Professor Billiar, or Rozanne Mungai.

Training

There is no training required for running this system, however the procedure should be run with this SOP on hand following it step-by-step to prevent any complications

Revision Record

Editor	Changes Made	Date
Rachel Drasser	Added Schematics and changed some information according to Rozanne’s feedback	04/27/2023

- a. Place the petri dish top back on the reservoir and check for any leaks in the system and ensure there is still cell media flowing through
- b. Close the incubator and continue the test

1. Roles and Responsibilities

This system was designed by the 2022-2023 Fluid Flow Simulation of a Heart Valve MQP team, if there are any questions about the system contact a member of this team, their advisor Professor Billiar, or Rozanne Mungai.

2. Training

There is no training required for running this system, however the procedure should be run with this SOP on hand following it step-by-step to prevent any complications

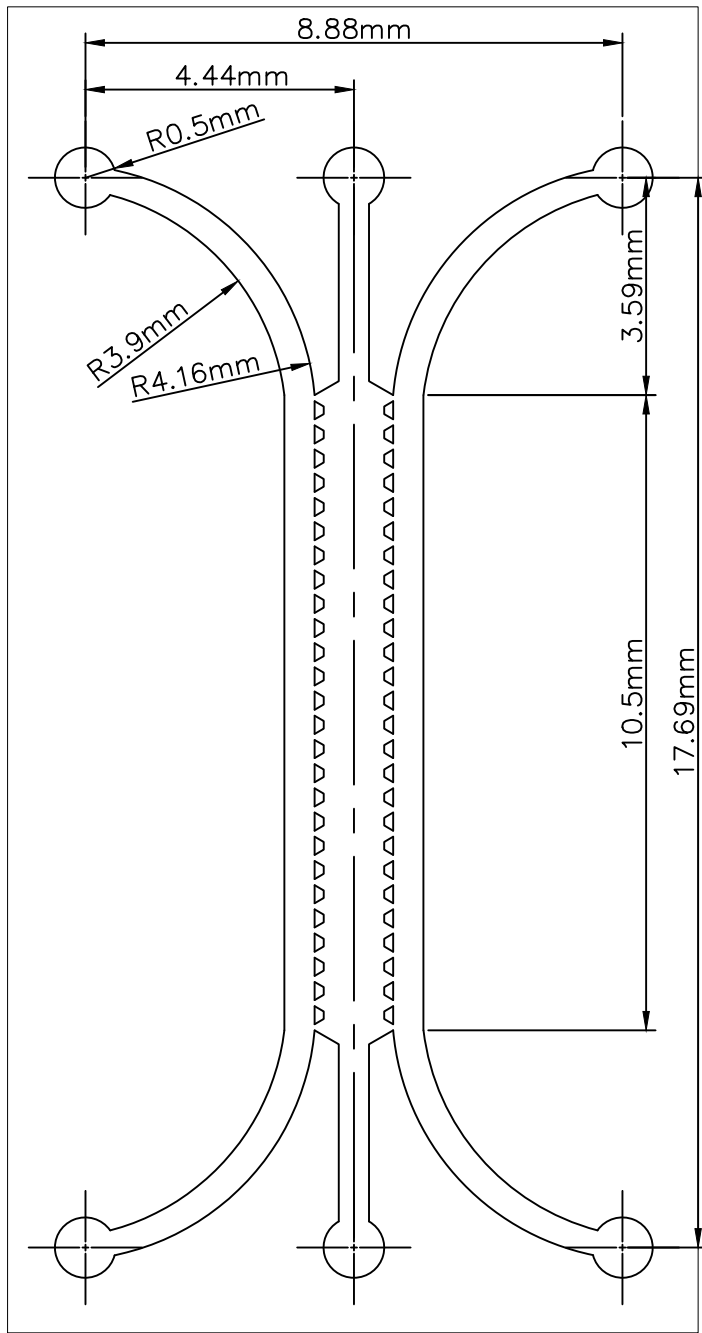
3. Revision Record

Editor	Changes Made	Date

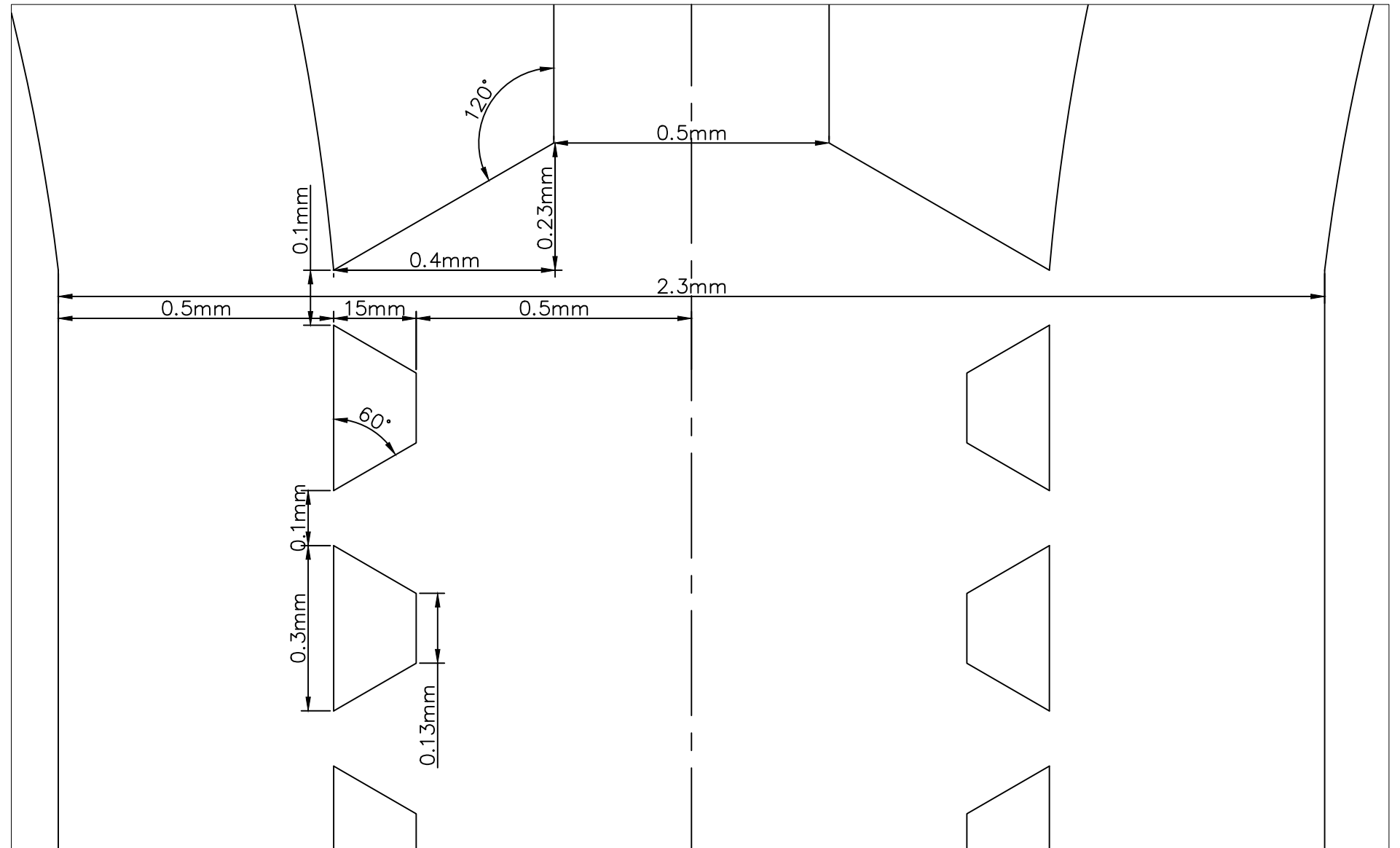
Appendix L: AutoCAD Drawings of Microfluidic Designs

[AutoCAD Drawings](#)

RevNo	Revision note	Date	Signature	Checked



SCALE: 8:1

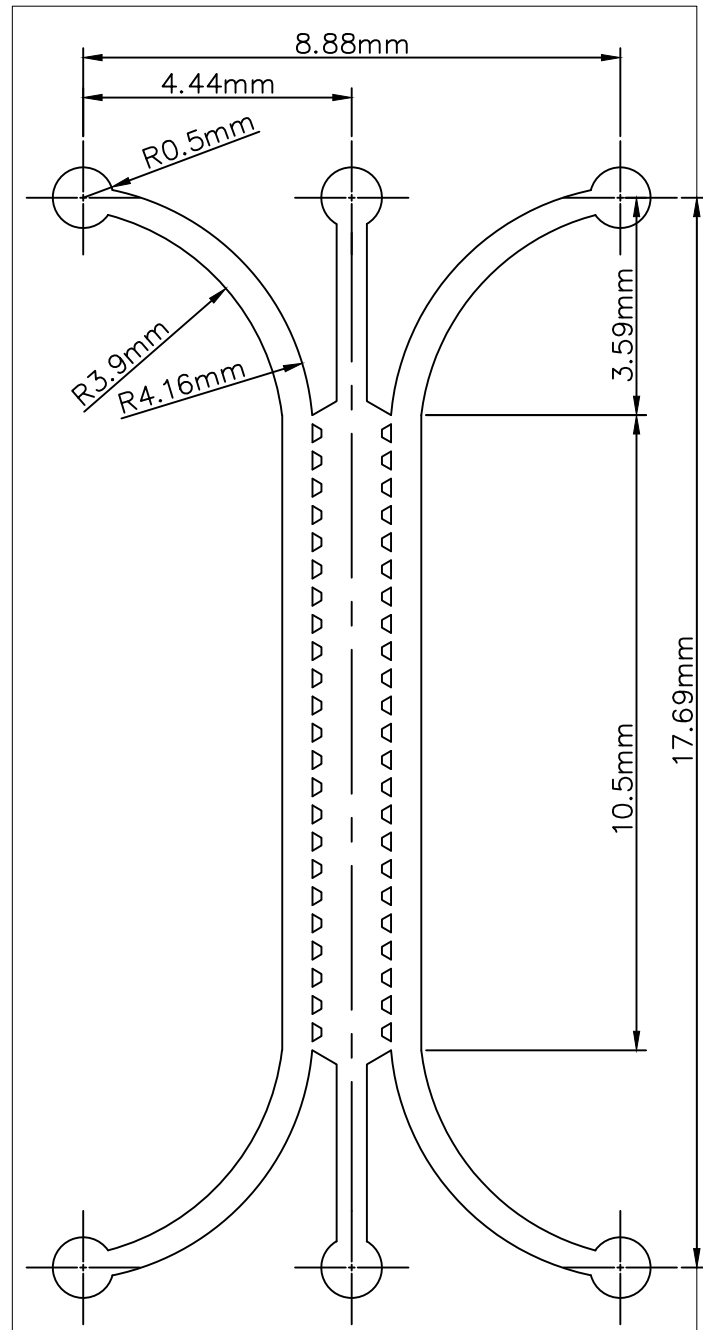


SCALE: 100:1

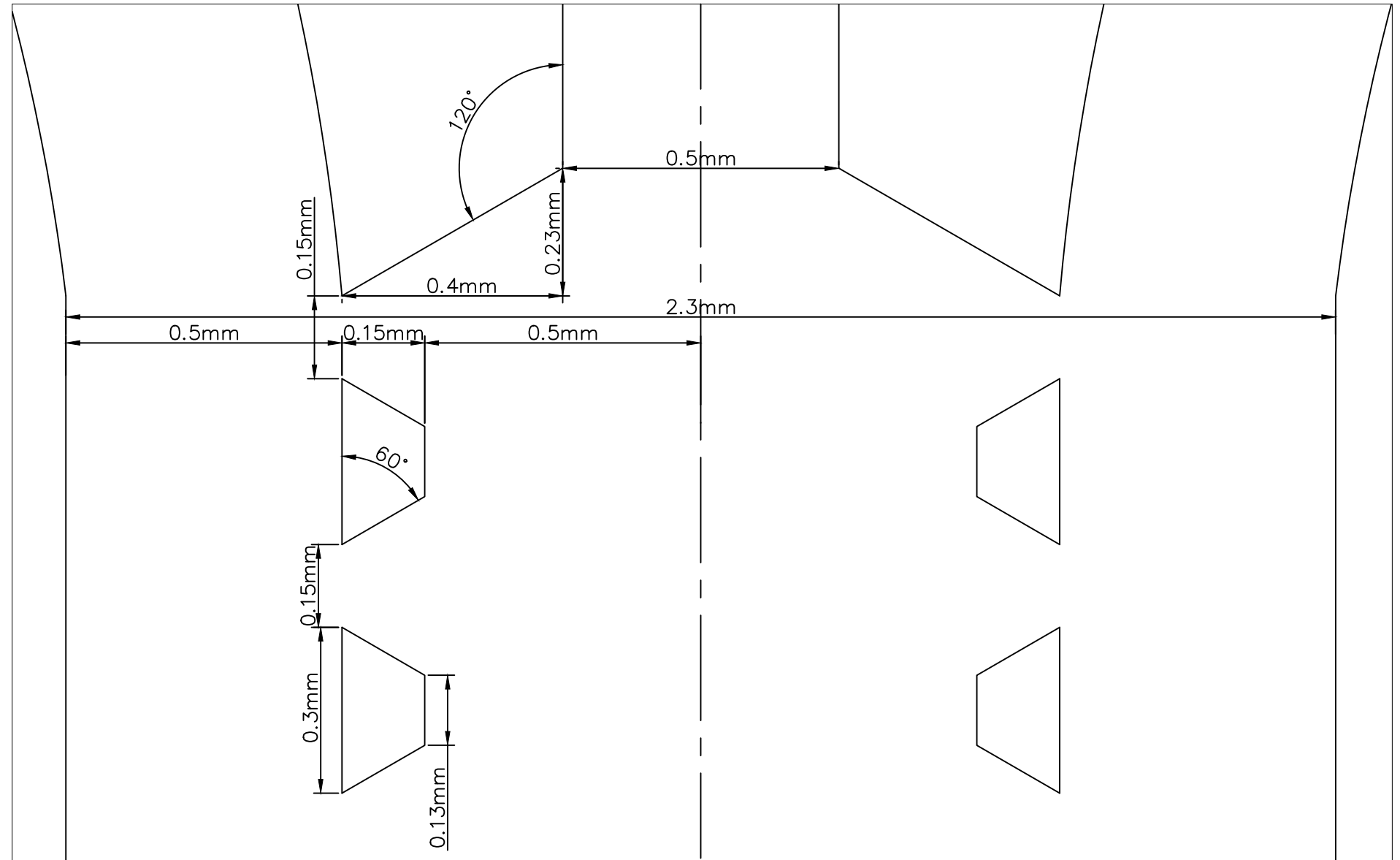
FILE NAME	AIM1 AIM_Exact.dwg	FSCM NO	SHEET	AIM1	SCALE	Check View
SIZE	A4					
DRAWN	3/24/2023					
CHECK	3/26/2023					
APPR.						
ISSUED						
REV						
CONTRACT NO			DWG NO	AIM1 - AIM_EXACT		



RevNo	Revision note	Date	Signature	Checked



SCALE: 8:1

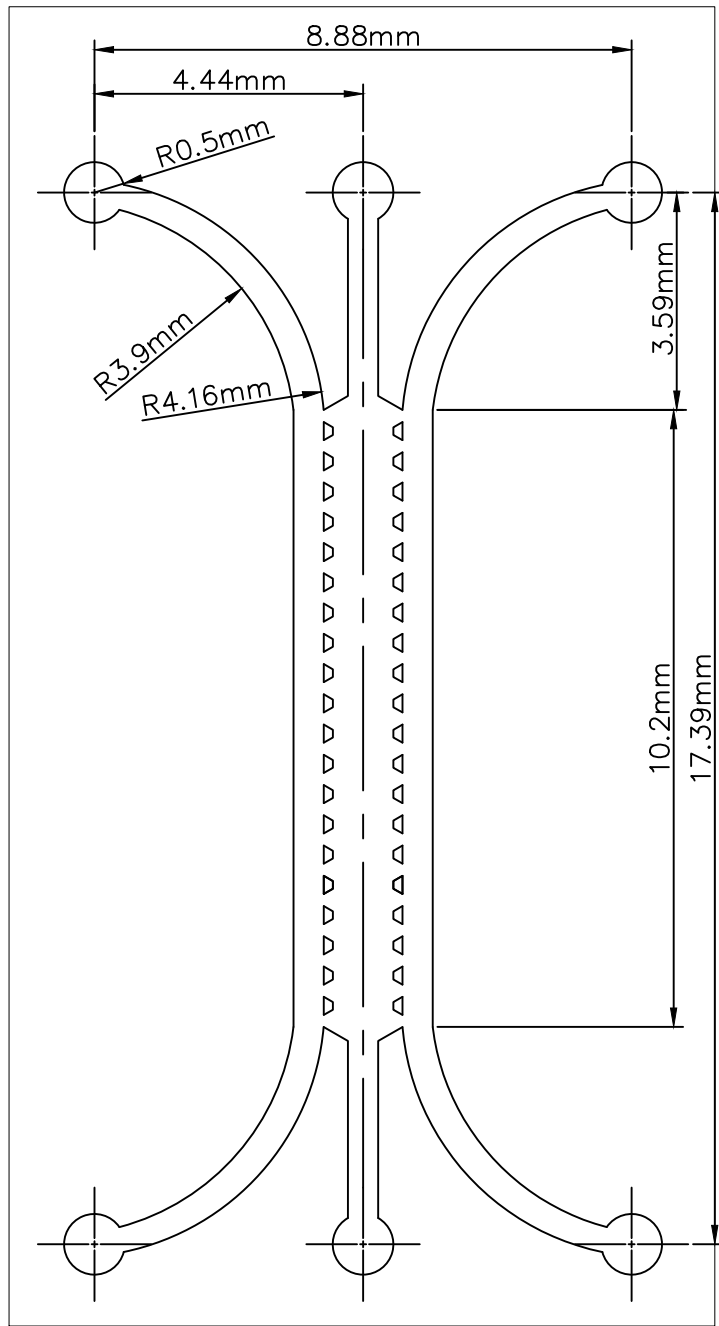


SCALE: 100:1

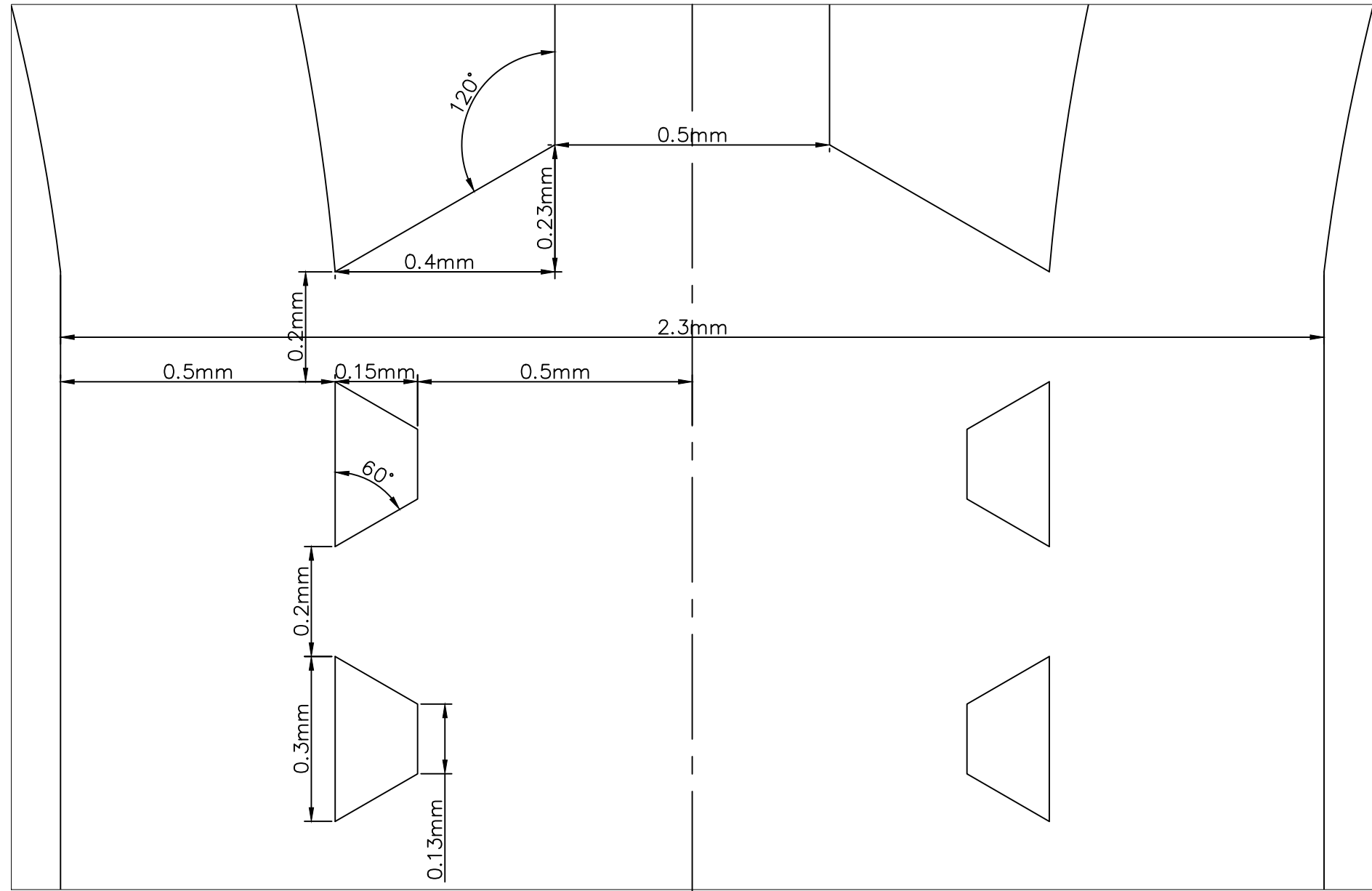
FILE NAME	AIM2 AIM_PS150.dwg	FSCM NO	SHEET	AIM2	SCALE	Check View
SIZE	A4					
DRAWN	3/24/2023					
CHECK	3/26/2023					
APPR.						
ISSUED						
REV						
CONTRACT NO						
			DWG NO	AIM2 - AIM_PS150		



RevNo	Revision note	Date	Signature	Checked



SCALE: 8:1

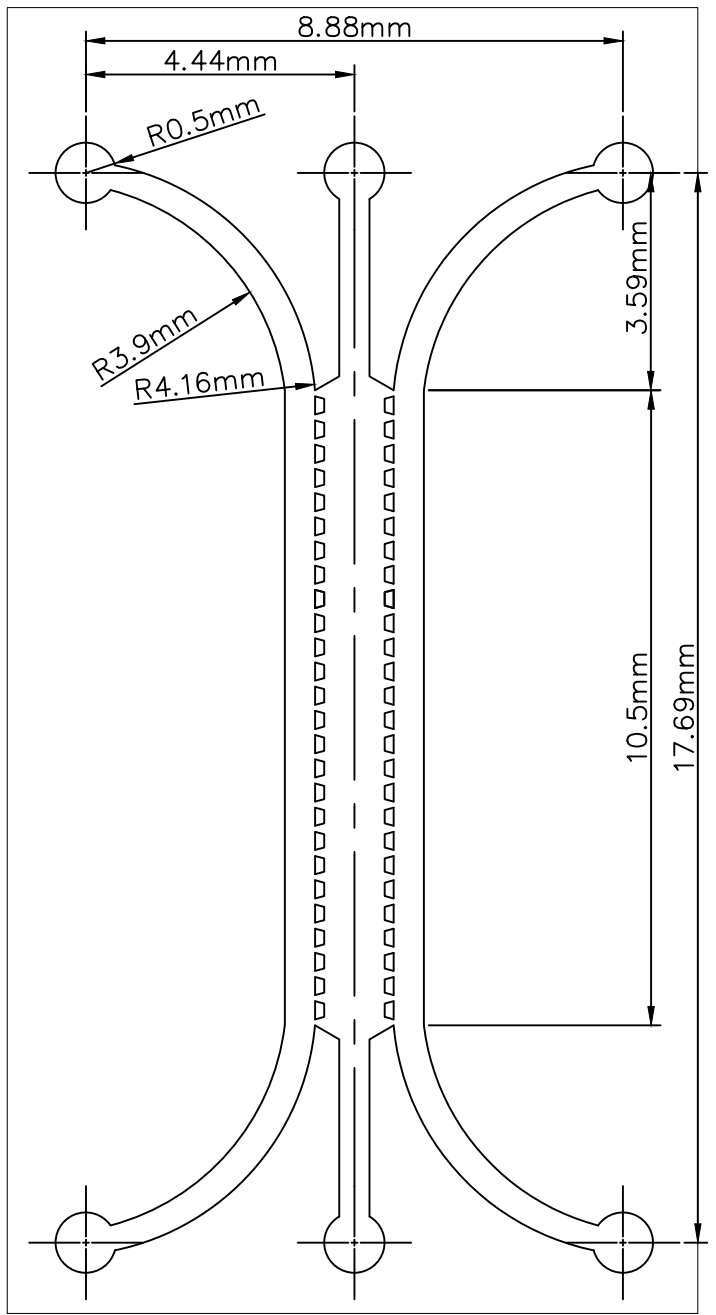


SCALE: 100:1

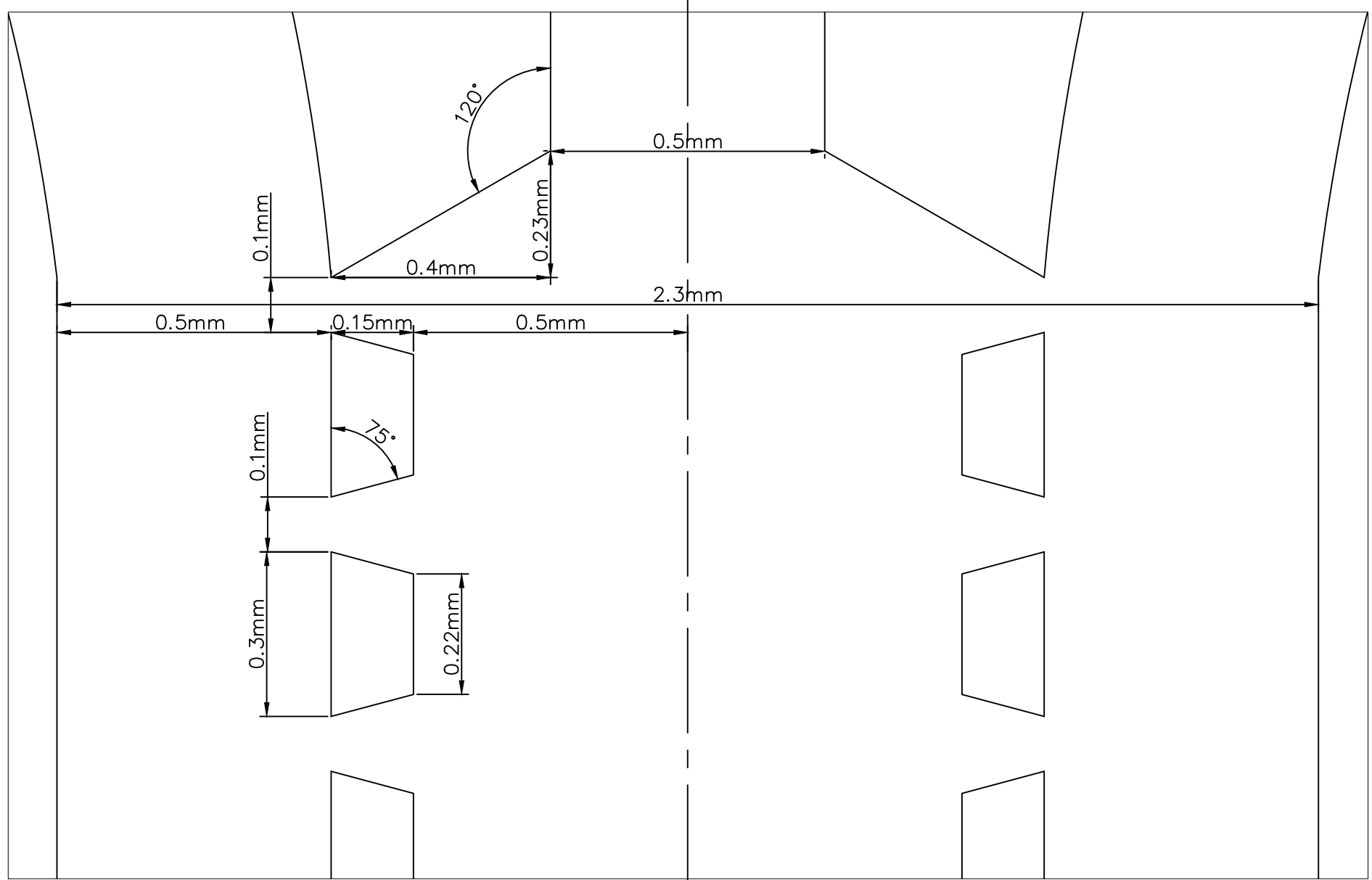
FILE NAME	AIM3 AIM_PS200.dwg	FSCM NO	SHEET	AIM3	SCALE	Check View
SIZE	A4					
DRAWN	3/24/2023					
CHECK	3/26/2023					
APPR.						
ISSUED						
REV						
CONTRACT NO						
			DWG NO	AIM3 - AIM_PS200		



RevNo	Revision note	Date	Signature	Checked



SCALE: 8:1

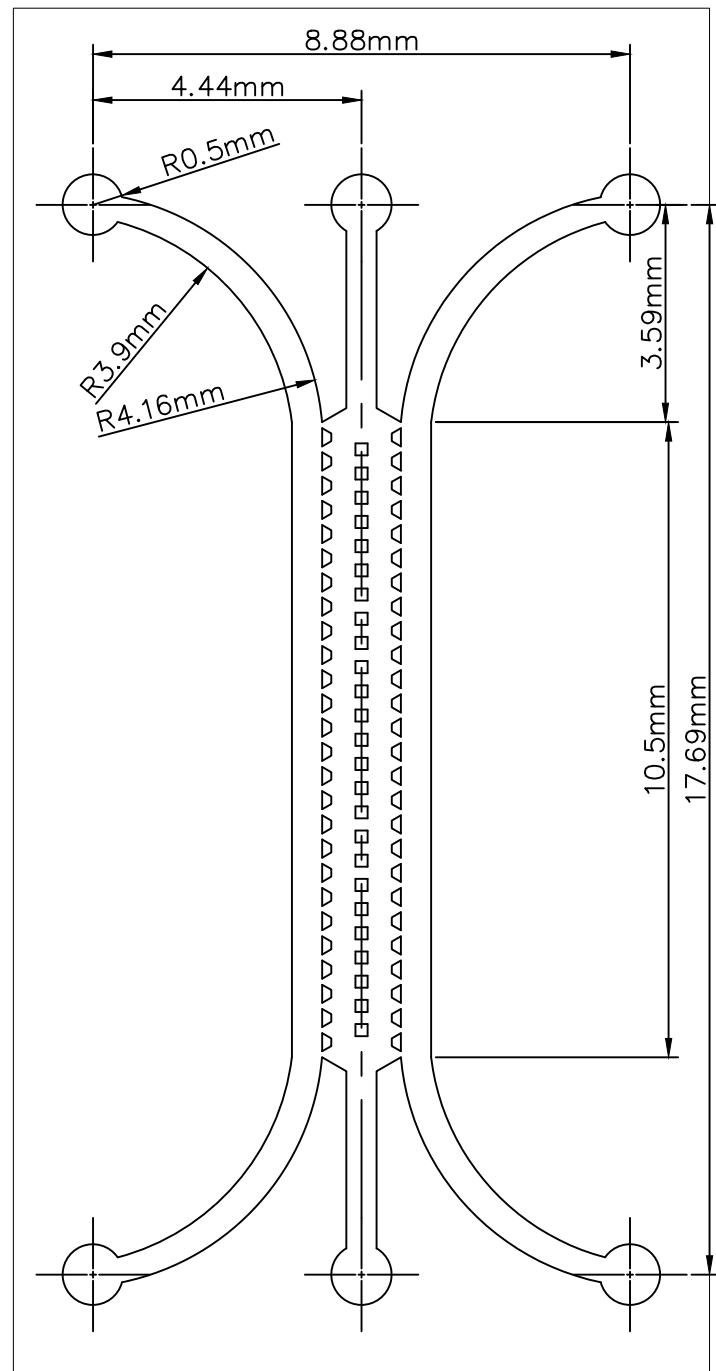


SCALE: 100:1

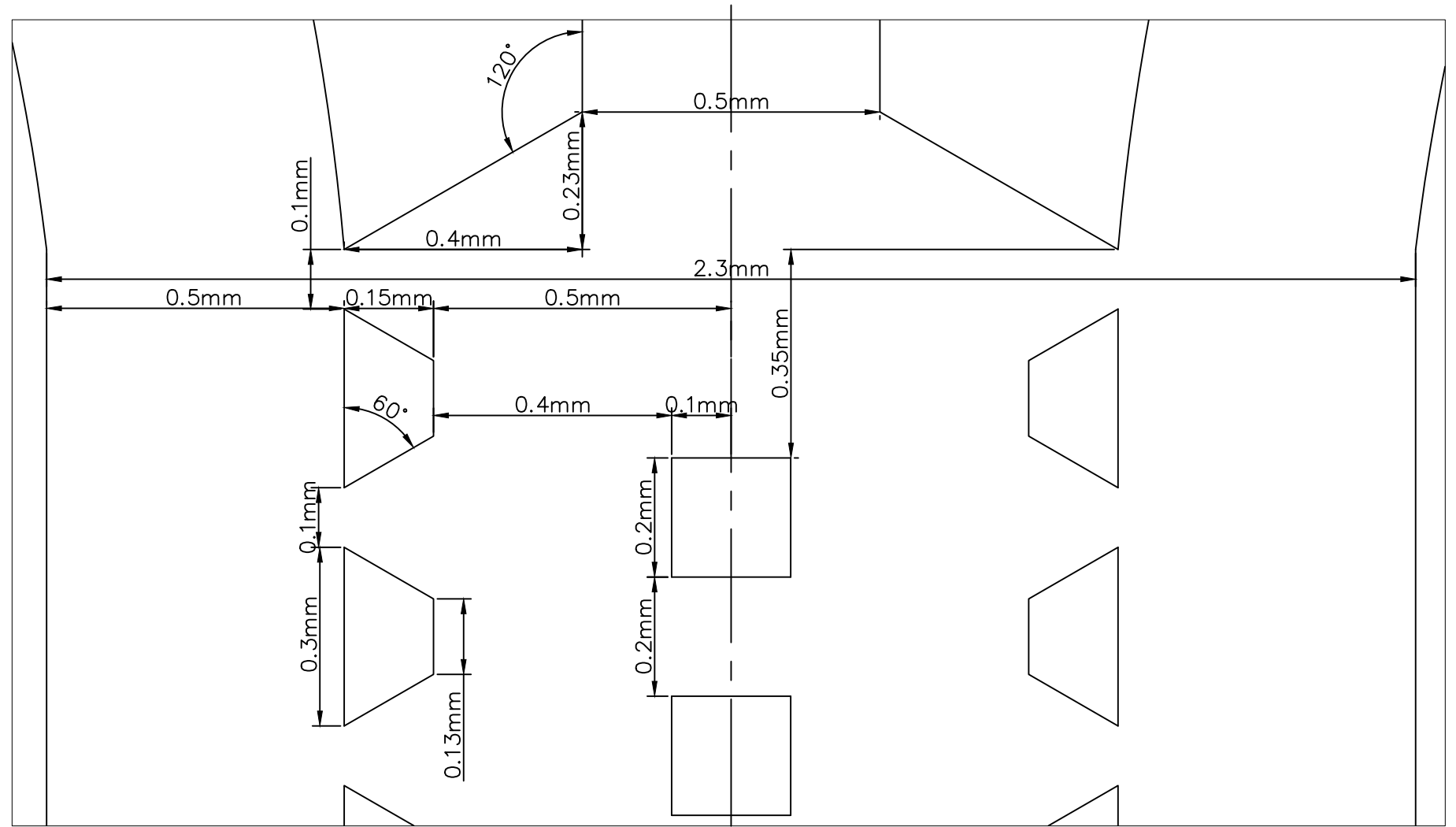
FILE NAME	AIM4 AIM_PA75.dwg	FSCM NO	SHEET	AIM4	SCALE	Check View
SIZE	A4					
DRAWN	3/24/2023					
CHECK	3/26/2023					
APPR.						
ISSUED						
REV						
CONTRACT NO			DWG NO	AIM4 - AIM_PA75		



RevNo	Revision note	Date	Signature	Checked



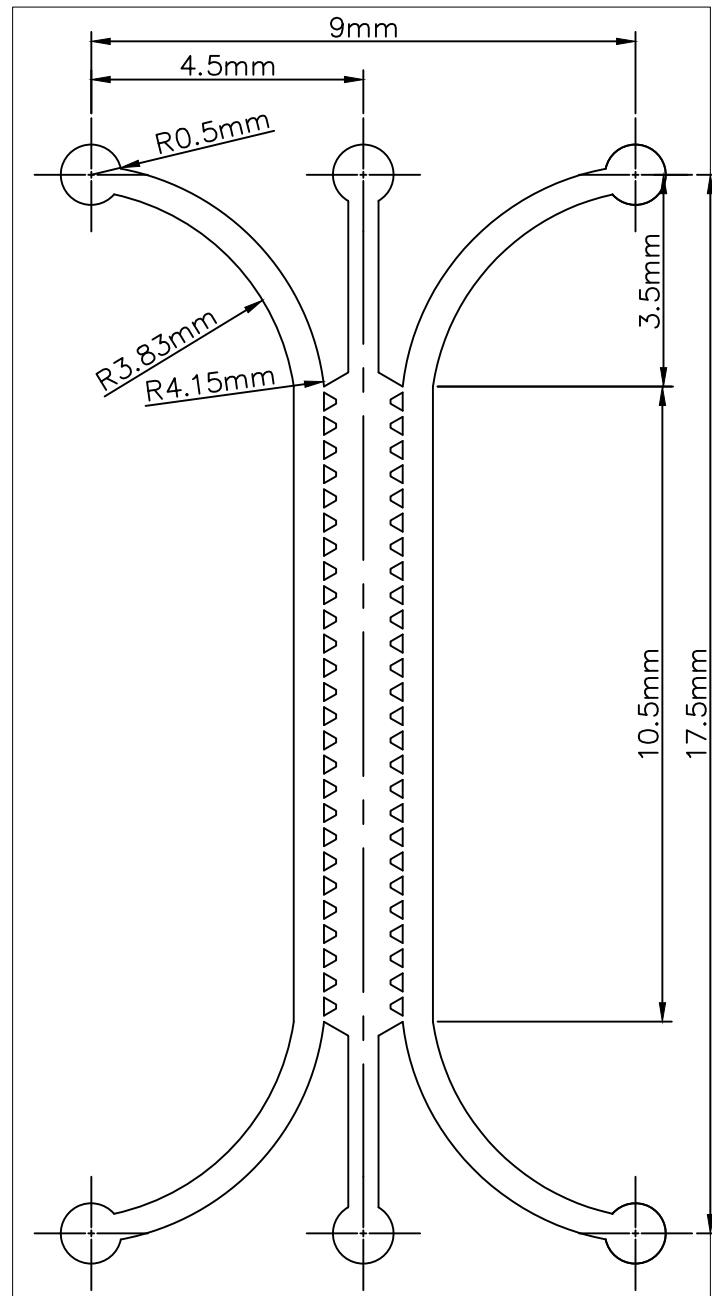
SCALE: 8:1



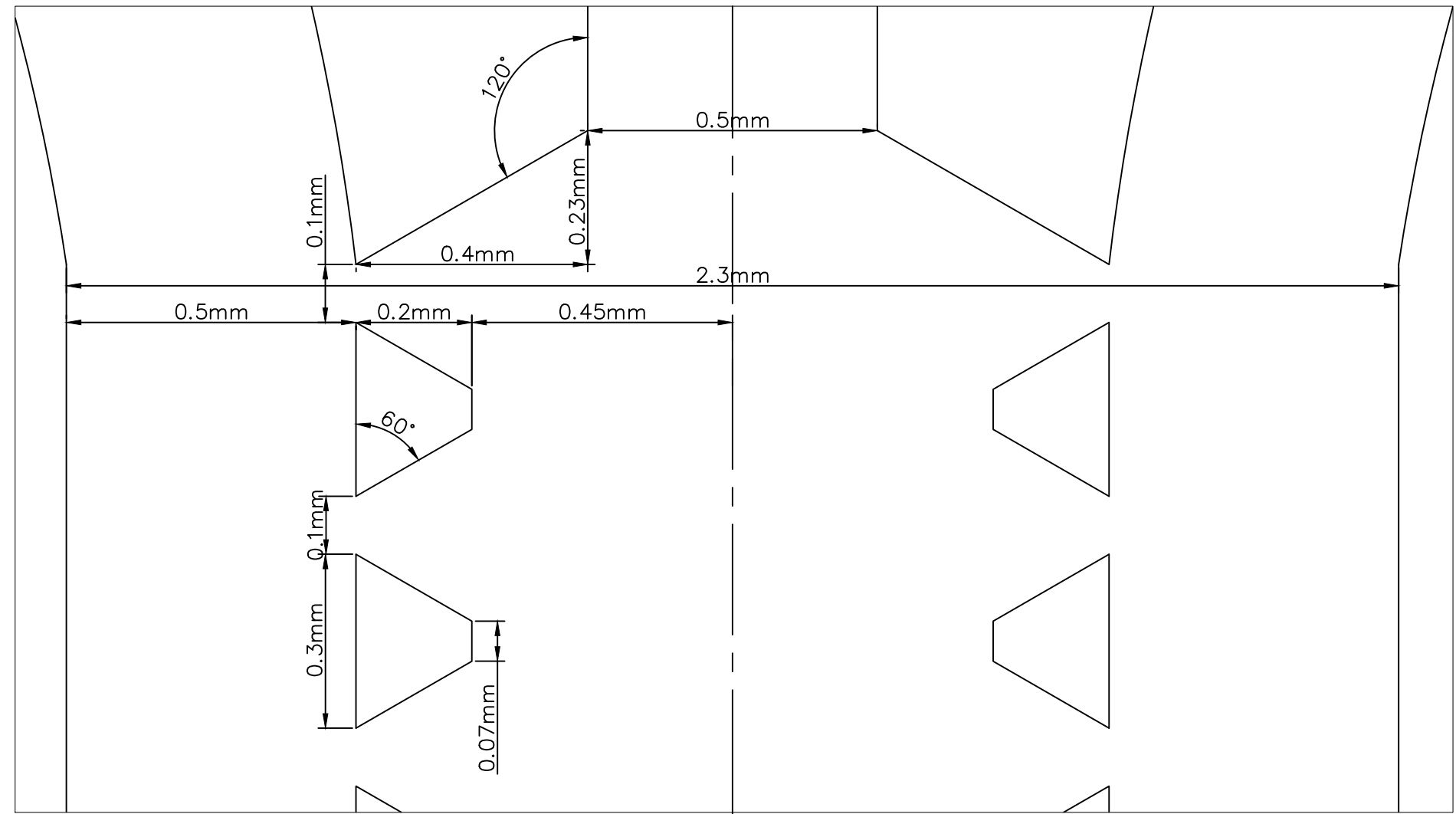
SCALE: 100:1

FILE NAME	AIM5 AIM_IP.dwg	FSCM NO	SHEET	AIM5	SCALE	Check View
SIZE	A4					
DRAWN	3/24/2023					
CHECK	3/26/2023					
APPR.				AIM_IP		
ISSUED						
REV						
CONTRACT NO			DWG NO	AIM5 - AIM_IP		

RevNo	Revision note	Date	Signature	Checked



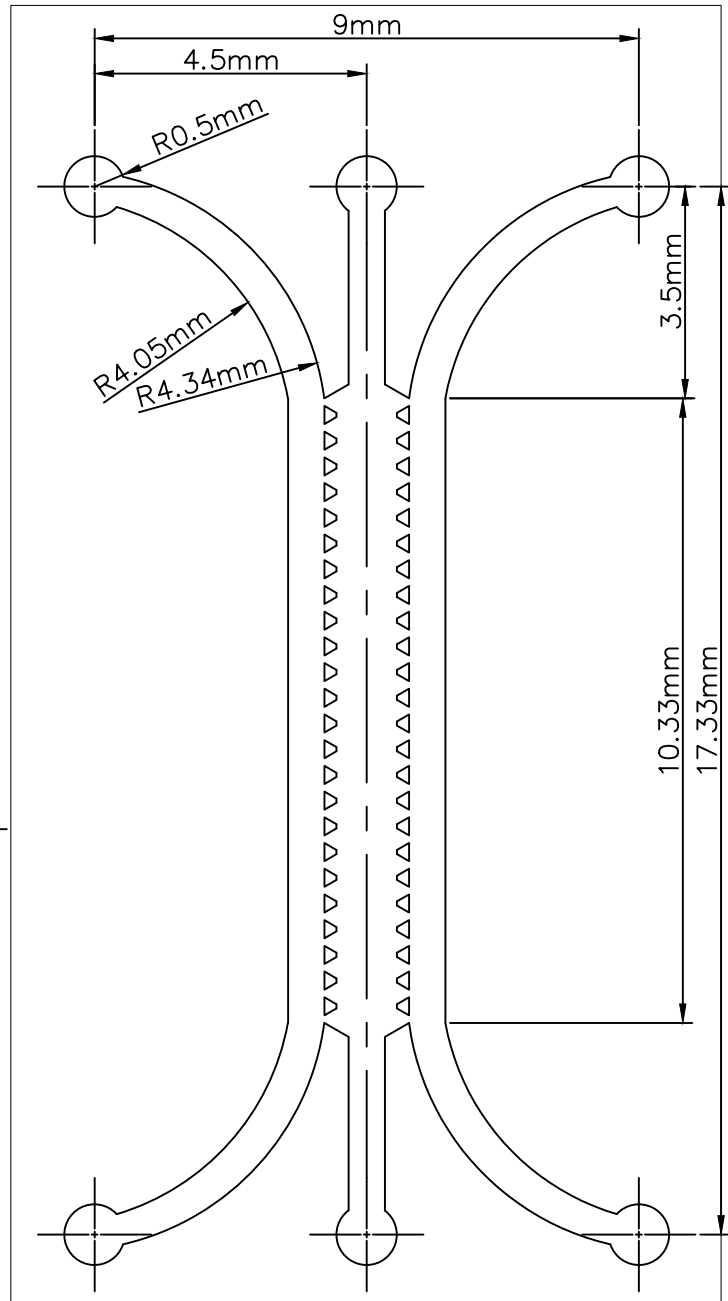
SCALE: 8:1



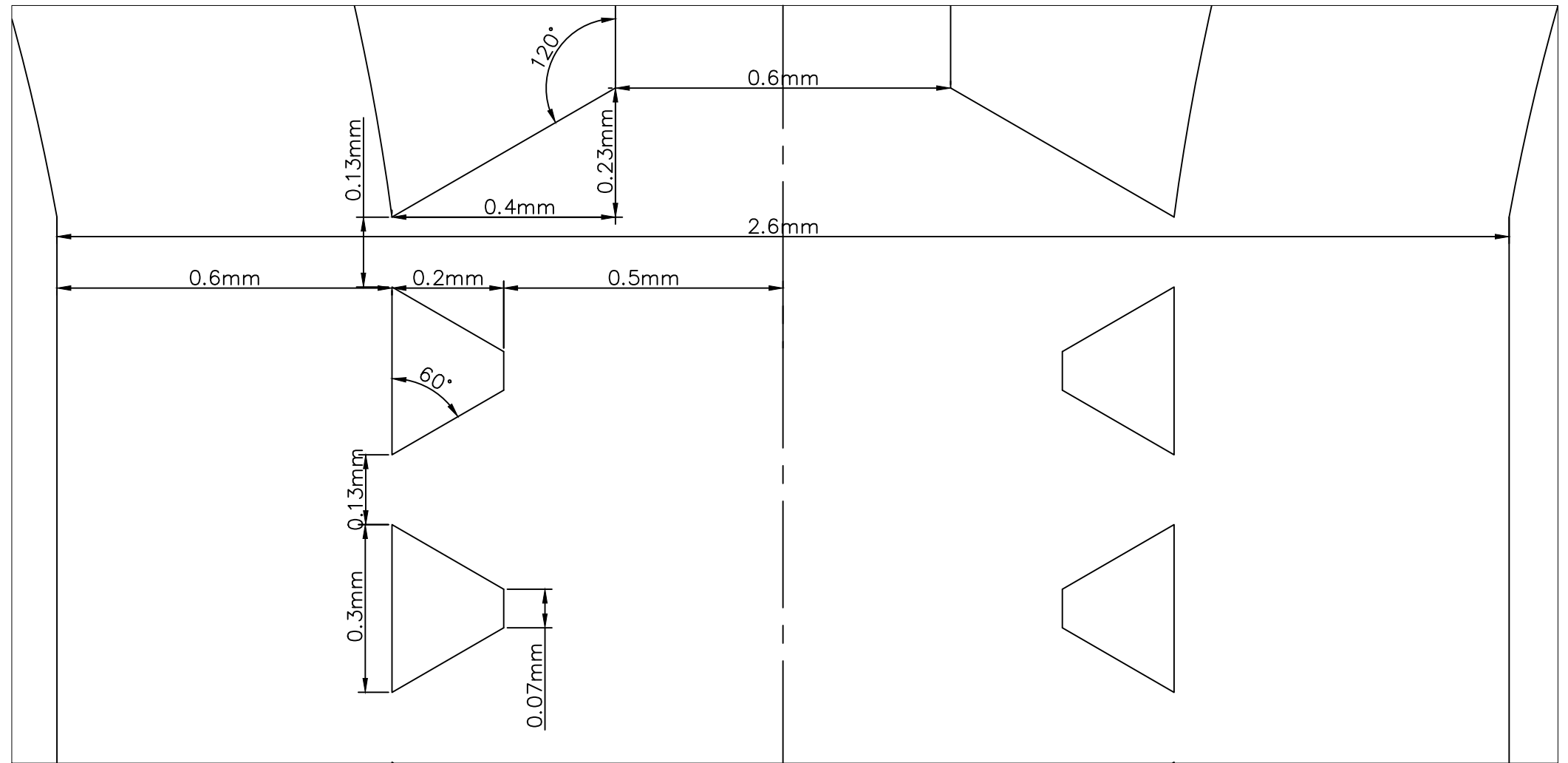
SCALE: 100:1

FILE NAME	F1 Farahat.dwg	FSCM NO	SHEET	SCALE
SIZE	A4		F1	Check View
DRAWN	3/24/2023		FARAHAT_EXACT	
CHECK	3/26/2023			
APPR.			F1 - FARAHAT_EXACT	
ISSUED				
REV			DWG NO	
CONTRACT NO				

RevNo	Revision note	Date	Signature	Checked



SCALE: 8:1

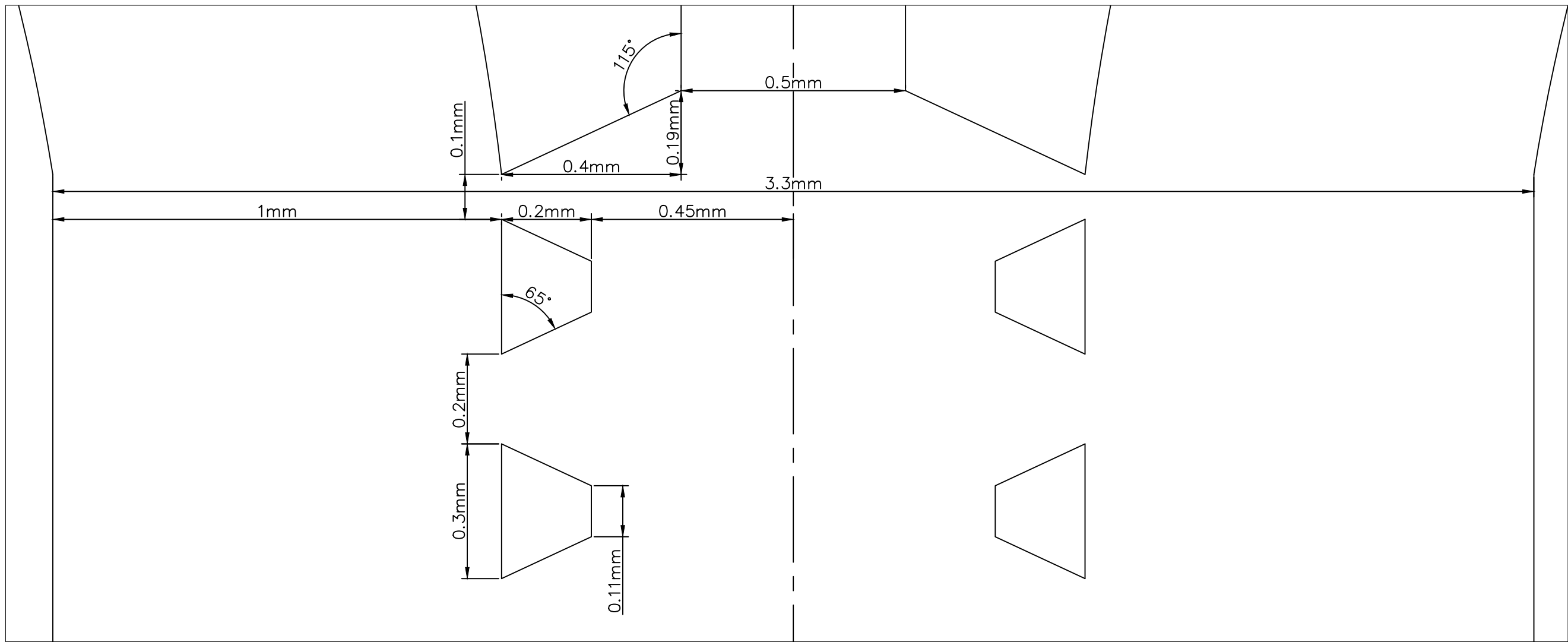


SCALE: 100:1

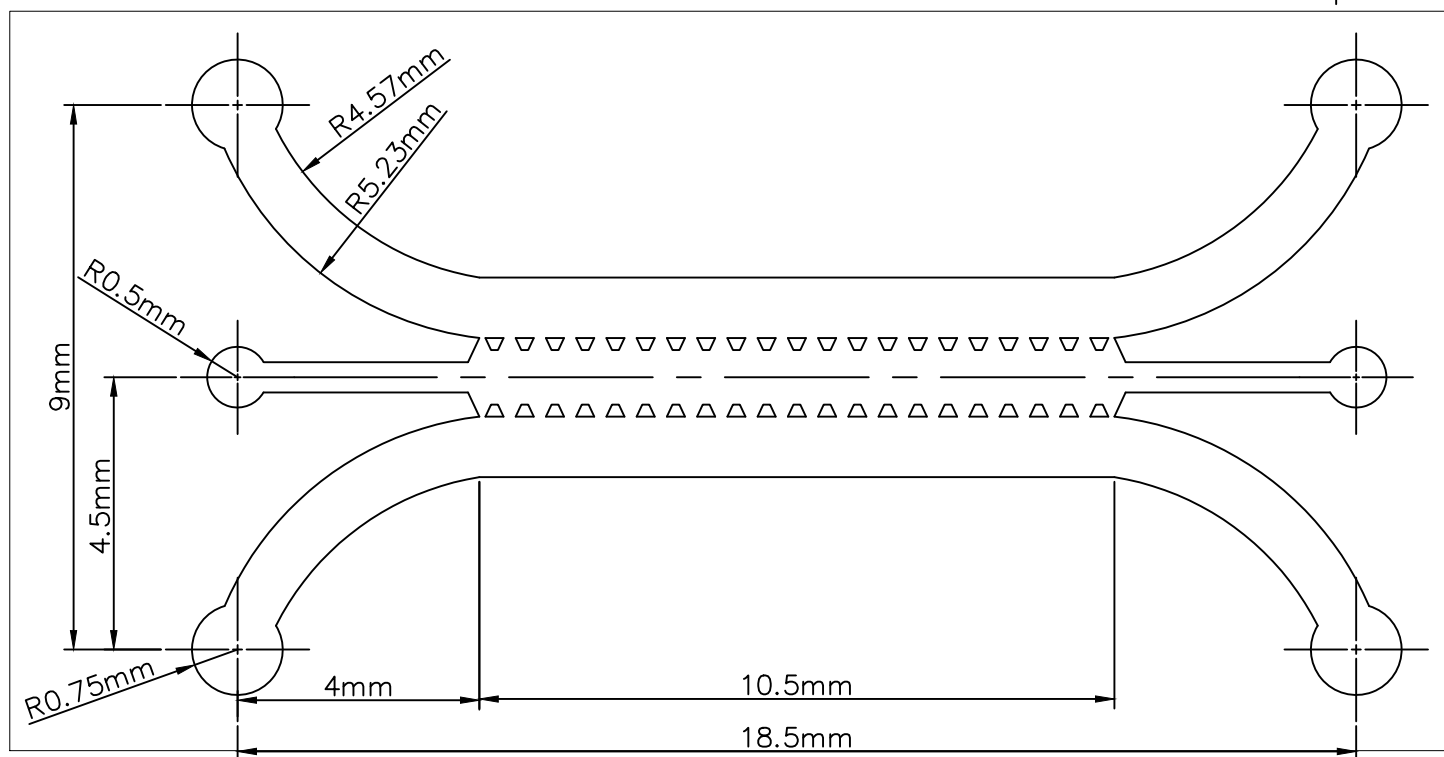
FILE NAME	P1 Polacheck 1.dwg	FSCM NO	SHEET	P1	SCALE	Check View
SIZE	A4					
DRAWN	3/24/2023					
CHECK	3/26/2023					
APPR.						
ISSUED						
REV						
CONTRACT NO			DWG NO	P1 - POLACHECK_EXAC		



RevNo	Revision note	Date	Signature	Checked



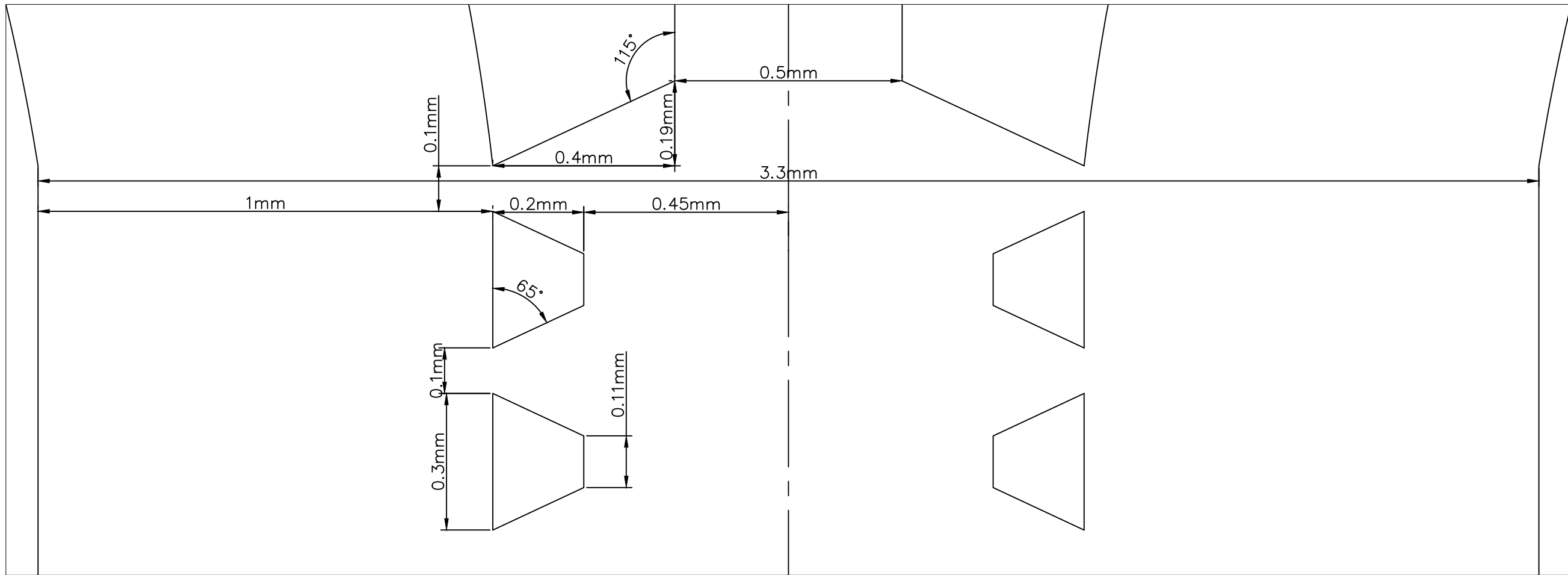
SCALE: 100:1



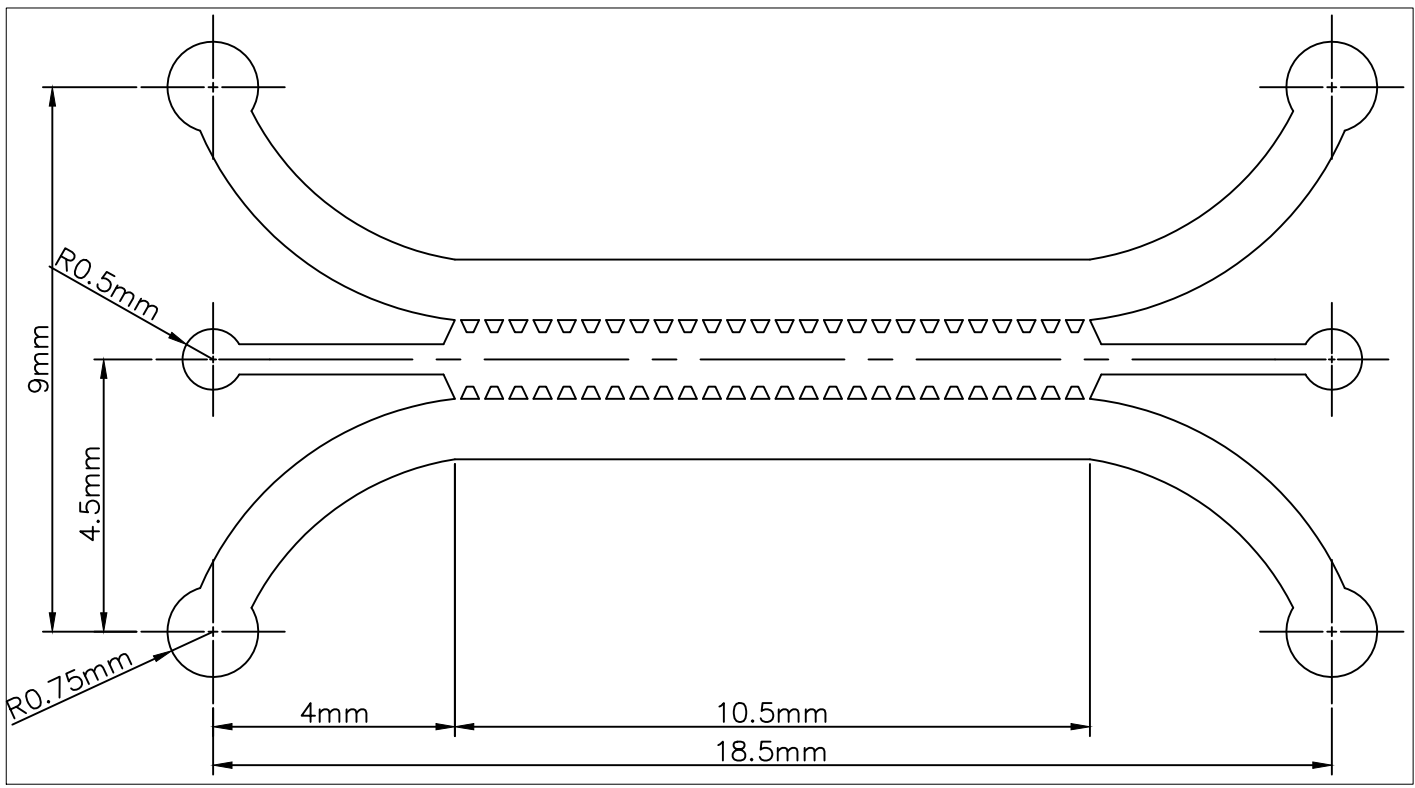
SCALE: 8:1

FILE NAME	Y1 Yoon_Exact.dwg	FSCM NO	SHEET	Y1	SCALE	1:1
SIZE						
DRAWN	3/25/2023					
CHECK						
APPR.						
ISSUED						
REV						
CONTRACT NO						
			YOON_EXACT			
			DWG NO			
			Y1 - YOON_EXACT			

RevNo	Revision note	Date	Signature	Checked



SCALE: 100:1



SCALE: 8:1

FILE NAME	Y2 Yoon_PS100.dwg	FSCM NO	SHEET	Y2	SCALE	1:1
SIZE						
DRAWN	3/25/2023					
CHECK						
APPR.						
ISSUED						
REV						
CONTRACT NO						
			Y00N_PS100			
			DWG NO			
			Y2 - Y00N_PS100			